This is to certify that the
dissertation entitled

CHARACTERIZATION OF MOLECULAR MOTION IN
SELECTED LIPID BILAYER SYSTEMS

presented by
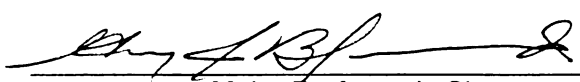
KELLY GREENOUGH

has been accepted towards fulfillment
of the requirements for the

_____Doctoral_____ degree in _____Chemistry_____

_____
Major Professor's Signature

_____7/2/07_____
Date

PLACE IN RETURN BOX to remove this checkout from your record.
TO AVOID FINES return on or before date due.
MAY BE RECALLED with earlier due date if requested.

DATE DUE	DATE DUE	DATE DUE

CHARACTERIZING MOLECULAR MOTION IN SELECTED LIPID BILAYER
SYSTEMS

By

Kelly Greenough

A DISSERTATION

Submitted to
Michigan State University
in partial fulfillment of the requirements
for the degree of

DOCTOR OF PHILOSOPHY

Department of Chemistry

2007

ABSTRACT

CHARACTERIZING MOLECULAR MOTION IN SELECTED LIPID BILAYER SYSTEMS

By

Kelly Greenough

Plasma membranes are central to the existence and function of cellular systems. These membranes are known to contain a large number of constituents and as our understanding of these complex and dynamic systems has evolved, it has become clear that even simple lipid bilayer membranes are heterogeneous, highly dynamic structures. The complexity of these structures makes studies regarding the environment inside membranes difficult. For this reason, experiments are performed using model lipid bilayers. We have produced model lipid bilayers in the form of unilamellar vesicles and have chosen a chemical probe, 6-(N-(7-nitrobenz-2-oxa-1,3-diazol-4-yl)amino) (NBD) to incorporate into our bilayer systems. NBD is a well characterized fluorophore with strong one- and two-photon absorption bands. Two phospholipids were chosen, 1,2-dilauroyl-*sn*-glycero-3-phosphocholine (DLPC) and 1,2-distearoyl-*sn*-glycero-3-phosphocholine (DSPC), as were cholesterol and sphingomyelin in order to promote phase segregation in the model lipid bilayers. The fluorescence lifetime and anisotropy behavior of NBD in vesicles were measured using time correlated single photon counting (TCSPC). We utilized both one- and two-photon excitation to allow determination of the Cartesian components of the chromophore rotational diffusion coefficient as a function of its local

environment. Fluorescence lifetime data indicated that NBD, regardless of being present as a free or tethered probe, resides in the polar region of the lipid bilayer. One- and two-photon anisotropy data have been demonstrated to provide complementary information regarding molecular motions of the chemical probe in the membrane environment and indicate changes in bilayer organization upon the addition of cholesterol and sphingomyelin.

To my husband

ACKNOWLEDGEMENTS

I would like to first thank my advisor Gary Blanchard for all of the support and encouragement he gave me in my years at MSU. He always made it a point to be available and approachable to all of his students. I very much appreciated his confidence in me even when I did not believe in myself. I know that I was extremely lucky to have joined his group, and also very fortunate to have known him.

I would also like to give a special thanks to my friend and colleague, Monika Dominska. She gave me great ideas for my research and was always there when I needed someone to talk to. She is such a talented and knowledgeable individual – she is truly the "Boss". I will miss our daily lattes, which was often the best part of my day.

I would like to say thank you to my parents, Chuck and Susie Patching, who have always been there for me and who continue to go above and beyond to help me out. Much of my success in life I attribute to the fact that I have such incredible and supportive parents.

I would like to say thanks to my sister, Amy Winston, who has always believed in my ability to earn my Ph.D., and encouraged me to pursue this goal from the beginning.

A special thanks goes to my brother Tim Patching who was always my "good luck charm" - especially when I was taking cumulative exams.

Finally, my greatest thank you goes to my husband Dan Greenough. From the beginning, he supported my decision to go back to school, even if it meant completely disrupting our lives, because that was what I wanted. He was the one who was there with me every day throughout this program, standing beside me no matter what. I cannot count

the number of times I wanted to just give up on myself, but he continued to believe in me and picked me up when I was at my lowest. I truly could not have gotten my degree without him. Out of everything I have ever achieved in my life, I am most proud that I am his wife.

TABLE OF CONTENTS

LIST OF TABLES

CHAPTER 1

INTRODUCTION

Lipid bilayers have attracted a great deal of attention in recent years due to the crucial role they play in cellular processes. Plasma membranes are central to the function of cells as they serve as a barrier to the external environment and support transmembrane proteins. These proteins play a key role in metabolic reactions, viral and bacterial infection, nutrient transport to cells, as well as drug delivery. In order to gain an understanding of these processes, knowledge of the membranes and the environment within lipid bilayers must first be gained.

Cell membranes were first described as lipid bilayers by Gorter and Grendel in 1925,[1,2] and the lipid bilayer structure became the accepted model for cell membranes after further studies by Davson and Danielli in 1935.[3] However, at that time, it was believed that the lipids constituting a membrane were fixed, with proteins covering the outside of the bilayer. The fluid mosaic model introduced by Singer and Nicolson in 1972[3,4] proposed that the lipids constituting the membrane are not fixed, but rather are fluid. This led to the idea of biomembranes as lipid matrices containing both peripheral and integral proteins. A key element in this model is that the proteins and lipids composing the bilayer have motional freedom. The fluid mosaic model is not entirely sufficient to describe the bilayer and the motions within it, because the lipids exist in several phases, and other components of the membrane (i.e. cholesterol) affect mobility within the bilayer.[3,4] Dynamics of proteins and lipids within the bilayer membrane facilitate life processes, and in order to fully understand how such processes affect

cellular functions, it is first necessary to understand the structure and organization of the membrane.

A major function of membrane lipids is to form amphipathic bilayers that surround cells. Three common classes of lipids found in mammalian cell membranes include glycerophospholipids, sphingolipids, and sterols, yet there is great variety in the identity of the lipid head groups, and both length and unsaturations present in the acyl chains. A characteristic of lipid bilayers is their transition temperature, T_m, the point at which the lipid layer transitions from the solid phase, s, to a liquid disordered phase, l_d. At a temperature above the transition temperature, the lipid monolayer or bilayer is fluid and disorganized, lateral motion of lipid molecules is rapid, and there is very loose lipid packing. At a temperature below the transition temperature, the lipids exist in a solid, gel-like state, and lipid molecules that comprise the monolayer or bilayer are tightly packed together.

Recent research has shown that plasma membranes are exceedingly complex heterogeneous structures, and are composed of multiple different constituents.[4-9] In studies utilizing biomimetic membranes, it has been found that, upon mixing, rather than random blending of lipids resulting in a homogeneous bilayer, the formation of micro-domains is seen.[5,8,10-18] These structures, which are sometimes referred to as "lipid rafts", have been found to be enriched in cholesterol and sphingomyelin,[6,7,10,14,19-26] yet the question remains if these lipid raft structures form in actual plasma membranes.

The formation of such structures was first realized when certain membrane fragments were found to be insoluble in cold non-ionic detergents such as Triton X-100.[27]

These detergent-resistant membranes, or DRMs, were enriched in cholesterol and sphingolipids. It became apparent that detergents could solubilize membrane domains in different physical states differentially.[27] Insoluble domains were classified as a "liquid-ordered" (l_o) phase, because they shared characteristics of both the l_d and s phases – high lipid packing density, similar to the solid phase, yet like the l_d phase in that relatively rapid lateral motion of lipid molecules is possible. The l_o state is distinct and coexists with l_d or solid states.

Although the existence of lipid raft domains has yet to firmly be established in plasma membranes, several studies have been performed that specifically address the question as to whether raft structures exist, and under what circumstances they form. Various methods have been used to explore lipid raft formation including fluorescence microscopy, fluorescence recovery after photobleaching (FRAP), single particle tracking (SPT), nuclear magnetic resonance (NMR), atomic force microscopy (AFM) and others.[7-9,13-15,28-33] Time-resolved fluorescence techniques have been used widely to investigate biomimetic membranes due to the high sensitivity of such experiments.

The long term goal of this project is to quantitate the chemical, physical and viscoelastic properties of lipid bilayer membranes. We produced model lipid bilayers in the form of vesicles by the extrusion method.[34-36] This technique uses an extruder composed of two syringes and a polycarbonate membrane with pores of specific diameters. A lipid solution is forced through the membrane several times, and the result is lipid vesicles with a diameter roughly equal to that of the pore sizes. Extrusion has been shown to reproducibly produce unilamellar vesicles of a desired diameter. We formed such structures with fluorescent molecular probes embedded within and tethered to the

bilayer, and monitored the lifetime and motional properties of the probe molecules using time-correlated single photon counting (TCSPC). Specifically, experiments designed to determine fluorescence lifetime and molecular reorientation have assisted in our understanding of the polarity, viscosity, and organization within lipid bilayers. The model bilayers used in this study were composed mainly of phospholipids, similar to plasma membranes but, in order to study possible lipid raft structures, cholesterol and sphingomyelin were used as well. Our experiments determine how the bilayer properties change as a function of bilayer composition.

We used time-resolved fluorescence spectroscopy to probe lipid bilayer heterogeneity and to examine the environment within a lipid bilayer membrane. In such experiments, a fluorescent probe is selected, incorporated into the model bilayer, and fluorescence lifetime and depolarization measurements provide insight into the chromophore environment. For this work, experiments utilizing both one- and two-photon excitation were used in order to determine the rotational diffusion coefficient of the chromophore embedded in the bilayer.

All lifetime and anisotropy data were acquired using a time correlated single photon counting (TCSPC) system (Figure 1.1). The source laser is a CW mode-locked Nd:YAG laser (Coherent Antares 76-S) that produces 30 W average power at 1064 nm with 100 ps pulses at 76 MHz repetition rate. The second (3W average power) or third harmonic (1 W average power) of the output of this laser excites a cavity dumped dye laser (Coherent 702-2). For our experiments, based on the absorption properties of the chromophore used, output was produced using a Rhodamine 610 dye (Exciton, 532 nm pump) which produced light at ~650 nm for two- photon excitation experiments, or with

4

Stilbene 420 dye (Exciton, 355 nm pump), producing ~460 nm light for one photon

excitation experiments. The dye laser output is typically 5 ps pulses at a repetition rate of

3.8 MHz for both excitation wavelengths. The dye output beam is split into a reference

channel and a sample beam.
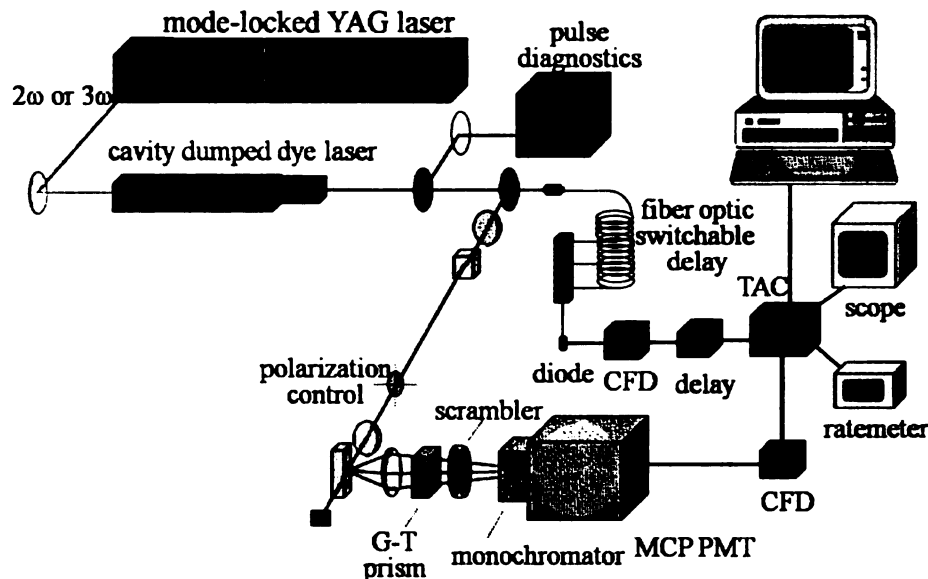
**Figure 1.1 The time correlated single photon counting (TCSPC)
system**

The sample is excited by a vertically polarized pulse and is collected 90° to the

excitation beam. Fluorescence was collected at 0°, 54.7° and 90° with respect to the

vertically polarized excitation pulse. Fluorescence signals are spectrally filtered using a

subtractive double monochromoator (American Holographic DB10-S) which reduces the

effects of dispersion-induced time broadening of the collected light,[37] and are detected

using a Hamamatsu R3809U microchannel plate photomultiplier tube (MCP-PMT)

detector. The signals are processed using a Tennelec 454 quad constant fraction

discriminator and Tennelec 864 time-to-amplitude converter (TAC) and biased amplifier.

The TAC measures the time between the excitation pulse and the first arriving photon,

5

and is operated in reverse time mode to avoid dead-time limitations of the electronics.[37,38] The TAC counts are observed with an oscilloscope and are sent to a Tennelec PCA-II multichannel analyzer (MCA). Collection wavelength, polarization and data acquisition were controlled using National Instruments LabVIEW® 7.1 software.

The emission transients collected at 54.7° provide fluorescence lifetime data, while those collected at 0° and 90° are used for fluorescence depolarization measurements. Lifetime values provide information on the polarity of the environment in which the probe molecule localizes. Specifically, in lipid bilayer environments where drastic differences in polarity exist, the lifetime values can yield detailed information regarding the chromophore's surroundings, such as whether the probe molecule is in the non-polar lipid tail region, near the glycerol backbone region, or near the bilayer-aqueous layer interface. In addition, chromophores with unique fluorescent properties can be selected to provide further detail on the specific location of probe molecules, and the polarity of those surroundings. The decay functionality also provides insight as to the number of environments sensed by the chromophore; a single exponential anisotropy decay indicates the chromophore population exists in a single environment, or at least a group of rapidly-exchanging environments, while a double exponential anisotropy decay indicates the chromophore population is sampling multiple, distinct non-exchanging environments.

Time-resolved fluorescence anisotropy measurements provide information about the rotational dynamics of the molecule of interest. In such experiments, randomly oriented sample molecules in the ground state are excited by the vertically polarized excitation beam. The molecules in the sample with their absorption dipoles oriented

parallel to the incident light will be preferentially excited, leading to a non-random excited state population. The primary means in which the sample molecules restore their initial random orientation is through rotational diffusion. The rotational motion of a molecule in solution or in a lipid bilayer is determined by a number of factors, including the size and shape of the molecule, the viscosity of its environment, and the nature of the chromophore's interactions with neighboring molecules. Depending on these various factors, the rotational motions of the probe molecules may be inhibited, and it is useful to follow the rotational relaxation of solute molecules after photoselection. Fluorescence depolarization measurements can provide direct measurements of the rotational decay time, τ_{or}, which help characterize rotational dynamics by allowing determination of the rotational diffusion coefficient. Such experiments have been used extensively to investigate the environment in both solvents and model membranes[30,38-44], and utilized that information to gain insight about the organization in these systems.

Anisotropy measurements have been used extensively to investigate the rotational dynamics of molecules in a range of environments, and there is a well established theoretical framework for such measurements.[37,38,40,45] In these experiments, emission transients are collected at 0° (parallel) and 90° (perpendicular) relative to the vertically polarized excitation pulse. The raw data are combined to generate the induced orientational anisotropy function (Eqn.1.1):

$$R(t) = \frac{I_{\parallel}(t) - I_{\perp}(t)}{I_{\parallel}(t) + 2I_{\perp}(t)}$$

(1.1)

7

Where $I_{\parallel}(t)$ is the emission intensity collected at 0° relative to the excitation polarization,

and $I_{\perp}(t)$ is the emission intensity collected at 90° relative to the excitation polarization.

The value of R(t) is then plotted vs. time (Figure 1.2), and can exhibit up to five

exponential decay components, but the typical case is to observe one or two components.

As the molecules re-randomize, the anisotropy decays exponentially in time, until the

sample molecules are once again randomly oriented and the value of R is zero.
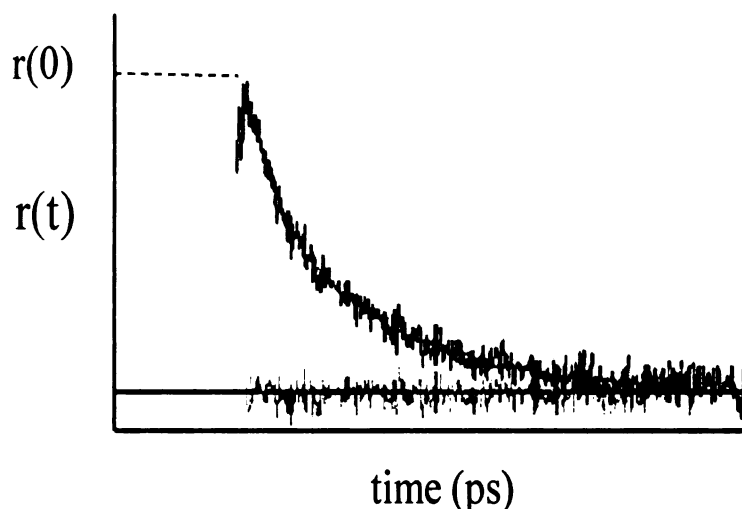
Figure 1.2 An experimental single exponential anisotropy decay

The reorientation time, τ_{or}, reflects rotational motion of the chromophore. For

chromophore molecules that are free to rotate in solution, the anisotropy decay curve

yields the reorientation time, and for a spherical molecule, τ_{or} is related to the rotational

diffusion constant, D, by the modified Debye-Stokes-Einstein equation[46-48]:

$$\tau_{OR} = \frac{\eta V f}{k_b T S}$$

(1.2)

8

where η is the viscosity of the surrounding medium, V is the hydrodynamic volume of the probe molecule, T is the absolute temperature, k_B is the Boltzmann constant, f is a frictional coefficient with values from 0 to 1, and S is a shape factor that is dependent on the shape of the probe molecule.

In most cases, the probe molecule is not perfectly spherical, but has an ellipsoid shape, and the relationship between the decay functionality of R(t) and the rotational diffusion coefficients and the angle between the absorption and emission transition dipole moments has been described in detail by Chuang and Eisenthal.[40] They treated the form of R(t) for a general ellipsoid, and related the experimental anisotropy decay to both the orientation of the absorption and emission transition dipole moments and the rotational diffusion coefficient by choosing Cartesian axes such that the z-axis was perpendicular to the molecular plane, and the transition dipole lied along either the x- or y-axis.[37,38,40,45] They treated the form of R(t) for a general ellipsoid, using two limiting cases, termed *prolate* or *oblate* rotors, where the rotational motion around the axis that is distorted is no longer equal to the rotation about the other axes. In the case of a prolate rotor, the rotational diffusion coefficient about the x-axis is greater than that about either the y- or z-axes. In the case of an oblate rotor, rotations about the z-axis are slower than rotations about either the y- or x-axes. These differences are reflected in the values of the rotational diffusion coefficients.

When the motional freedom of a molecule is restricted in some manner, such as incorporation into a bilayer structure and/or tethered to an interface, the data are usually treated using the hindered rotor model.[32,37,44,49-53] This model takes into account the fact that the initially non-random chromophore population is not free to re-randomize

completely. The inability to re-randomize completely is manifested as a non-zero anisotropy decay at long times. The decay time constant τ, is related to θ_0, the semi-angle of the cone which the tethered molecule sweeps out, and the "wobbling" diffusion coefficient D_w which describes the motion about it's tethering bond:[32,37,44,49-53]

$$\tau = \frac{7\theta_o^2}{24D_w}$$

(1.3)

While the cone angle is a useful measure of the average disorder in the system, D_w provides limited detail on chromophore motion. However, the Cartesian components of D_w can be separated to give a more complete picture of chromophore dynamics.

For a hindered rotor, the anisotropy decays according to Equation 1.4. $R(0)$ is the initial anisotropy value, and $R(\infty)$ is related to the size of the cone in which the chromophore resides. A large cone angle means a large volume is swept out by the chromophore indicative of an environment where the chromophore has substantial freedom. Conversely, a small cone angle is reflective of the chromophore residing in a comparatively restricted environment.

$$R(t) = R(\infty) + [R(0) - R(\infty)]\exp\left(-t/\tau_{OR}\right)$$

(1.4)

For either model used, depending on the orientation of the probe molecule's transition dipole moments, there can be ambiguity in resolving the Cartesian components of the rotational diffusional coefficient. Using one-photon anisotropy experiments in this work, determination of only one of the Cartesian components of the rotational diffusion coefficients is possible. Therefore the diffusion coefficients found by single photon

excitation do not provide a full description of rotational dynamics. For this reason, we have also used the induced orientational anisotropy function using two-photon excitation.

In 1931, Maria Göppert-Mayer first predicted the ability of a molecule to simultaneously absorb two photons.[54] It was believed that two photons, of energies $h\nu_1$ and $h\nu_2$, when summed would correspond to an excited state of an atom. It was not until the 1960's, with the invention of the laser that two photon absorption was experimentally observed. Kaiser and Garrett first observed the phenomenon in $CaF_2:Eu^{2+}$ crystals in 1961.[54,55]

Two photon excitation (TPE) is a third order non-linear process where the intensity of the fluorescence signal is dependent on the square of the incident power:[55]

$$I \propto P^2 \qquad\qquad\qquad (1.5)$$

Therefore, high peak intensities are necessary. TPE offers several advantages over one-photon excitation (OPE).[56] First, because of the longer wavelength, resonant one photon absorption does not occur, minimizing sample heating and damage. The laser source is focused onto a small area to achieve the high intensity necessary for two photon absorption, resulting in less background interference. Another advantage of two-photon excitation is the different selection rules for electronic transitions than for one-photon excitation. Two-photon absorption requires an even-parity transition, while one-photon absorption requires an odd parity transition between the ground and excited states. Thus the ground and excited states can have the same parity in two-photon excitation. This property of two photon excitation was widely used in the 1970's to assign symmetry properties to previously inaccessible excited states.[57-59] In two-photon excitation, two

photons are absorbed simultaneously, and so two electric field vectors are needed to describe the interaction with the process, therefore the amplitude for the process is given by the double projection of two field vectors onto a molecular tensor, represented by a 3x3 matrix:[57,60,61]

$$S = \begin{pmatrix} S_{xx} & S_{xy} & S_{xz} \\ S_{yx} & S_{yy} & S_{yz} \\ S_{zx} & S_{zy} & S_{zz} \end{pmatrix}$$

(1.6)

Reorientation dynamics probed by two-photon excited fluorescence can provide more detailed information regarding rotational diffusion than by utilizing one-photon excitation. The Johnson group and others have established a theoretical framework with which to interpret anisotropy data gathered using two photon excitation.[30,61-65] An added benefit in utilizing TPE for study of lipid bilayers is that it uses lower energy photons so thermal damage of the bilayer structure is less likely. This characteristic of TPE makes it a particularly valuable technique for studying fragile biological membranes.

Reorientational dynamics probed by two-photon excited fluorescence can provide complementary information regarding rotational motion of molecules. When used in combination, data acquired using both means of excitation allow determination of the Cartesian components of the rotational diffusion coefficient. For both modes of excitation, the motional dynamics of the molecules is similar, however, the initial anisotropic distribution of excited state molecules is dependent on different factors for the two means of excitation. These experiments, in turn, give different experimental reorientation times, and thus different molecular information.

For both one- and two-photon excitation, the value of the initial anisotropy depends on the extent of photo-selection. If the molecule's absorption transition moment is oriented parallel to the excitation, they have the highest probability of absorption. That probability for molecules to be excited by one-photon excitation is proportional to $\cos^2\theta$, and for two-photon excitation, the probability of absorption is proportional to $\cos^4\theta$, where θ is the angle between the incident electric field polarization and the axis along which the transition moment lies. Therefore, the two experiments yield different initial distributions of excited molecules as displayed in Figure 1.3.

one-photon   two-photon   two-photon
              (linear)   (circular)
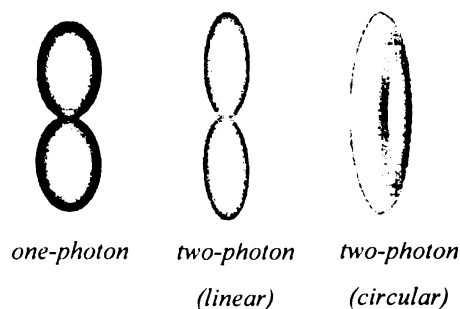
Figure 1.3 The initial orientational distributions of excited state molecules for one-photon, two-photon linear, and two-photon circular polarization

For one-photon excitation, the anisotropy depends on the relationship between the absorption and emission transition dipole moments (μ_{ab} and μ_{em}, respectively), while for two-photon experiments, R(t) depends on the molecular tensor, S, and the emission transition dipole moment (Eqns 1.7).

$$r_{OPE}(t) = r_1(0)\left(\mu_{ab}(0) \cdot \mu_{em}(t)\right)$$

$$r_{TPE}(t) = r_2(0)\left(S(0) \cdot \mu_{em}(t)\right) \tag{1.7}$$

13

The molecules comprising the initial excited state distribution will re-randomize to become randomly oriented again, and by comparing the experimental data for one- and two-photon excitation, a more complete and less ambiguous picture of the rotational diffusion coefficients is determined.

For our experiments, we have chosen probes from the 7-nitrobenz-2-oxa-1,3-diazole (NBD) family. The fluorescence behavior of this chromophore has been shown to depend sensitively on its environment.[39,41,66-68] Chapter 2 examines three substituted NBD chromophores and discusses the role of the side group in mediating solution phase rotational motion. Initial experiments in which an NBD chromophore has been incorporated into a bilayer are presented in Chapter 3 where NBD-hexanoic acid was inserted into a lipid bilayer composed of phospholipids, cholesterol, and a sphingolipid. Experiments utilizing tethered chromophores and embedding them in lipid bilayers are outlined in Chapter 4. Chapter 5 discusses experiments dealing with lipids with different headgroups. Finally, Chapter 6 provides some final conclusions as well as presents ideas for future research.

Literature Cited

(1)   Chapman, D. *Langmuir* **1993**, *9*, 39.

(2)   Gorter, E., Grendel, F. *J. Exp. Med.* **1925**, *41*, 439.

(3)   Singer, S. J., Nicholson, G.L. *Science* **1972**, *172*, 720.

(4)   Subczynski, W. K. e. a. *Cell. Mol. Bio Lett.* **2003**, *8*, 147.

(5)   Scherfeld, D.; Kahya, N.; Schwille, P. *Biophysical Journal* **2003**, *85*, 3758.

(6)   Stottrup, B. L., Stevens, D.S., Kellar, S.L. *Biophysical Journal* **2005**, *88*, 269.

(7)   Veatch, S. L. a. K., S. L. *Biophysical Journal* **2003**, *85*, 3074.

(8)   Veatch, S. L. a. K., Sarah L. *Biochimica et Biophysica Acta* **2005**, *1746*, 172.

(9)   Wilson, B. S. e. a. *Molecular Biology of the Cell* **2004**, *15*, 2580.

(10)   Wisniewska, A.; Draus, J.; Subczynski, W. K. *Cellular & Molecular Biology Letters* **2003**, *8*, 147.

(11)   Crane, J. M., Tamm, L.K. *Biophysical Journal* **2004**, *86*, 2965.

(12)   Dietrich, C., Bagatolli, L.A., Volovyk, Z.N., Thompson, N.L., Levi, M., Jacobson, K., Gratton, E. *Biophysical Journal* **2001**, *80*, 1417.

(13)   Hancock, J. F. *Molecular Cell Biology* **2006**, *7*, 456.

(14)   Hao, M.; Maxfield, F. R. *Journal of Fluorescence* **2001**, *11*, 287.

(15)   Prenner, E., Honsek, G., Honig, D., Mobius, D., Lohner, K. *Chemistry and Physics of Lipids* **2007**, *145*, 106.

(16)   Silvius, J. R. *Biochimica et Biophysica Acta* **2005**, *1746*, 193.

(17)   Simons, K.; van Meer, G. *Biochemistry* **1988**, *27*, 6197.

(18)   Suzuki, T., Suzuki, Y. *Biol. Pharm. Bull.* **2006**, *29*, 1538.

(19)   Jacobson, K., Dietrich, C. *Trends in Cell Biology* **1999**, *9*, 87.

(20)   Bittman, R., Kasireddy, C. R. , Mattjus, P., Slotte, J.P. *Biochemistry* **1994**, *33*, 11776.

(21)   Garmy, N., Taieb, N., Nouara, Y., Fantini, J. *Journal of Lipid Research* **2007**.

(22)   Ramstedt, B., Slotte, J.P. *FEBS Letters* **2002**, *531*, 33.

(23)   Rog, T., Pasenkiewicz-Gierula, M. *Biophysical Journal* **2006**, *91*, 3756.

(24)   Smaby, J. M., Brockman, H.L., Brown, R.E. *Biochemistry* **1994**, *33*, 9135.

(25)   Smaby, J. M., Momsen, M., Kulkarni, V. S., Brown, R.E. *Biochemistry* **1996**, *35*, 5696.

(26)   Terova, B., Heczko, R., Slotte, J.P. *Biophysical Journal* **2005**, *88*, 2661.

(27)   Xin-Min, L. M., M.M., Smaby, J. M., Brockman, H. L., Brown, R. E. *Biochemistry* **2001**, *40*, 5954.

(28)   London, E., Brown, D.A. *Biochimica et Biophysica Acta* **2000**, *1508*, 182.

(29)   Birch, D. J. S. *Spectrochimica Acta, Part A: Molecular and Biomolecular Spectroscopy* **2001**, *57A*, 2313.

(30)   Girard, C.; Martin, O. J. F.; Dereux, A. *Physical Review Letters* **1995**, *75*, 3098.

(31)   Johnson, J. M.; Ha, T.; Chu, S.; Boxer, S. G. *Biophysical Journal* **2002**, *83*, 3371.

(32)   Korchowiec, B., Paluch, M., Corvis, Y., Rogalska, E. *Chemistry and Physics of Lipids* **2006**, *144*, 127.

(33)   Lipari, G.; Szabo, A. *Biophysical Journal* **1980**, *30*, 489.

(34)   Polozov, I. V. a. G., Klaus. *Biophysical Journal* **2006**, *90*, 2051.

(35)   Hunter, D. G.; Frisken, B. J. *Biophysical Journal* **1998**, *74*, 2996.

(36)   Moscho, A.; Orwar, O.; Chiu, D. T.; Modi, B. P.; Zare, R. N. *Proceedings of the National Academy of Sciences of the United States of America* **1996**, *93*, 11443.

(37)   Patty Philipus, J.; Frisken Barbara, J. *Biophysical Journal* **2003**, *85*, 996.

(38)   Lakowicz, J. R. *Principles of Fluorescence Spectroscopy*, 2nd ed., 1999.

(39)   Blanchard, G. J. *Applied Spectroscopy* **2001**, *55*, 110A.

(40)   Chattopadhyay, A.; London, E. *Biochimica et Biophysica Acta, Biomembranes* **1988**, *938*, 24.

(41)   Chuang, T. J.; Eisenthal, K. B. *Journal of Chemical Physics* **1972**, *57*, 5094.

(42)   Dela Cruz, J. L.; Blanchard, G. J. *Journal of Physical Chemistry A* **2001**, *105*, 9328.

(43)   Greenough, K. P.; Blanchard, G. J. *Journal of Physical Chemistry B* **2006**, *110*, 6351.

(44)   Koan, M. M.; Blanchard, G. J. *Journal of Physical Chemistry B* **2006**, *110*, 16584.

(45)   Mazeres, S.; Schram, V.; Tocanne, J.-F.; Lopez, A. *Biophysical Journal* **1996**, *71*, 327.

(46)   McPhie, P. *Principles of Fluorescence Spectroscopy, Second ed. Joseph R. Lakowicz*, 2000; Vol. 287. pp. 291-333.

(47)   Blanchard, G. J. *Journal of Chemical Physics* **1987**, *87*, 6802.

(48)   Edward, J. T. *Journal of Chemical Education* **1970**, *47*, 261.

(49)   Zwanzig, R.; Harrison, A. K. *Journal of Chemical Physics* **1985**, *83*, 5861.

(50)   Perrin, F. *Journal de Physique et le Radium* **1936**, *7*, 1.

(51)   Karpovich, D. S.; Blanchard, G. J. *Langmuir* **1996**, *12*, 5522.

(52)   Kinosita, K., Jr.; Ikegami, A.; Kawato, S. *Biophysical Journal* **1982**, *37*, 461.

(53)   Kinosita, K., Jr.; Kawato, S.; Ikegami, A. *Biophysical Journal* **1977**, *20*, 289.

(54)   Szabo, A. *Journal of Chemical Physics* **1984**, *81*, 150.

(55)   Tao, T. *Biopolymers.* **1969**. 8. 609.

(56)   So, P. T., Masters, B. R. *Micros. Res. and Tech.* **2004**, *69*, 3.

(57)   Garrett, C. G. B., Kaiser, W. . *Phys. Rev. Lett.*, *7*, 229.

(58)   Jovin, T. M. e. a. *Biophysical Journal* **2000**, *78*, 1589.

(59)   McClain, W. M., Harris, R. A. *Excited States*; Vol. 3. pp.1-56.

(60)   McClain, W. M. *Journal of Chemical Physics* **1972**, *57*, 2264.

(61)   McClain, W. M. *Journal of Chemical Physics* **1973**, *58*, 324.

(62)   Blanchard, G. J., Jiang, Y. *Journal of Physical Chemistry* **98**, *98*, 6436.

(63)   Wan, C.; Johnson, C. K. *Journal of Chemical Physics* **1994**, *101*, 10283.

(64)   Callis, P. R. *Journal of Chemical Physics* **1993**, *99*, 27.

(65)   Chen, S. Y.; Van Der Meer, B. W. *Biophysical Journal* **1993**, *64*, 1567.

(66)   Johnson, C. K.; Wan, C. *Topics in Fluorescence Spectroscopy* **1997**, *5*, 43.

(67)   Wan, C.; Johnson, C. K. *Chemical Physics* **1994**, *179*, 513.

(68)   Fery-Forgues, S.; Fayet, J.-P.; Lopez, A. *Journal of Photochemistry and Photobiology, A: Chemistry* **1993**, *70*, 229.

CHAPTER 2

EVALUATING THE ROLE OF CHROMOPHORE SIDE GROUP IDENTITY IN MEDIATING SOLUTION PHASE ROTATIONAL MOTION

Introduction

The motion of a molecule in solution is controlled by a number of factors, ranging from its size, shape and polarity to the nature of its interactions with its immediate environment. It is these interactions that play a critical role in mediating processes such as chemical reaction kinetics, for example. As a result of a broad effort over the past decade or more, a series of chromophores has been identified that are capable of providing information on their local environment with both their time- and frequency-domain responses. Molecules such as pyrene are known to exhibit solvent-polarity dependent fluorescence spectral profiles, and the fluorescence lifetime of this molecule depends sensitively on the amount of oxygen present.[1] Other chromophores have been developed that are tethered to specific structures, allowing them to locate in comparatively well-defined regions of heterogeneous systems. The so-called lock-and-key approach to the examination of crystallization phenomena makes use of chromophores that have as pendant side groups the crystallizing entity.[2-4] This approach to the optical interrogation of molecular-scale phenomena has proven to be useful to a broad range of biological and chemical investigations.

One chromophore that has been used widely for the study of biological and biomimetic systems is 7-nitrobenz-2-oxa-1,3-diazole, NBD.[5-12] The reason for the

popularity of this chromophore is that its fluorescence spectral profile and lifetime both depend sensitively on the polarity of its immediate environment. In addition, the chromophore NBD is amenable to synthetic substitution or modification of its amine side group, rendering it useful for localization within heterogeneous systems. A variety of sterols, lipids and other compounds are available with a pendant NBD chromophore. A recurring question in these studies is the role that the chromophore side group plays in mediating its dynamics. In an effort to address this issue, we have undertaken a study of the reorientation and fluorescence lifetime of NBD possessing several different side groups in a series of polar protic and aprotic solvents. Our data indicate that the reorientation dynamics of the NBD chromophore depend on the identity of the chromophore side group to a limited extent and that we can account for the experimental data in the context of a combination of frictional and dielectric interactions between the dipolar chromophore and its immediate environment.

Experimental

Materials. The fluorescent probes (figure 2.1) succinimidyl 6-(N-(7-nitrobenz-2-oxa-1,3-diazol-4-yl)amino) hexanoate (SNBD) and 6-(N-(7nitrobenz-2-oxa-1,3-diazol-4-yl)amino hexanoic acid (NBDHA) were obtained from Molecular Probes Inc. and used without further purification. The probe 4-benzylamino-7-nitrobenzofurazan (BBD) was purchased from Sigma-Aldrich and was also used as received. The solvents methanol, 1-propanol, 1-butanol, 1-pentanol, dimethyl sulfoxide (DMSO), N,N-dimethylformamide (DMF) and acetonitrile (ACN) were purchased from Sigma-Aldrich in their highest purity available and were used as received. Ethanol (95%) was distilled in-house. For time-resolved fluorescence measurements, the chromophore concentrations were 10^{-4} M or less in all cases.

Steady State Measurements. All absorption spectra were recorded on a Cary model 300 double beam UV-Visible absorption spectrometer, with 1 nm spectral resolution. All emission spectra were recorded on a Spex Fluorolog 3 spectrometer at a spectral resolution of 3 nm for both excitation and emission monochromators.

Time Correlated Single Photon Counting Measurements. All fluorescence lifetime and anisotropy data were collected using a time correlated single photon counting (TCSPC) system that has been described in detail elsewhere.[13] We provide a brief recap of its salient properties here. The source laser is a CW mode-locked Nd:YAG laser (Coherent Antares 76-S) that produces 100 ps 1064 nm pulses at 76 MHz repetition rate. The second or third harmonic of the output of this laser is used to excite a cavity dumped dye laser (Coherent 702-2), operating with Rhodamine 610 dye (Exciton, 532

nm pump) for two photon excitation experiments, or with Stilbene 420 dye (Exciton, 355 nm pump) for one photon excitation experiments. The dye laser outputs were 5 ps pulses at a repetition rate of 4 MHz for both output wavelengths (460 nm and 650 nm). Fluorescence transients centered between 535 and 545 nm were detected using a Hamamatsu R3809U microchannel plate photomultiplier tube detector with a Tennelec 454 quad constant fraction discriminator and Tennelec 864 time-to-amplitude converter and biased amplifier used for signal processing. Data were collected using a virtual instrument (VI) written with LabVIEW® 7.1 software. For this system the instrument response time is typically 35 ps fwhm. Fluorescence transients were collected at polarizations of 0°, 54.7° and 90° with respect to a vertically polarized excitation pulse.
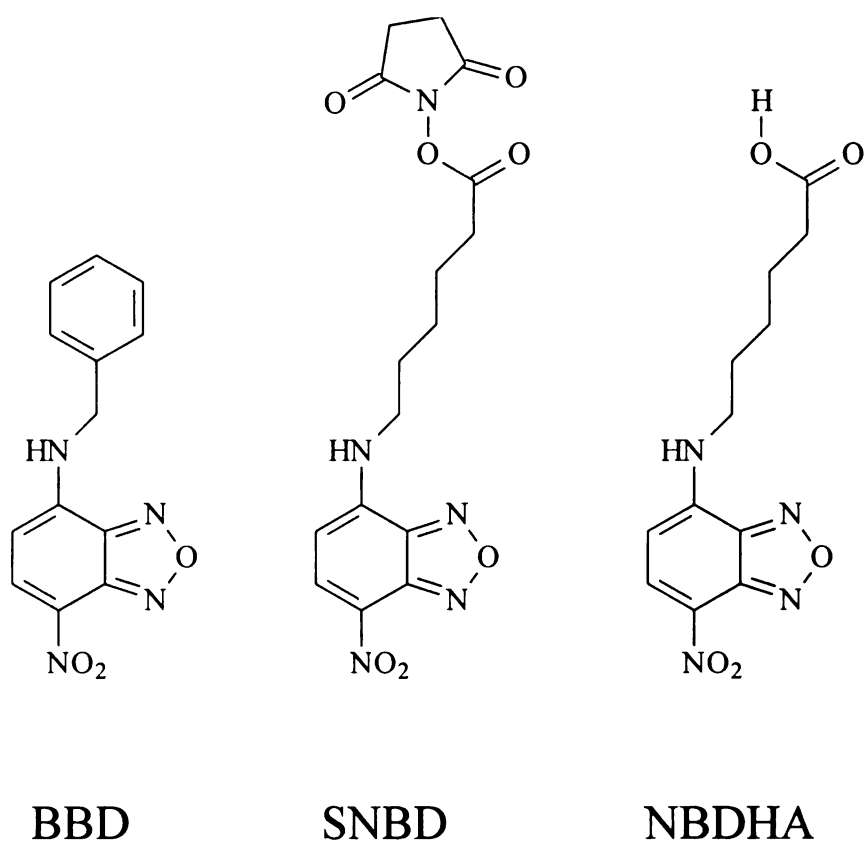
Figure 2.1 Structures of the substituted NBD chromophores used in this work.

Results and Discussion

There are several aspects of our experimental data on the chromophores SNBD, BBD and NBDHA that require discussion. The NBD chromophore is known to exhibit a steady state spectral response that depends on the polarity of its local environment. We show in Figs. 2-4 the absorption and emission spectra of the three chromophores in the solvents used here. We find that the steady state spectra of the chromophores changes very little with the identity of the alcohol solvent (Figs 2a – 4a), but that there is a marked variation in absorption and emission maxima in the polar aprotic solvents ACN, DMF and DMSO (Figs. 2b – 4b). For a given chromophore, the spectra in ACN are most similar to those in the alcohols, and greater red-shifting of both absorption and emission bands is seen for DMF and DMSO. Attempting to understand these spectral shifts in the context of solvent properties or polarity indices does not yield any insight into the chemical basis for these spectral shifts. Likewise, it appears that the Stokes shifts for these molecules do not change significantly or in a manner correlated to any solvent property or polarity index that we have tested. These spectra provide us with the information needed to perform the time-resolved experiments, but give limited insight into the chemical and/or physical basis for the observed band positions and Stokes shifts. For this reason, we have examined the emission bands of these chromophores in the time domain.

We consider next the relationship between the chromophore fluorescence lifetime and the polarity of the medium in which the chromophore resides. We note that the fluorescence lifetimes of BBD, SNBD and NBDHA are quite similar, and this is not surprising. The NBD chromophore is known to exhibit a solvent polarity-dependent

24

fluorescence lifetime,[5-7,9-11] but the issue of what comprises "solvent polarity" is not well understood. We have examined whether or not there is a correlation between the fluorescence lifetime of the NBD chromophore and a variety of solvent properties such as dielectric constant, refractive index, Debye dielectric relaxation time and solvent viscosity. We have found no correlation between fluorescence lifetime and any of these solvent properties, which is not surprising. The nanosecond time scale over which the chromophore population decays following excitation differs from the characteristic time scales which the above parameters sense, in many cases by several orders of magnitude. The interactions between solvent and solute must derive from dipole-dipole and dipole-induced dipole coupling, but the typical measures of solvent-solvent coupling listed above do not access the region(s) of the frequency-dependent dielectric response of the medium that dominate solvent-solute interactions.[14,15]

The literature is replete with attempts to create solvent polarity scales, with the most notable being the py scale,[16,17] the π^* scale[18-21] and the $E_T(30)$ scale.[22,23] The py scale is based on the emission spectrum of pyrene, which is sensitive to solvent mediation of the vibronic coupling between its S_1 and S_2 electronic states.[1] For the π^* and $E_T(30)$ scales, the solvent "polarity" is gauged by the spectral shifts of a polar dye molecule, with the mechanism(s) of these spectral shifts not being well understood at the molecular level. Perhaps because of this lack of fundamental understanding, these latter two solvent polarity scales have been related to various solvent properties through phenomenological linear free energy relationships, with each factor weighted according to the creator(s) of
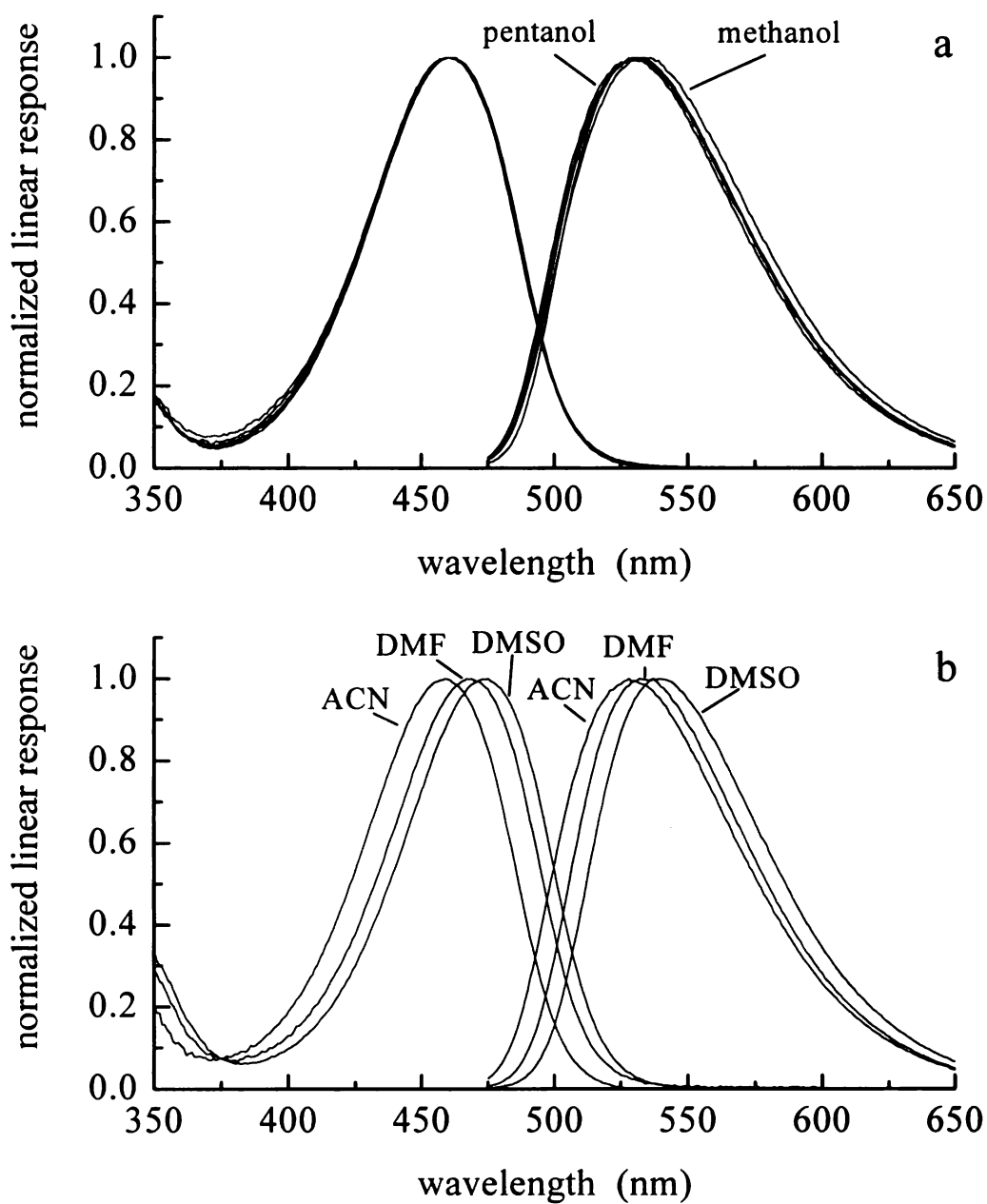
Figure 2.2 (a) Normalized absorption and emission spectra of BBD in the n-alcohols methanol through 1-pentanol. (b) Normalized absorption and emission spectra of BBD in the polar aprotic solvents acetonitrile (ACN), N,N-dimethyl formamide (DMF) and dimethyl sulfoxide (DMSO).
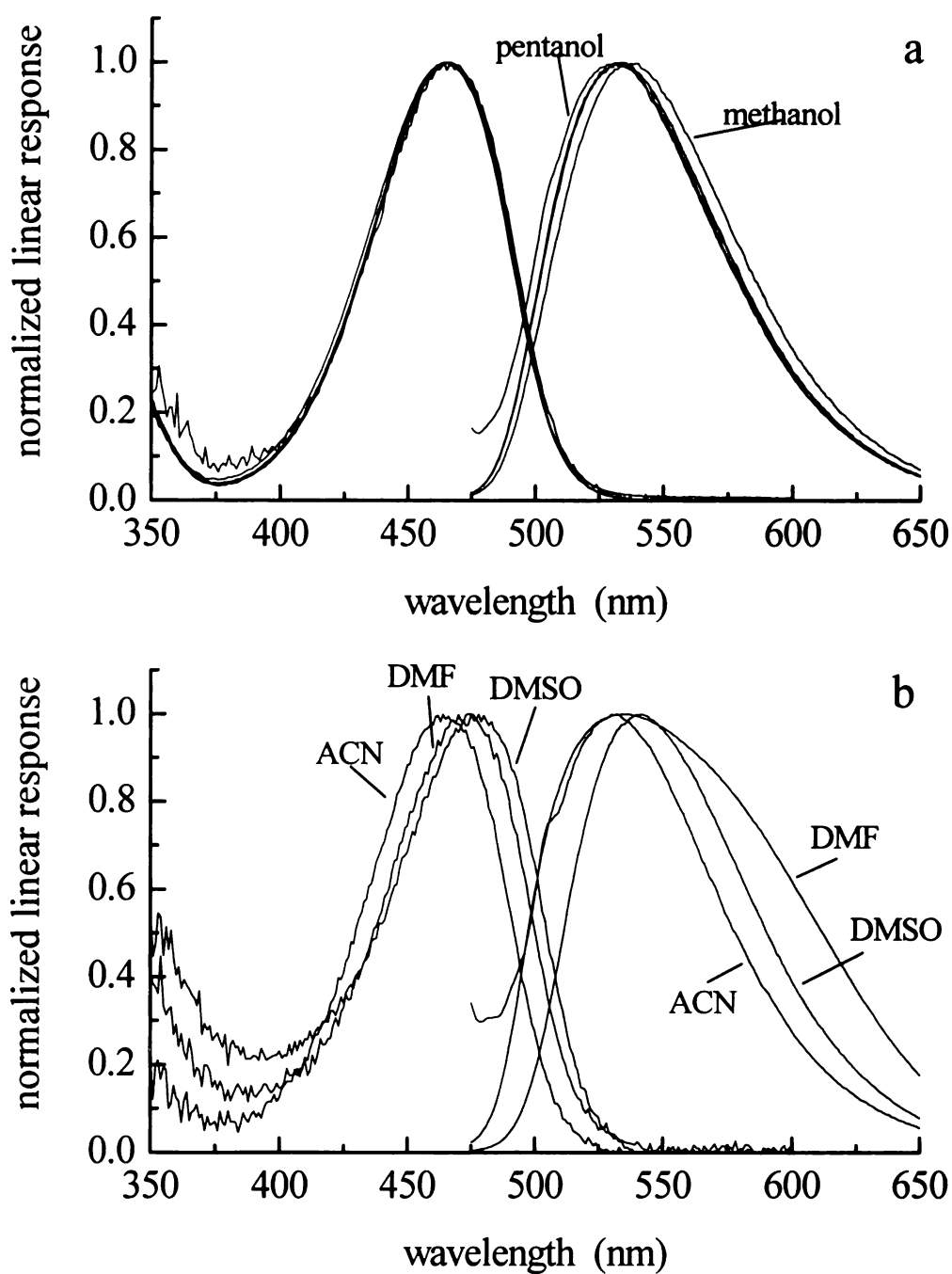
Figure 2.3. (a) Normalized absorption and emission spectra of SNBD in the n-alcohols methanol through 1-pentanol. (b) Normalized absorption and emission spectra of SNBD in the polar aprotic solvents acetonitrile (ACN), N,N-dimethyl formamide (DMF) and dimethyl sulfoxide (DMSO).

27
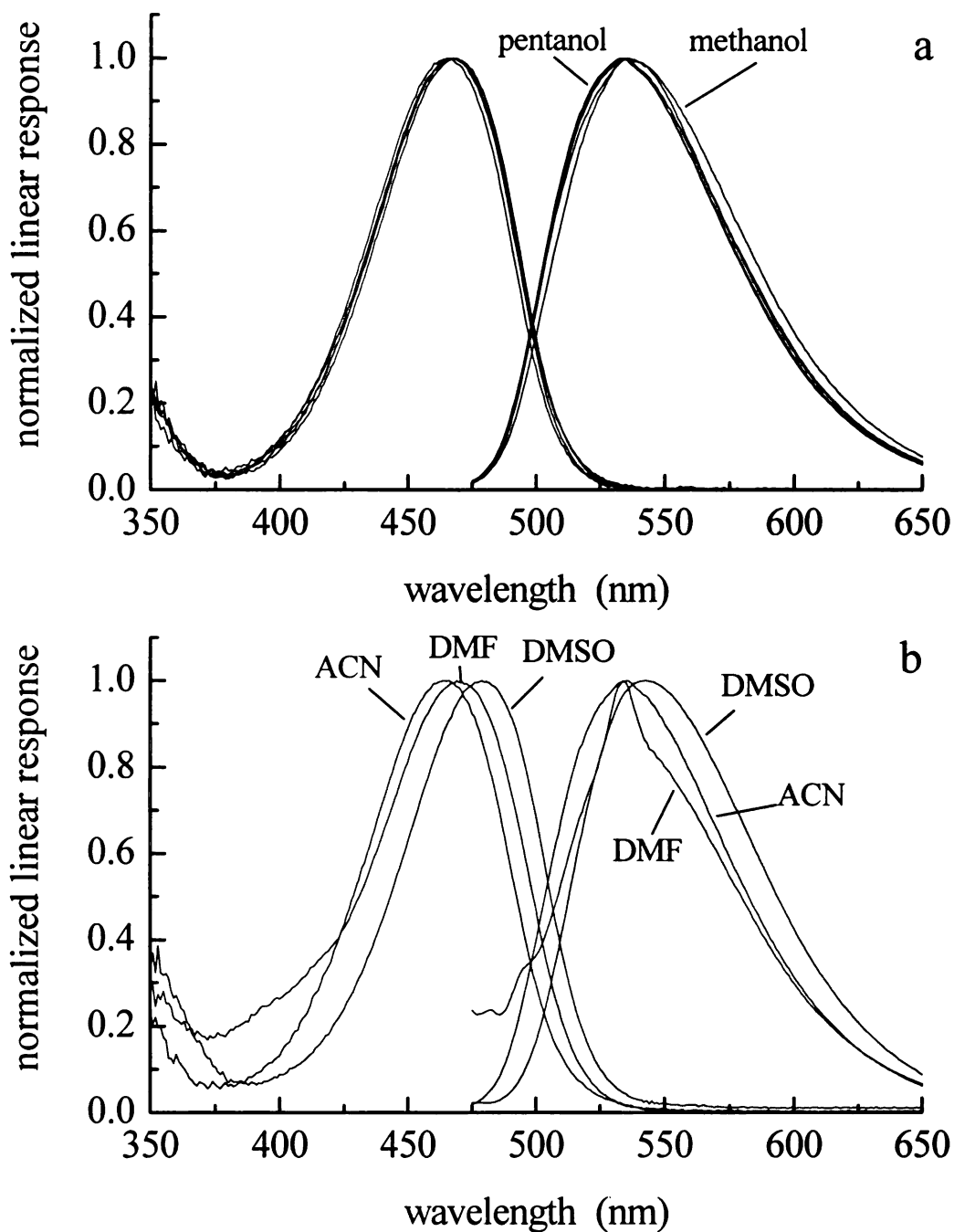
Figure 2.4 (a) Normalized absorption and emission spectra of NBDHA in the n-alcohols methanol through 1-pentanol. (b) Normalized absorption and emission spectra of NBDHA in the polar aprotic solvents acetonitrile (ACN), N,N-dimethyl formamide (DMF) and dimethyl sulfoxide (DMSO).

the polarity scale. It is useful to note that despite the success of these polarity scales, the system properties that are empirically factored into them are, for the most part, related to the polarizability of the solvent in some manner. These polarity scales can, in fact prove useful, as is the case here. We find that the fluorescence lifetime of the NBD chromophore correlates reasonably well with the $E_T(30)$ polarity scale (Fig. 2.5, Table 2.1). This information is useful for predictive or comparative purposes of estimating the polarity of the chromophore local environment. Because NBD derivatives find wide use in the interrogation of biological systems such as lipid bilayer structures, the correlation we report in Fig. 2.5 is of potential utility in understanding the average chemical environments of complex biological systems. Unfortunately, the analogous correlation does not exist in the frequency domain, between the steady state spectral maxima and the $E_T(30)$ scale. This is not surprising given the extent to which inhomogeneous broadening contributes to the spectral features of this complex organic chromophore.

We note that as the solvent polarity increases, the lifetime of the chromophore(s) decreases. This is expected because of the polar nature of the chromophore. Despite the poorly defined term of solvent polarity, we expect qualitatively that as the strength of (polar) interactions increases between solvent and solute, the more opportunity there is for structural and/or electronic wavefunction distortion of the solute. Such interactions between solvent and solute serve to increase the opportunity for nonradiative decay from the solute excited state.

We consider next the rotational diffusion properties of these chromophores. Because the theoretical foundation of reorientation measurements is well established, there is a wealth of information available from this type of measurement. We use both

29
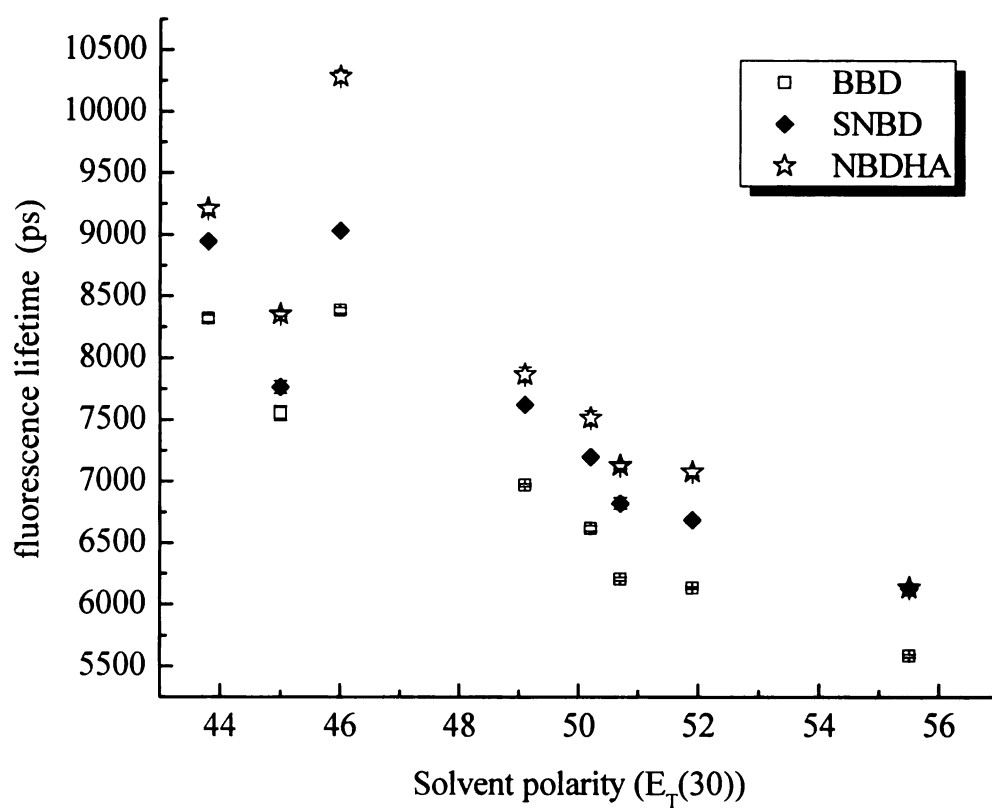
Figure 2.5 Dependence of chromophore fluorescence lifetime on solvent polarity. The solvent polarity is given in the form of the $E_T(30)$ scale, and the fluorescence lifetimes are in ps. □ = BBD, ◆ = SNBD and ☆ = NBDHA.

Table 2.1 Fluorescence lifetimes of the chromophores BBD, SNBD and NBDHA in the solvents used in this work. Solvent polarities according to the $E_T(30)$ scale were taken from Ref. [22]. Uncertainties reported here are ±1σ for at least six individual determinations. Lifetimes were the same for both one and two photon excitation to within the uncertainty of the measurement.

Solvent	$E_T(30)$ polarity	BBD τ_{fl} (ps)	SNBD τ_{fl} (ps)	NBDHA τ_{fl} (ps)
ACN	46.0	8385±22	9031±5	10283±51
MeOH	55.5	5585±13	6129±14	6136±21
DMF	43.8	8319±27	8944±16	9208±35
EtOH	51.9	6136±10	6685±24	7078±32
PrOH	50.7	6208±16	6822±46	7129±22
DMSO	45.0	7553±60	7764±52	8354±19
BuOH	50.2	6620±20	7199±17	7515±59
PeOH	49.1	6972±12	7622±23	7866±60

one photon and two photon excitation because they provide complementary information. For both modes of excitation, we monitor emission from the same excited state. We recap the information available from the two excitation methods and what we can extract from the experimental data for BBD, SNBD and NBDHA.

One-Photon Excited Fluorescence Anisotropy. In one-photon excited anisotropy measurements, the sample is excited by a vertically polarized light pulse, and the resulting emission is collected parallel and perpendicular to the incident beam. The induced orientational anisotropy is given by

$$R\ (t) = \frac{I_{\parallel}(t) - I_{\perp}(t)}{I_{\parallel}(t) + 2I_{\perp}(t)} \tag{2.1}$$

Where $I_{\parallel}(t)$ is the intensity of emission collected at a polarization angle of 0° with respect to the incident vertical polarization, and $I_{\perp}(t)$ is the intensity of emission collected at a polarization angle of 90° with respect to the incident polarization. Chemically useful information is contained in the decay time constant(s) of R(t), Eq. 1. R(t) can contain up to five exponential decays in theory, but only one or two decays are observed experimentally. The values of R(0) can range from -0.2 to 0.4 for one-photon excited anisotropy measurements, depending on the angle between the excited and emitting transition dipole moments.

The relationship between the anisotropy decay obtained experimentally and the molecular properties of the rotating molecule have been described by Chuang and Eisenthal.[24] These molecular properties include the rotational diffusion constants and the angle between the excited and emitting transition dipole moments. The typical

assignment of Cartesian axes to the chromophore are to have the z-axis perpendicular to the molecular π system plane, and the transition dipole lying either along the x (long) axis or the y (short) axis of the molecular plane. We follow this convention for the NBD chromophores considered here. Two limiting cases can be examined to evaluate the functionality of the anisotropy decay. By estimating the shape of the volume swept out by the rotating molecule as oblate ($D_z \neq D_x = D_y$), or prolate ($D_x \neq D_y = D_z$) rotors, we can simplify Chuang and Eisenthal's equations significantly. Even with these simplifications, there remains ambiguity in determining whether the prolate or oblate rotor shape best represents the molecule in question because of the orientation of the transition dipoles relative to the rotor axes. For parallel absorbing and emitting transition dipole moments, oriented along the long (x) axis of the ellipsoid of rotation, the functional forms of R(t) are[24]

$$\text{oblate} \quad R(t) = 0.1 \exp(-(2D_x + 4D_z)t) + 0.3\exp(-6D_x t) \quad (2.2)$$

$$\text{prolate} \quad R(t) = 0.4\exp(-6D_z t) \quad (2.3)$$

Similarly, for parallel absorbing and emitting transitions that are short (y) axis polarized,

$$\text{oblate} \quad R(t) = 0.4\exp(-(4D_x + 2D_z)t) \quad (2.4)$$

$$\text{prolate} \quad R(t) = 0.1\exp(-(4D_x + 2D_z)t) + 0.3\exp(-6D_z t) \quad (2.5)$$

For the NBD derivatives we have examined, all anisotropy decays are single exponential, (an example is provided in Fig. 2.6) a condition consistent with either a prolate rotor with a long-axis polarized transition, or an oblate rotor with a short axis polarized transition.

Because of this ambiguity, we have also used two photon excitation to provide complementary information and thus resolve the Cartesian components of the rotational diffusion constant.

Two-Photon Excited Fluorescence Anisotropy. Two photon excitation involves the photoselection of an anisotropic orientational distribution via the two-photon tensor, S, in contrast to the transition dipole moment, μ, accessed by one-photon excitation. Which two photon tensor elements are accessed depends on the polarization of the incident light. Induced orientational anisotropy decay functions are generated for both linearly ($r_1(t)$) and circularly ($r_2(t)$) polarized excitation and are given by:

$$r_1(t) = \frac{I_\parallel^{linear}(t) - I_\perp^{linear}(t)}{I_\parallel^{linear}(t) + 2I_\perp^{linear}(t)}$$

$$r_2(t) = \frac{I_\parallel^{circular}(t) - I_\perp^{circular}(t)}{2I_\parallel^{circular}(t) + I_\perp^{circular}(t)}$$

(2.6)

For both excitation polarizations, the anisotropy decays are characterized by two time constants, τ_0 and τ_2, weighted according to the spectroscopic and dynamical properties of the chromophore.[25-27]

$$r_1(t) = r_1(0)\left[c_0 \exp(-t/\tau_0) + c_2 \exp(-t/\tau_2)\right]$$

$$r_2(t) = r_2(0)\left[d_0 \exp(-t/\tau_0) + d_2 \exp(-t/\tau_2)\right]$$

(2.7)

The anisotropy decay for either two photon excitation polarization should contain two exponentials, but this is not seen in all cases. Our data are characterized by a single exponential decay time constant, and there are two possible explanations for this finding.

34
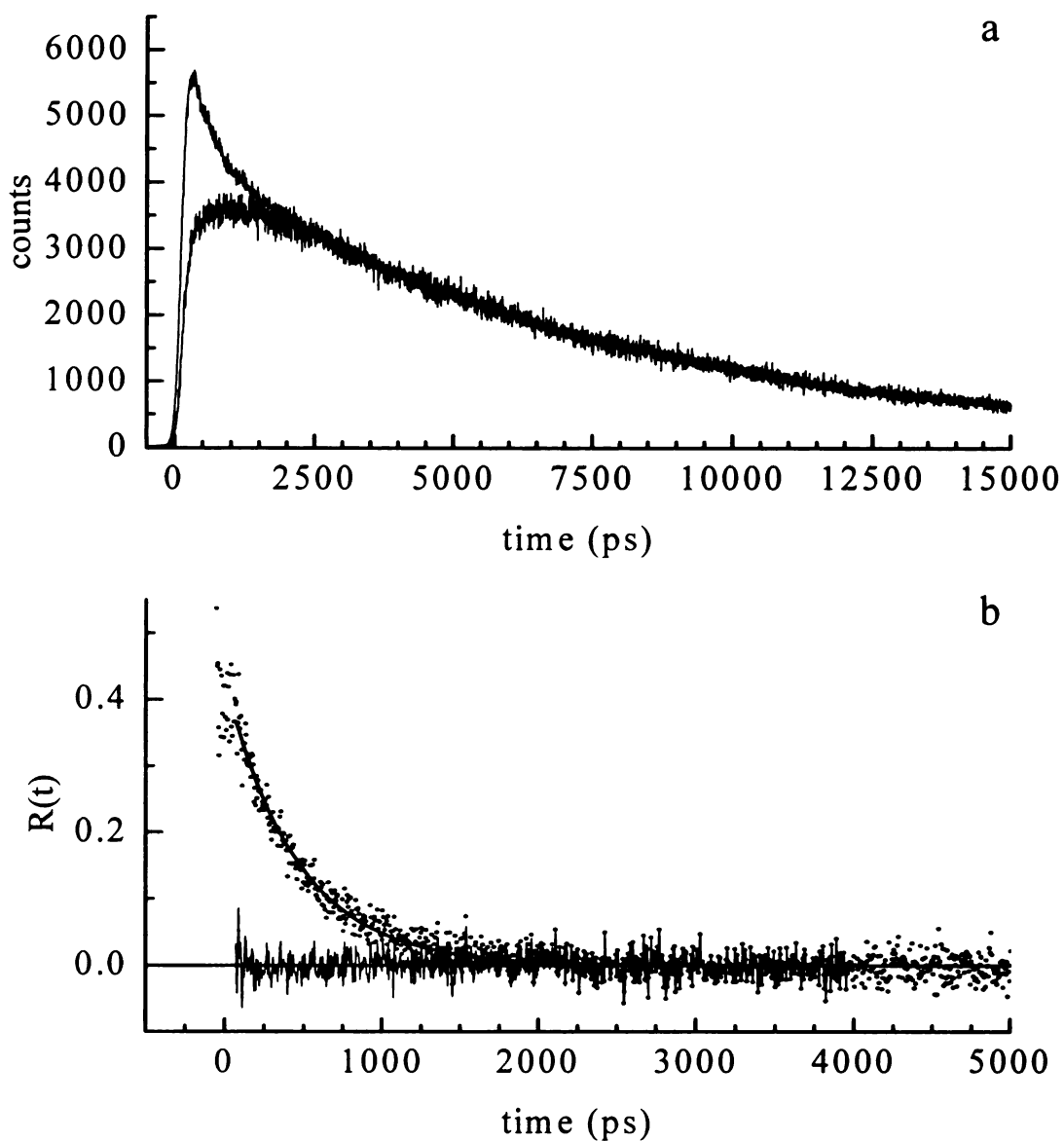
Figure 2.6 (a) Representative $I_{\parallel}(t)$ and $I_{\perp}(t)$ data for SNBD in 1-pentanol with one photon excitation. (b) Corresponding R(t) function generated from the data according to Eq. 1. The line through the data is the best fit single exponential decay function, with the residuals of the fit being distributed around zero intensity.

The first is that the two time constants τ_0 and τ_2 are similar enough that they cannot be resolved outside of the experimental uncertainty. The other possibility is that some of the prefactors in Eqs. 2.7 are too small to observe. The prefactors c_i and d_i have been described in detail elsewhere,[8,25-27] and we present them for the illustrative purposes.

$$c_0 = \frac{(\sqrt{3}a + b)\left[3(\sqrt{3}a + b)S_{xx}^2 + 3(-\sqrt{3}a + b)S_{yy}^2 + 2bS_{xx}S_{yy} + 4bS_{xy}^2\right]}{7N^2(3S_{xx}^2 + 3S_{yy}^2 + 2S_{xx}S_{yy} + 4S_{xy}^2)}$$ (2.8)

$$c_2 = \frac{(a - \sqrt{3}b)\left[3(a - \sqrt{3}b)S_{xx}^2 + 3(a + \sqrt{3}b)S_{yy}^2 + 2aS_{xx}S_{yy} + 4aS_{xy}^2\right]}{7N^2(3S_{xx}^2 + 3S_{yy}^2 + 2S_{xx}S_{yy} + 4S_{xy}^2)}$$ (2.9)

$$d_0 = \frac{(\sqrt{3}a + b)\left[(\sqrt{3}a + b)S_{xx}^2 + (-\sqrt{3}a + b)S_{yy}^2 - 4bS_{xx}S_{yy} + 6bS_{xy}^2\right]}{14N^2(S_{xx}^2 + S_{yy}^2 - S_{xx}S_{yy} + 3S_{xy}^2)}$$ (2.10)

$$d_2 = \frac{(a - \sqrt{3}b)\left[(a - \sqrt{3}b)S_{xx}^2 + (a + \sqrt{3}b)S_{yy}^2 - 4aS_{xx}S_{yy} + 6aS_{xy}^2\right]}{14N^2(S_{xx}^2 + S_{yy}^2 - S_{xx}S_{yy} + 3S_{xy}^2)}$$ (2.11)

$$a = \sqrt{3}(D_y - D_x)$$
$$b = 2D_z - D_y - D_x + 2\Delta$$
$$N^2 = a^2 + b^2$$
$$\Delta = (D_x^2 + D_y^2 + D_z^2 - D_xD_y - D_yD_z - D_xD_z)^{1/2}$$ (2.12)

In order to determine more information about the rotational diffusion coefficients, we return to the limiting cases of prolate ($D_x \neq D_y = D_z$) and oblate ($D_z \neq D_x = D_y$) rotors. Using these ellipsoidal shapes to simplify Eqs. 2.12 we obtain the prefactors in Eqs.2.8-2.11 for the terms c and d as follows:

Prolate: $\sqrt{3}a + b = 2\sqrt{3}(D_z - D_x)$ $a - \sqrt{3}b = 0$

Oblate: $\sqrt{3}a + b = 4(D_z - D_x)$ $a - \sqrt{3}b = 4\sqrt{3}(D_x - D_z)$

Given the fact that we obtain a single exponential anisotropy decay for both one photon (Fig. 2.6) and two photon (Figs. 2.7, 2.8) excitation in these experiments, the experimental data are most consistent with the NBD chromophores reorienting as prolate rotors in the systems we have examined. For a prolate rotor, the time constant τ_0 for two photon excitation is

$$\tau_0 = \frac{S_{xx}^2(7D_x + 17D_z) - 4S_{yy}^2(2D_x - D_z) + (S_{xx}S_{yy} + 2S_{xy}^2)\left(\dfrac{3(D_z^2 + 2D_zD_x)}{2D_x + D_z} + 4D_x - D_z\right)}{8(D_z^2 + 2D_xD_z)(6S_{xx}^2 - 3S_{yy}^2 + S_{xx}S_{yy} + 2S_{xy}^2)} \qquad (2.13)$$

By setting $S_{yy} = 1$ and extracting normalized values of S_{xx} and S_{xy} from $r_1(0)$ and $r_2(0)$, then using the value of D_z obtained from the one photon measurements (Eq. 2.3), we can extract D_x from the two photon excitation data. We present in Tables 2.2-2.4 the experimental reorientation times and the resulting values of D_z and D_x that we extract from our anisotropy data as a function of chromophore and solvent. As expected, the reorientation times for one photon excitation and two photon excitation of each chromophore differ, in some cases quite noticeably. This is an expected result, as is clear from comparing Eq. 2.3 with Eq. 2.13, for example. These data show that while there are subtle differences between the substituted chromophores, they all produce qualitatively the same result of $D_z/D_x \sim 2$. This finding is significant in that it implies that the side groups exert a limited influence on the motional properties of

37
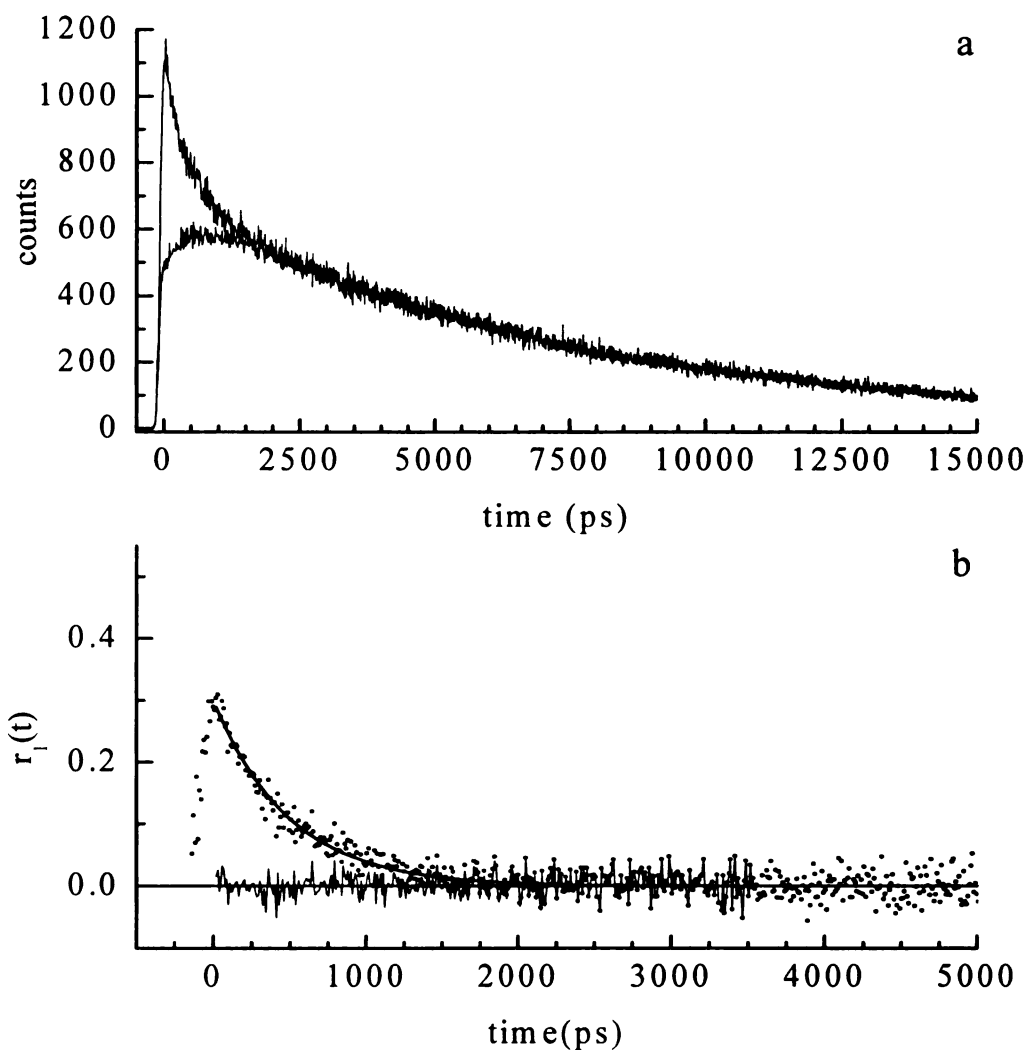
Figure 2.7 (a) Representative $I_{\parallel}(t)$ and $I_{\perp}(t)$ data for SNBD in 1-pentanol with linearly polarized two photon excitation. (b) Corresponding R(t) function generated from the data according to Eq. 2.6. The line through the data is the best fit single exponential decay function, with the residuals of the fit being distributed around zero intensity.
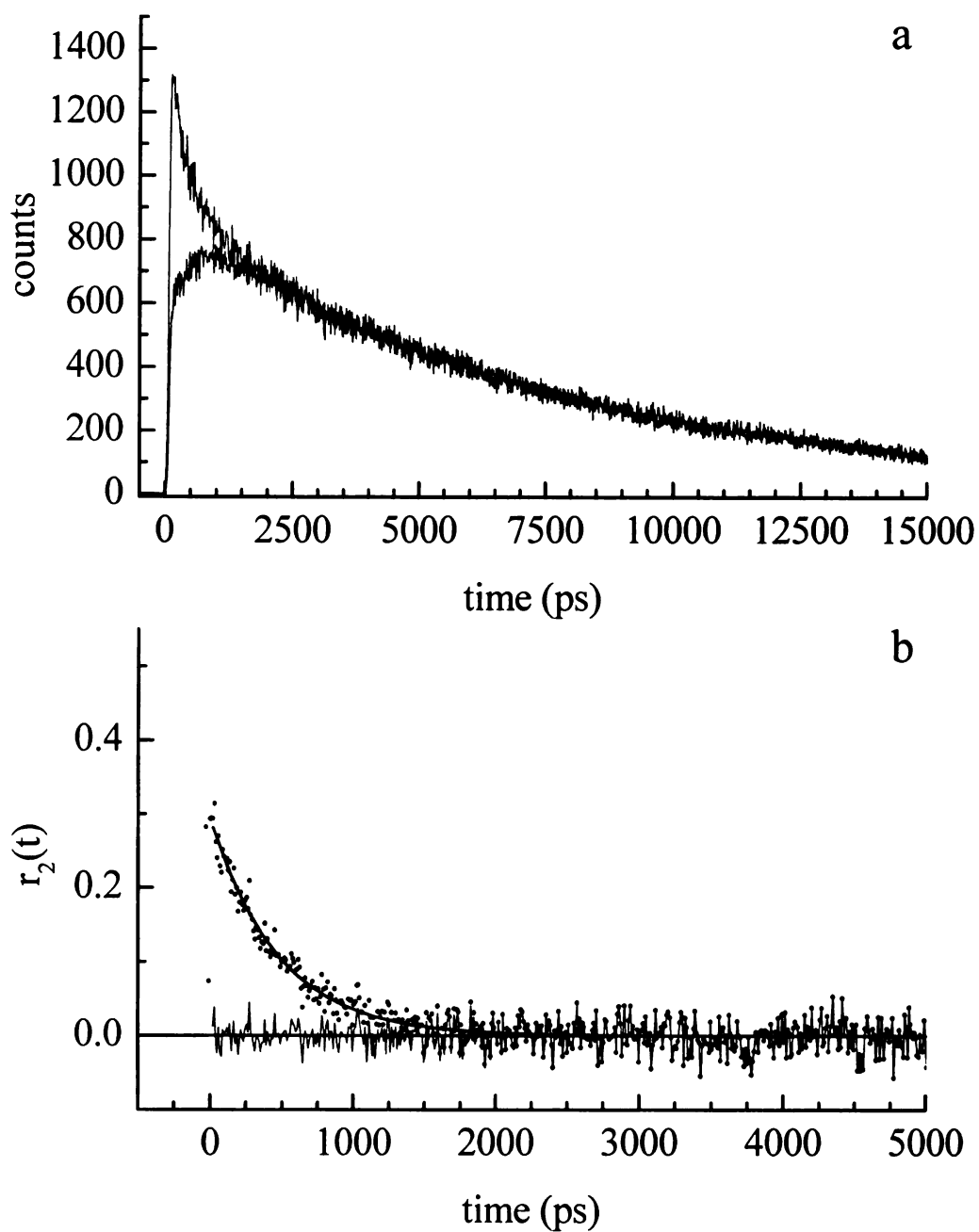
Figure 2.8. (a) Representative $I_{\parallel}(t)$ and $I_{\perp}(t)$ data for SNBD in 1-pentanol with circularly polarized two photon excitation. (b) Corresponding R(t) function generated from the data according to Eq. 2.6. The line through the data is the best fit single exponential decay function, with the residuals of the fit being distributed around zero intensity.

these molecules, which is likely the result of averaging motions over a large number of side group conformations for all three chromophores.

We note that the assignment of a prolate effective rotor shape for these chromophores is based on the observation of single exponential decays for both the one and two photon excitation data. It is, of course, possible that there could be two exponential decays present in our data that remain unresolved either due to the similarity of the time constants or to the limited S/N ratio of the experimental data. In the limit that the time constants are too similar to resolve, the physical picture that emerges from a prolate rotor would change little, and the conclusions drawn from interpreting the data as single exponentials would not change. If the latter were the case, we would expect to see at least hints of deviation from single exponential behavior in the residuals of the fits to the data. In no cases do we observe any such indication. While the interpretation of our data are ultimately limited by the S/N ratio of the data, as is the case for many experimental studies, the consistency and reproducibility of our findings lend confidence to our interpretation of single exponential anisotropy decays.

We consider next how to relate our findings to solvent-solute interactions. The relationship between molecular rotational motion and the properties of the surrounding solvent medium has been described by the modified Debye-Stokes-Einstein model,[28]

$$\tau_{DSE} = \frac{\eta V f}{k_B T S} \tag{2.14}$$

Table 2.2 Experimental reorientation times for BBD using one photon excitation (1) and two photon excitation with linear polarization (2L) and circular polarization (2C). Values of D_x and D_z are extracted from the experimental data according to Eqs. 2.3 and 2.13. Uncertainties reported here are $\pm 1\sigma$ for at least six individual determinations.

Solvent	Viscosity η, (cP)	$\tau_{OR}(1)$ (ps)	$\tau_{OR}(2L)$ (ps)	$\tau_{OR}(2C)$ (ps)	D_z (MHz)	D_x (MHz)	D_z/D_x
ACN	0.37	88±9	72±15	92±9	1894	959	2.0
MeOH	0.54	96±13	79±11	79±6	1736	900	1.9
DMF	0.79	102±3	103±6	123±14	1634	846	1.9
EtOH	1.07	139±10	148±15	140±6	1199	595	2.0
PrOH	1.95	199±10	205±7	199±11	838	419	2.0
DMSO	1.99	170±27	151±4	196±23	980	428	2.3
BuOH	2.54	267±25	249±19	252±7	624	304	2.1
PeOH	3.61	333±19	365±32	346±24	501	247	2.0

Table 2.3. Experimental reorientation times for SNBD using one photon excitation (1) and two photon excitation with linear polarization (2L) and circular polarization (2C). Values of D_x and D_z are extracted from the experimental data according to Eqs. 2.3 and 2.13. Uncertainties reported here are $\pm 1\sigma$ for at least six individual determinations.

Solvent	Viscosity η, (cP)	$\tau_{OR}(1)$ (ps)	$\tau_{OR}(2L)$ (ps)	$\tau_{OR}(2C)$ (ps)	D_z (MHz)	D_x (MHz)	D_z/D_x
ACN	0.37	125±3	81±22	76±2	1333	826	1.6
MeOH	0.54	182±15	113±6	112±2	916	497	1.8
DMF	0.79	177±5	140±7	136±11	942	535	1.8
EtOH	1.07	238±25	179±2	195±118	700	396	1.8
PrOH	1.95	351±31	292±14	328±7	474	269	1.8
DMSO	1.99	285±15	239±18	288±18	585	322	1.8
BuOH	2.54	398±18	324±19	396±5	419	246	1.7
PeOH	3.61	477±19	465±14	499±19	349	187	1.9

Table 2.4. Experimental reorientation times for NBDHA using one photon excitation (1) and two photon excitation with linear polarization (2L) and circular polarization (2C). Values of D_x and D_z are extracted from the experimental data according to Eqs. 2.3 and 2.13. Uncertainties reported here are $\pm 1\sigma$ for at least six individual determinations.

Solvent	Viscosity η, (cP)	$\tau_{OR}(1)$ (ps)	$\tau_{OR}(2L)$ (ps)	$\tau_{OR}(2C)$ (ps)	D_z (MHz)	D_x (MHz)	D_z/D_x
ACN	0.37	50±3	52±3	49±3	3370	1887	1.8
MeOH	0.54	131±24	112±10	111±10	1270	610	2.1
DMF	0.79	162±11	134±13	109±3	1030	599	1.7
EtOH	1.07	174±6	158±13	180±21	960	566	1.7
PrOH	1.95	302±13	283±12	339±50	550	324	1.7
DMSO	1.99	273±10	204±22	250±16	610	352	1.7
BuOH	2.54	570±26	402±20	426±56	290	165	1.8
PeOH	3.61	724±15	456±4	539±35	230	128	1.8

Where the time constant for rotational motion, τ_{DSE}, is determined from the anisotropy decay data. The term η is the solvent bulk viscosity, V is the hydrodynamic volume[29] of the rotating moiety, f is a frictional interaction term, taken to be 1 for polar systems, and S is the shape factor derived by Perrin[30] to account for non-spherical solutes. The quantity τ_{DSE} is equal to $6D^{-1}$, where $D = \frac{1}{3}(D_x+D_y+D_z)$. We can thus relate the predictions of the DSE model to the experimental data.

We show in Tables 2.2-2.4 the experimentally measured one photon excited reorientation times, and compare these data to the predictions of the DSE model with S = 0.667, calculated for a prolate rotor with an aspect ratio of two[31,32] (Table 2.5). In all cases, the experimental reorientation times are longer than those predicted by Eq. 2.14 (Fig. 2.9), dashed line vs. experimental data). Such a relationship between experiment and model has been seen for a number of molecules,[33-35] and the origin(s) of such a discrepancy have been ascribed to a number of factors. Certainly, some portion of this difference arises from the DSE model itself. Eq. 2.14 was derived for an ellipsoidal solute reorienting in a continuum solvent, thereby accounting only for frictional interactions. To compound matters, the estimation of V and S can give rise to significant uncertainty because of the intrinsic dynamics and variability in the range of structural conformations that these chromophores can take on over time. Also, depending on the solvent system used, strong and persistent solvent-solute interactions can give rise to a rotating entity that is larger, on average, than the bare chromophore.[4,34,35] Such a solvent-attachment approach to understanding experimental reorientation data has been useful for solvents capable of hydrogen bonding.[36] For solvents that are not capable of

Table 2.5. Calculated dielectric friction time constants, DSE reorientation time constants and their sum, reported at τ_{OR}. Solvent properties viscosity, dielectric constant and Debye dielectric relaxation time constant are from references [34,37,38]. For the calculation of τ_{DSE} (S=0.667) (Eq. 2.14), V = 215 Å^3 for BBD; V = 297 Å^3 for SNBD; V = 245 Å^3 for NBDHA.[29] For the calculation of τ_{df}, a = 3.7 Å and μ^* = 10.6 D for BBD; a = 4.1 Å and μ^* = 12.2 D for SNBD; a = 3.9 Å and μ^* = 9.9 D for NBDHA.

Solvent	Viscosity	Dielectric	τ_D	BBD			SNBD			NBDHA		
				τ_{df}	τ_{DSE}	τ_{OR}	τ_{df}	τ_{DSE}	τ_{OR}	τ_{df}	τ_{DSE}	τ_{OR}
	η, (cP)	Const., ε_0	(ps)	(ps)	(ps)	(ps)	(ps)	(ps)	(ps)	(ps)	(ps)	(ps)
ACN	0.37	38.0	4	0.2	30	30	0.2	40	40	0.2	33	33
MeOH	0.54	33.7	56	3.4	42	45	3.4	58	61	2.5	48	51
DMF	0.79	36.7	12	0.8	61	62	0.8	85	86	0.6	70	71
EtOH	1.07	24.5	337	30.6	82	113	29.3	115	144	24	94	118
PrOH	1.95	20.5	430	46.5	151	198	44.4	210	254	36	174	210
DMSO	1.99	46.5	21	0.8	153	154	0.8	214	215	0.6	177	178
BuOH	2.54	17.5	668	75.4	198	273	72.1	271	343	58	225	283
PeOH	3.61	13.9	927	129	280	409	123	388	511	99	321	420
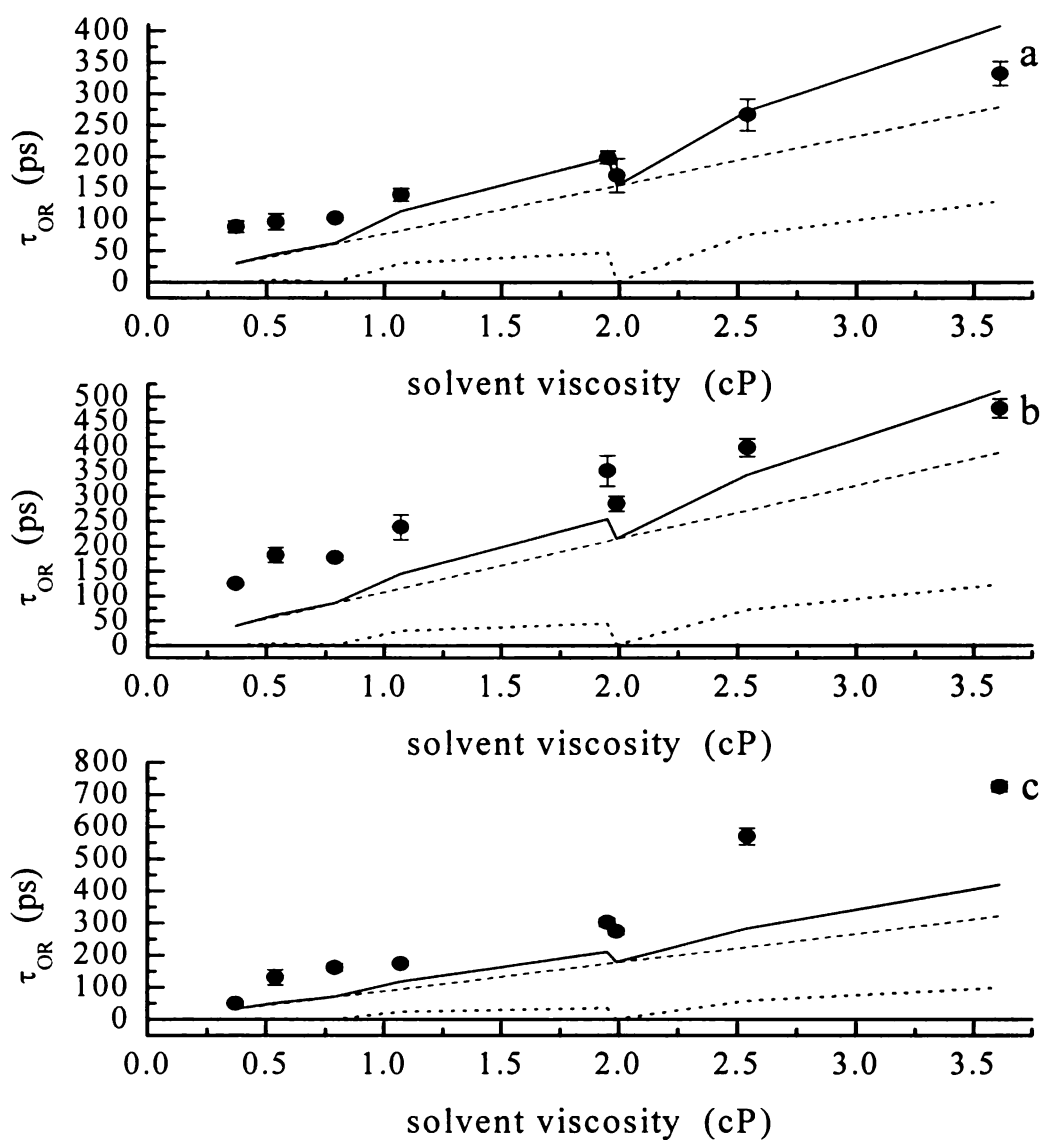
Figure 2.9 (a) One photon experimental reorientation times (●) for BBD as a function of solvent viscosity. The dashed line is calculated from the DSE model (Eq. 2.14), the dotted line is the calculated dielectric friction contribution (Eq. 2.15) and the solid line is the sum of the two model contributions. (b) One photon experimental reorientation times (●) for SNBD as a function of solvent viscosity, with the dashed, dotted and solid lines having the same assignments as for panel (a). (c) One photon experimental reorientation times (●) for NBDHA as a function of solvent viscosity, with the dashed, dotted and solid lines having the same assignments as for panel (a).

forming H-bonds, such an explanation is not appropriate. Another approach to understanding such data has been to postulate that the reorienting molecule, in certain circumstances, can possess added effective volume owing to the conformation of its side groups. As noted above, such an explanation is difficult to support because of the labile nature of the side groups that would have to be responsible for creating any such "volume", and the fact that within the most widely accepted model for the calculation of hydrodynamic volume, there is no means to account for conformational variations within a given molecule.[29] A third explanation for the difference between experiment and theory is that the frictional interactions between the solvent and solute are very strong, giving rise to values of f that exceed unity. Such interactions have been examined theoretically[39] but values of f in excess of unity derived from experimental data are necessarily suspect. Assigning physical or chemical significance to such an explanation would hinge of the identification of strong, persistent solvent-solute interactions such as hydrogen bonding or dipole-dipole interactions.

In addition to the reasons put forth above, there can be other contributions to the interactions between solvent and solute. The dielectric coupling between the solvent medium and the solute can also contribute to the solute reorientation times. Dielectric friction is a mechanism for solvent-solute interactions that has a well established theoretical foundation[40-48] and it has proven useful in explaining a host of reorientation data for sometimes complex systems.[37] In this model, there are two contributions to solvent-solute interactions; viscoelastic frictional forces, which are accounted for through the DSE model (Eq. 2.14), and dielectric interactions, which can be modeled by:

$$\tau_{df} = \frac{\mu^{*2}(\varepsilon - 1)\tau_D}{k_B Ta^3(2\varepsilon + 1)^2} \tag{2.15}$$

Where μ^* is the solute excited state dipole moment, ε is the zero-frequency dielectric constant of the solvent medium, τ_D is the Debye relaxation time of the solvent and a is the radius of the sphere approximating the solute cavity in the solvent. In this model, the contribution of dielectric friction to the overall reorientation time of the chromophore depends on the solute property μ^{*2}/a^3, which effectively represents the torque exerted on the solvent by the solute as it moves, the solvent susceptibility to this force, and the characteristic time constant for solvent motions, τ_D. It is this latter term that plays a dominant role in determining the contribution from dielectric friction. For hydrogen-bonding solvents, τ_D is relatively long, reflecting the extensive H-bonding network formed in alcohols, and in aprotic solvents, τ_D is short, mediated primarily by dipole-dipole or dispersion interactions. This dependence on τ_D provides an important signature that can be compared to experimental data, as we consider below.

A word is in order about the values of μ^* we used in the calculation of τ_{df}. We have calculated the excited state dipole moments for BBD, SNBD and NBDHA at the semi-empirical level, using Hyperchem® v. 6.0 with the PM3 parameterization. While it would be preferable to obtain an experimental estimate of the dipole moments of these molecules, none of them exhibit a sufficient solavatochromaticity nor are there any reliable experimental data available on the ground state dipole moments of these molecules. Thus we are left to estimate the values of μ^*, and experience has indicated

that the PM3 parameterization provides useful results for polar organic chromophores such as NBD.

We show in Table 2.5 and Figs. 2.9 the comparison of our experimental data to model predictions where τ_{OR} (solid line) is the sum of τ_{DSE} (Eq. 2.14, dashed line) and τ_{df} (Eq. 2.15, dotted line). There are a number of interesting features to be noted in the comparison of the experimental data to the model. First, we note that in all cases the experimental reorientation time is longer than that calculated by the model. As discussed above, this systematic difference between model and data can be accounted for either in the context of an underestimation of the frictional terms, a systematic error in the calculation of the hydrodynamic volume, V, or direct solvent-solute interactions. We note that the data for NBDHA, the only solute studied here that has a side group capable of participating strongly in H-bonding interactions, provides the greatest difference between model and experiment. It is likely that strong solvent-solute interactions, in some cases approaching "solvent attachment," are responsible for at least a portion of this difference. We also consider that for BBD and SNBD, the experimental reorientation times do not regress to a prediction of $\tau_{OR} \sim 0$ for zero viscosity. Such behavior has been seen before and it has sometimes been explained in the context of the inertial contributions of molecular motion in the limit of zero viscosity. When inertial contributions are calculated for dyes similar in size to these NBD derivatives, the inertial contributions account for only a few ps at most.[49] Another possible explanation is that for low solvent viscosities there is a different boundary condition for frictional solvent-solute interactions than there is for higher viscosity systems. We work with several solvents of relatively low viscosity (ACN, MeOH, DMF) and if such a change in

boundary condition were to occur with increasing viscosity, it is likely that we would sense it. The origin of the non-zero intercept for the data in Figs. 2.9 will require further investigation to understand in detail.

For all of the chromophores we have examined here, there is a significant feature in the experimental data. The data for 1-propanol (η=1.95 cP) and DMSO (η=1.99 cp) are consistent in that for all chromophores the reorientation time of DMSO is always faster than that of 1-propanol (Figs. 2.9). This finding stands in contrast to the DSE model (Eq. 2.14) but is predicted accurately in the context of dielectric friction contributions to the data (Eq. 2.15). The apparent anomaly results from the short τ_D of DMSO compared to that for 1-propanol, and this feature is modeled well by Eq. 2.15. This feature is not seen as prominently for the other polar aprotic solvents that are characterized by short τ_D values because the τ_D values for the alcohols in the same viscosity range are also short. There is insufficient contrast between methanol and acetonitrile to resolve contributions from dielectric friction, but there is a small observable effect for DMF and a prominent effect seen for comparing DMSO to 1-propanol data (Fig. 2.9). We take the comparison of the functional form of the data and the model to indicate that dielectric friction does, in fact, contribute to our results.

The offset between experiment and model cannot be explained fully in the context of the DSE model. It is also possible that the contribution from dielectric friction has not been estimated correctly owing to the limitations of the model. The systematic difference between model and experiment could result from our use of the calculated solute excited state dipole moments, or from the limitations associated with the assumption of the spherical solute shape, as implied by the a^3 term. In Table 2.5, where the frictional and

dielectric contributions to the overall model reorientation time are indicated, it is clear that dielectric friction plays a more important role in alcohols than it does in aprotic solvents, underscoring the importance of persistent solvent organization as expressed through τ_D. While we have found literature values for τ_D, we recognize that this is a difficult quantity to obtain and that there may be significant uncertainties in the values we use. We note that for both the frictional and dielectric contributions to the model, when there is a systematic difference between model and experiment, the implication is that one of the quantities used in the calculations is consistently under-estimated. It is also possible that there are other contributions to the experimental data that remain unaccounted for, such as changes in the frictional boundary condition between solvent and solute as the ratio of solvent to solute size varies systematically. If there is any indication of such an effect, it appears to be most prominent for BBD (Fig. 2.9a) and SNBD (Fig. 2.9b), where the smallest solvents appear to be modeled least well. Such a finding would appear to stand in conflict with the DSE model, which was derived under the assumption of a continuum solute, a condition approximated most closely by small solvents and large solutes. Regardless of these subtle features in the data, there is overall good agreement between model and experiment, as shown in Fig. 2.9.

We recognize that invoking dielectric friction as a contributor to our experimental data is difficult to verify by other means, especially in light of other systems that have shown varying contributions from this same effect. Several studies have concluded that dielectric friction does not contribute significantly to their data, even with polar solvents and solutes.[50,51] In those cases, coumarin derivatives were used as the solutes and the interpretation of the data may have been complicated by the presence of multiple excited

electronic states in close energetic proximity.[52] In other cases, where systems where comparatively less polar chromophores such as DPP and DMDPP have been used, dielectric friction can contribute to the motional behavior of these molecules.[53] It would appear that the contribution of dielectric friction to experimental reorientation data can be important, but the extent to which dielectric friction contributes is system-dependent. The fact that the functional form of our experimental data match relatively well with the predictions of Eq. 2.15 suggest that NBD derivatives do in fact experience dielectric friction in polar solvents.

Conclusions

We have shown in this work that, despite the different side groups present on the NBD chromophores, the dynamics of the molecules are fundamentally quite similar. In all cases the fluorescence lifetime of the NBD chromophore exhibits the same solvent polarity-dependence, indicating that the side groups are neither coupled strongly to the electronic excited state of the NBD chromophore, nor is there a significant steric interaction between side group and chromophore that interferes with chromophore-solvent interactions.

The rotational diffusion data for both one and two photon excitation of the NBD chromophore reveal remarkably similar motional behavior for the three molecules, analogous to the lifetime data. The use of both one and two photon excitation provides complementary information and allows the evaluation of the ratio of the Cartesian components of the rotational diffusion constant. For the three molecules we have studied, $D_z/D_x \sim 2$. When our experimental reorientation data are compared to the well-established Debye-Stokes-Einstein model, we find that in all cases the experimental reorientation time is substantially longer than predicted. We account for this discrepancy to a substantial extent by considering the role that dielectric friction plays. When dielectric friction is accounted for, the reorientation times predicted by model are much more similar to the experimental data, including the apparent discrepancy between H-bonding alcohol solvents and polar aprotic solvents. Taken collectively, our measurements show that the identity of the side group on the NBD chromophore plays little measurable role in determining the dynamics of the NBD chromophore, and that

both frictional and dielectric effects must be taken into account to understand the

comparatively strong interactions between NBD and polar solvents.

Literature Cited

(1)   Karpovich, D. S.; Blanchard, G. J. *Journal of Physical Chemistry* **1995**, *99*, 3951.

(2)   Rasimas, J. P.; Berglund, K. A.; Blanchard, G. J. *Journal of Physical Chemistry* **1996**, *100*, 17034.

(3)   Rasimas, J. P.; Berglund, K. A.; Blanchard, G. J. *Journal of Physical Chemistry* **1996**, *100*, 7220.

(4)   Rasimas, J. P.; Blanchard, G. J. *Journal of Physical Chemistry* **1995**, *99*, 11333.

(5)   Chapman, C. F.; Liu, Y.; Sonek, G. J.; Tromberg, B. J. *Photochemistry and Photobiology* **1995**, *62*, 416.

(6)   Chattopadhyay, A.; London, E. *Biochimica et Biophysica Acta, Biomembranes* **1988**, *938*, 24.

(7)   Fery-Forgues, S.; Fayet, J.-P.; Lopez, A. *Journal of Photochemistry and Photobiology, A: Chemistry* **1993**, *70*, 229.

(8)   Greenough, K. P.; Blanchard, G. J. *Journal of Physical Chemistry B* **2006**, *110*, 6351.

(9)   Lin, S.; Struve, W. S. *Photochemistry and Photobiology* **1991**, *54*, 361.

(10)   Mazeres, S.; Schram, V.; Tocanne, J.-F.; Lopez, A. *Biophysical Journal* **1996**, *71*, 327.

(11)   Mukherjee, S.; Chattopadhyay, A.; Samanta, A.; Soujanya, T. *Journal of Physical Chemistry* **1994**, *98*, 2809.

(12)   Tsukanova, V.; Grainger, D. W.; Salesse, C. *Langmuir* **2002**, *18*, 5539.

(13)   Dewitt, L.; Blanchard, G. J.; Legoff, E.; Benz, M. E.; Liao, J. H.; Kanatzidis, M. G. *Journal of the American Chemical Society* **1993**, *115*, 12158.

(14)   Garg, S. K.; NSmyth, C. P. *Journal of Physical Chemistry* **1965**, *69*, 1294.

(15)   Nee, T. W.; Zwanzig, R. *Journal of Chemical Physics* **1970**, *52*, 6353.

(16)   Dong, D. C.; Winnik, M. A. *Photochemistry and Photobiology* **1982**, *35*, 17.

(17)   Dong, D. C.; Winnik, M. A. *Canadian Journal of Chemistry* **1984**, *62*, 2560.

(18)   Kamlet, M. J.; Abboud, J. L.; Taft, R. W. *Journal of the American Chemical Society* **1977**, *99*, 6027.

(19)   Kamlet, M. J.; Hall, T. N.; Boykin, J.; Taft, R. W. *Journal of Organic Chemistry* **1979**, *44*, 2599.

(20)   Taft, R. W.; Abboud, J. L.; Kamlet, M. J. *Journal of the American Chemical Society* **1981**, *103*, 1080.

(21)   Brady, J. E.; Carr, P. W. *Journal of Physical Chemistry* **1982**, *86*, 3053.

(22)   Reichardt, C. *Angewandte Chemie International Edition in English* **1979**, *18*, 98.

(23)   Elias, H.; Dreher, M.; Neitzel, S.; Volz, H. *Zeitschrift fuer Naturforschung, Teil B: Anorganische Chemie, Organische Chemie* **1982**, *37B*, 684.

(24)   Chuang, T. J.; Eisenthal, K. B. *Journal of Chemical Physics* **1972**, *57*, 5094.

(25)   Johnson, C. K.; Wan, C. *Topics in Fluorescence Spectroscopy* **1997**, *5*, 43.

(26)   Wan, C.; Johnson, C. K. *Journal of Chemical Physics* **1994**, *101*, 10283.

(27)   Wan, C.; Johnson, C. K. *Chemical Physics* **1994**, *179*, 513.

(28)   Debye, P. *Polar Molecules*; Chemical Catalog Co.: New York, 1929.

(29)   Edward, J. T. *Journal of Chemical Education* **1970**, *47*, 261.

(30)   Perrin, F. *Journal de Physique et le Radium* **1936**, *7*, 1.

(31)   Blanchard, G. J. Ultrafast Stimulated Emission Spectroscopy. In *Topics in Fluorescence Spectroscopy. Volume 5. Nonlinear and Two-Photon Induced Fluorescence*; Lakowicz, J. R., Ed.; Plenum Press: New York, 1997; Vol. 5; pp 255.

(32)   Cantor, C. R.; Schimmel, P. R. *Biophysical Chemistry, Vol. 1*; Mir: Moscow, USSR, 1984; Vol. 1.

(33)   Dutt, G. B.; Srivatsavoy, V. J. P.; Sapre, A. V. *Journal of Chemical Physics* **1999**, *110*, 9623.

(34)   Blanchard, G. J. *Journal of Physical Chemistry* **1988**, *92*, 6303.

(35)   Blanchard, G. J.; Cihal, C. A. *Journal of Physical Chemistry* **1988**, *92*, 5950.

(36)   Stevenson, S. A.; Blanchard, G. J. *Journal of Physical Chemistry A* **2006**, *110*, 3426.

(37)   Simon, J. D.; Thompson, P. A. *Journal of Chemical Physics* **1990**, *92*, 2891.

(38)   Maroncelli, M.; MacInnis, J.; Fleming, G. R. *Science* **1989**, *243*, 1674.

(39)   Srinivas, G.; Bhattacharyya, S.; Bagchi, B. *Journal of Chemical Physics* **1999**, *110*, 4477.

(40)   Kivelson, D.; Spears, K. G. *Journal of Physical Chemistry* **1985**, *89*, 1999.

(41)   Madden, P.; Kivelson, D. *Journal of Physical Chemistry* **1982**, *86*, 4244.

(42)   Dote, J. L.; Kivelson, D. *Journal of Physical Chemistry* **1983**, *87*, 3889.

(43)   Dote, J. L.; Kivelson, D.; Knobler, C. M. *Journal of Chemical Physics* **1980**, *73*, 3519.

57

(44)   Dote, J. L.; Kivelson, D.; Schwartz, R. N. *Journal of Physical Chemistry* **1981**, *85*, 2169.

(45)   Cross, A. J.; Simon, J. D. *Journal of Chemical Physics* **1987**, *86*, 7079.

(46)   Hubbard, J. B.; Wolynes, P. G. *Journal of Chemical Physics* **1978**, *69*, 998.

(47)   van der Zwan, G.; Hynes, J. T. *Journal of Physical Chemistry* **1985**, *89*, 4181.

(48)   Vijayadamodar, G. V.; Chandra, A.; Bagchi, B. *Chemical Physics Letters* **1989**, *161*, 413.

(49)   Blanchard, G. J.; Wirth, M. J. *Journal of Physical Chemistry* **1986**, *90*, 2521.

(50)   Dutt, G. B.; Raman, S. *Journal of Chemical Physics* **2001**, *114*, 6702.

(51)   Horng, M.-L.; Gardecki, J. A.; Maroncelli, M. *Journal of Physical Chemistry A* **1997**, *101*, 1030.

(52)   Jiang, Y.; McCarthy, P. K.; Blanchard, G. J. *Chemical Physics* **1994**, *183*, 249.

(53)   Dutt, G. B. *ChemPhysChem* **2005**, *6*, 413.

CHAPTER 3

QUANTITATING THE DYNAMICS OF NBD HEXANOIC ACID IN HOMOGENEOUS SOLUTION AND IN SOLUTIONS CONTAINING UNILAMELLAR VESICLES

Introduction

Lipid bilayers have attracted a great deal of attention because of the central role these structures play in mediating life processes. As our understanding of these structures has improved, it has become clear that plasma membranes are exceedingly complex heterogeneous structures comprised of multiple different constituents, with the relative amount of each depending on the function of the cell. Early work on understanding plasma membranes pointed to the existence of some bilayer constituents that were not detergent-soluble, and more detailed analysis of these insoluble fractions revealed that they were enriched in cholesterol content. This finding, combined with work on multi-component model bilayer systems lead to the notion that "lipid rafts" may exist in cellular membranes.[1] Such rafts are thought to be regions of locally high cholesterol concentration, with sphingolipids playing a supportive role in raft formation owing to the ability of this family of lipids to hydrogen bond. While there is abundant evidence in the literature for phase separation in two and three component bilayer model systems,[2-4] the existence of lipid rafts in plasma membranes remains to be established firmly.

We are interested in biomimetic lipid bilayer structures because of the possibility that these structures can be used to support transmembrane proteins in their active forms.

A first step in this work is to understand the local environments formed by model bilayer structures as a function of their composition. In order to gain information on these heterogeneous systems from a molecular perspective, we are interested in imbedding selected chromophores in these structures. In this paper, we report on the optical properties of the chromophore (6-(N-(7nitrobenz-2-oxa-1,3-diazol-4-yl)amino hexanoic acid), NBDHA. The NBD chromophore is used widely for investigations of bilayer systems, and we focus here on both the details of chromophore motion in neat solvents and in solutions containing unilamellar vesicles. We have chosen to study the hexanoic acid derivative of this chromophore in an effort to understand where in the unilamellar vesicle structures such an amphiphilic chromophore will reside. Our specific choice of a chromophore possessing an amphiphilic side group that differs in structure from either the phospholipid or cholesterol bilayer constituents was deliberate. We are interested in understanding both polarity-mediated and structurally-mediated interactions within lipid bilayers, and this work centers on polarity-mediated interactions. We have chosen to use an NBD derivative because of the extensive knowledge base that already exists for this chromophore.[5-11] Our data in neat solvents reveal that NBDHA reorients as a prolate rotor with an aspect ratio $D_z/D_x \sim 2$. For NBDHA in vesicle-containing solutions, we find that the chromophore experiences the same environment regardless of vesicle composition or the specific phospholipid used. This finding, in conjunction with steady state absorbance and emission data, and fluorescence lifetime data, point to the NBDHA residing in close proximity to the head group region of the vesicles. Because the pK$_a$ of NBDHA is ca. 4.5 and the aqueous vesicle solutions are buffered to pH 8, the

60

chromophore exists in a predominantly deprotonated (anionic) form, facilitating

association with the phosphocholine headgroups of the lipids.

Experimental

Materials. The fluorescent probe 6-(N-(7nitrobenz-2-oxa-1,3-diazol-4-yl)amino hexanoic acid (NBDHA) was obtained from Molecular Probes Inc. and used without further purification. The solvents methanol, 1-propanol, 1-butanol, 1-pentanol, dimethyl sulfoxide (DMSO), N,N-dimethylformamide (DMF) and acetonitrile were purchased from Sigma-Aldrich in their highest purity available. Water and ethanol (95%) were distilled in-house. For time-resolved fluorescence measurements, the concentration of NBDHA in solvents and the concentration of NBDHA in the vesicles for one-photon experiments was 10^{-5} M, while the concentration of NBDHA in vesicles for two-photon experiments was 10^{-4} M.

For the construction of unilamellar vesicles, the lipids 1,2-Dilauroyl-sn-Glycero-3-Phosphocholine (DLPC, mp = -1°C), 1,2-Distearoyl-sn-Glycero-3-Phosphocholine (DSPC, mp = 55°C), egg sphingomyelin (SPM) and powdered cholesterol were obtained from Avanti Polar Lipids, Inc. Although DLPC and DSPC are not major components of plasma membranes, they were chosen based on their significant difference in transition temperatures. The vesicle constituents were prepared in a 1:1:1 mole ratio of phospholipid : cholesterol : sphingomyelin or a 2:1 mole ratio of phospholipid : cholesterol for the multicomponent systems. For the mixed lipid systems, the ratio of phospholipids used was 1:1. A total of nine vesicle systems were produced with varying composition. The vesicle compositions were as follows: DLPC, DLPC/cholesterol, DLPC/cholesterol/SPM, DSPC, DSPC/cholesterol, DSPC/cholesterol/SPM, DLPC/DSPC, DLPC/DSPC/cholesterol, and DLPC/DSPC/cholesterol/SPM. Chloroform was evaporated from the lipid solutions, then the vesicle constituents were dissolved in a

4:1 benzene:methanol solvent system, followed by another evaporation. The resulting lipid mixture was then dissolved in a 10 mM solution of Tris® buffer (Aldrich) in Milli-Q water. The Tris® buffer was adjusted for a pH ~ 8. An equal volume of the NBDHA-containing solution (2×10^{-4} M) was added next for a final total concentration of the vesicle constituents of 1 mg/mL, and 10^{-4} M in NBDHA. This probe concentration corresponds to ~7000 chromophore molecules per 100 nm diameter vesicle. The average distance between chromophores is calculated to be ~30 Å, a distance that could give rise to efficient Förster excitation transport. To test for this possibility, we compared our time-resolved and steady state data for 10^{-4} M solutions to the same data for 10^{-5} M solutions, and found that they were identical to within the experimental uncertainty.

We used the extrusion method[12-15] to produce small unilamellar vesicles of approximately 100 nm diameter. The lipid suspensions experienced five freeze-thaw-vortex cycles to aid in mixing of the constituents. The suspensions were frozen in liquid nitrogen for 5 minutes, followed by thawing in a hot water bath (5 minutes), then vortexed for approximately 2 minutes. For vesicle formation, a syringe-based mini-extruder from Avanti Lipids, Inc. was used. The lipid suspension was extruded eleven times through a polycarbonate filter with 100 nm diameter pores to produce vesicles. TEM measurements were used to verify vesicle size following extrusion.

Steady State Measurements. All absorption spectra were recorded on a Cary model 300 double beam UV-Visible absorption spectrophotometer, with 1 nm spectral resolution. All emission spectra were recorded on a Spex Fluorolog 3 spectrometer at a spectral resolution of 3 nm for both excitation and emission monochromators.

Time Correlated Single Photon Counting Measurements. All lifetime and anisotropy measurements of solvent and vesicle solutions were collected using a time correlated single photon counting (TCSPC) system. This system has been described in detail elsewhere and we provide only a brief recap of its salient features here. The source laser is a CW mode-locked Nd:YAG laser (Coherent Antares 76-S) that produces 100 ps 1064 nm pulses at 76 MHz repetition rate. The second or third harmonic of the output of this laser is used to excite a cavity dumped dye laser (Coherent 702-2), operating with Rhodamine 610 dye (Exciton, 532 nm pump) for two photon excitation experiments, or with Stilbene 420 dye (Exciton, 355 nm pump) for one photon excitation experiments. The dye laser outputs were 5 ps pulses at a repetition rate of 4 MHz for both excitation wavelengths. Fluorescence signals were detected using a Hamamatsu R3809U microchannel plate photomultiplier tube detector with a Tennelec 454 quad constant fraction discriminator and Tennelec 864 time-to-amplitude converter and biased amplifier used for signal processing. For this system the instrument response time is ~ 35 ps. Fluorescence was collected at 0°, 54.7° and 90° with respect to the vertically polarized excitation pulse.

Transmission Electron Microscopy. Samples were fixed with a 2% osmium tetroxide solution in 0.1 M cacodylate buffer (pH ~7.4). TEM images (Fig. 3.1) were acquired using a JEOL 100CX TEM operated at an accelerating voltage of 100 kV. The TEM data reveal an average vesicle size of 109 ± 28 nm based on 25 individual determinations.

200 nm
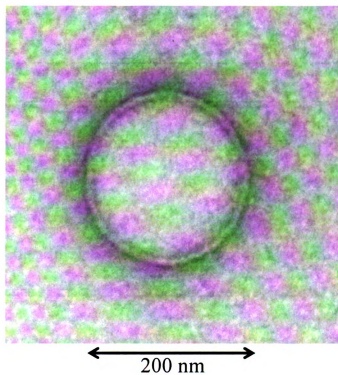
Figure 3.1 TEM image of unilamellar vesicles produced by extrusion. The average vesicle size is 109 ± 28 nm based on 25 individual determinations.

Background

In this section, we consider the theoretical framework within which we interpret time-resolved fluorescence anisotropy and molecular reorientation data for either one- or two-photon excitation. For either mode of excitation, we monitor emission from the S_1 state of the NBDHA chromophore. While the treatment of fluorescence anisotropy data has been reported elsewhere,[16-19] we believe it is important to provide a brief discussion of this subject to facilitate the interpretation of our experimental data. We start with a discussion of molecular reorientation data acquired using one photon excitation.

One-photon excited fluorescence anisotropy. For one photon excitation, the exciting pulse is polarized vertically and fluorescence transients are collected at 90° with respect to the excitation axis, at polarizations parallel (vertical) and perpendicular (horizontal) to the excitation polarization. These raw data are combined according to Eq. 3.1 to generate the induced orientational anisotropy function, R(t) (Eq. 3.1)

$$R(t) = \frac{I_{\parallel}(t) - I_{\perp}(t)}{I_{\parallel}(t) + 2I_{\perp}(t)} \qquad (3.1)$$

The chemically important information contained in R(t) is manifested in the number of exponential decays recovered, their relative fractional contribution, and the time constant(s) of the decay(s). While R(t) can contain up to five exponential decays, the most common case is for a one component decay, with a two component decay being observed under certain circumstances. The zero-time value(s) of R(t) range from -0.2 to 0.4 for one photon excitation, depending on the angle between the excited and emitting transition dipole moments.

The relationship between the decay functionality of R(t) and molecular properties including the rotational diffusion constants and the angle between the excited and emitting transition dipole moments was described by Chuang and Eisenthal.[16] That treatment considers the functional form of R(t) for an arbitrary ellipsoid of rotation, with limiting cases of either an oblate or prolate ellipsoid being used to simplify the general expression for R(t). Judicious assignment of Cartesian axes to the rotating molecule can serve to simplify the functionality of R(t). Generally, the excited transition dipole moment is taken as the x-axis, and for nominally planar molecules such as NBD the π-system defines the x-y plane. For an oblate rotor, $D_z \neq D_x = D_y$, and for a prolate rotor $D_x \neq D_y = D_z$.[16,18,19] For excitation and emission transition dipole moments aligned parallel to one another and along the long (x) axis, R(t) decays according to Eqs. 3.2

$$
\begin{aligned}
\text{oblate} \quad & R(t) = \left(\frac{1}{10}\right)\exp(-(2D_x + 4D_z)t) + \left(\frac{3}{10}\right)\exp(-6D_x t) \\
\text{prolate} \quad & R(t) = \left(\frac{4}{10}\right)\exp(-6D_z t)
\end{aligned}
\tag{3.2}
$$

If the transition moments are oriented along the z-axis, an oblate rotor will decay as a single exponential with an exponential term of $(4D_x + 2D_z)$.[16,18-20] These various possibilities have been treated elsewhere in detail, and for the outwardly simple case of a single exponential decay, there can be ambiguity in resolving the Cartesian components of D.[16] For this reason, we have also measured the induced orientational anisotropy function of NBDHA using two-photon excitation. While the essential physics of molecular motion remain the same regardless of the excitation mechanism, the means by which the initial anisotropic distribution is excited can have a profound influence on the functional form of the resulting fluorescence transients. By comparing the experimental

data for one- and two-photon excitation, we obtain a more complete and less ambiguous picture of the rotational diffusion constant for NBDHA in the various environments which we examine.

Two-photon excited fluorescence anisotropy. Reorientation dynamics probed by two photon excited fluorescence can, in principle, provide more detailed, or at least complementary information on the rotational motion that characterizes NBDHA in solution. We are interested in using two-photon excitation because it is a nonlinear process and thus provides selective excitation of the chromophore of interest without unwanted background absorption that can give rise to heating in thermally sensitive materials or in fragile biological systems. In our discussion of two-photon excited fluorescence anisotropy data, we follow the treatment put forth by the Johnson group.[21-23] Our goal is to relate the two-photon excited anisotropy decays of NBDHA in selected environments to the Cartesian components of its rotational diffusion constant.

Two-photon absorption is a third order nonlinear process, where two photons from the same incident electric field are absorbed simultaneously. Two-photon absorption is not an efficient process, and measuring the attenuation of the incident electric field is not a practical means of detection. Typically, for two-photon resonant excitation, the population placed in an excited electronic state as a result of two photon absorption relaxes by internal conversion to the S_1 state, where subsequent radiative decay is detected. The components of the molecular hyperpolarizability that can be accessed by the incident electric field(s) are represented by a tensor.[21-24]

$$S = \begin{bmatrix} S_{xx} & S_{xy} & S_{xz} \\ S_{yx} & S_{yy} & S_{yz} \\ S_{zx} & S_{zy} & S_{zz} \end{bmatrix}$$

For most planar chromophores such as NBD, a limited number of tensor elements contribute to two photon absorption, which are typically written as a 2x2 tensor, containing only S_{xx}, $S_{xy}(=S_{yx})$ and S_{yy}.[21-24] We are interested primarily in the *relative* values of the tensor elements S_{xx} and S_{xy}, and thus normalize these values to $S_{yy} = 1$.

Two-photon excitation provides information on the Cartesian components of the rotational diffusion constant of a chromophore that is complementary to that available from one photon excitation measurements. Because the details of the orientational anisotropy relaxation depend on both the shape of the initial photo-selected anisotropic population and on the two photon tensor elements accessed, the functional form of the anisotropy decay will depend on whether circularly or plane-polarized light was used for two photon excitation. The anisotropy functions generated from the linearly $(r_1(t))$ and circularly $(r_2(t))$ polarized light are given by

$$r_1(t) = \frac{I_{\parallel}^{linear}(t) - I_{\perp}^{linear}(t)}{I_{\parallel}^{linear}(t) + 2I_{\perp}^{linear}(t)}$$

$$r_2(t) = \frac{I_{\parallel}^{circular}(t) - I_{\perp}^{circular}(t)}{2I_{\parallel}^{circular}(t) + I_{\perp}^{circular}(t)}$$

(3.3)

Both zero-time anisotropies and anisotropy decay time constants are recovered from the experimental data. For both excitation polarizations, the transient anisotropy decays are characterized by the same two time constants, τ_0 and τ_2, each weighted according to the spectroscopic properties of the chromophores. The zero-time anisotropies for these two

different excitation polarizations are related to the two photon tensor elements according to Eq. 3.4, for systems where S_{xx}, S_{xy} ($=S_{yx}$) and S_{yy} are the dominant elements. [21-23]

$$r_1(0) = \frac{1}{7}\frac{2\left(S_{xx} + S_{yy}\right)^2 + \left(S_{xx} - S_{yy}\right)^2 + 4S_{xy}^2 + 9\left(S_{xx}^2 - S_{yy}^2\right)}{2\left(S_{xx} + S_{yy}\right)^2 + \left(S_{xx} - S_{yy}\right)^2 + 4S_{xy}^2}$$

$$r_2(0) = \frac{1}{7}\frac{3\left(S_{xx} - S_{yy}\right)^2 - \left(S_{xx} + S_{yy}\right)^2 + 12S_{xy}^2 + 6\left(S_{xx}^2 - S_{yy}^2\right)}{\left(S_{xx} + S_{yy}\right)^2 + 3\left(S_{xx} - S_{yy}\right)^2 + 12S_{xy}^2}$$

(3.4)

Knowing the experimental values of $r_1(0)$ and $r_2(0)$, we can determine the relative values of S_{xx} and S_{xy} when S_{yy} is normalized to unity. Because we are concerned with the relative values of the tensor elements and not their absolute magnitudes, normalization of the tensor elements to S_{yy} does not reduce the relevant information content of our measurements.

Rotational diffusion will re-randomize the initially anisotropic orientational distribution of the emitting molecules according to Eqs. 3.5, [21-23]

$$r_1(t) = r_1(0)\left[c_0\exp(-t/\tau_0) + c_2\exp(-t/\tau_2)\right]$$
$$r_2(t) = r_2(0)\left[d_0\exp(-t/\tau_0) + d_2\exp(-t/\tau_2)\right]$$

(3.5)

where τ_0 and τ_2 are two different relaxation time constants. The relative contribution of the two time constants is given by the prefactors c_i and d_i, which are in turn related to the rotational diffusion constant and the two photon tensor elements, as described in Eqs. 3.6 – 3.10:[21-23]

$$c_0 = \frac{(\sqrt{3}a + b)\left[3(\sqrt{3}a + b)S_{xx}^2 + 3(-\sqrt{3}a + b)S_{yy}^2 + 2bS_{xx}S_{yy} + 4bS_{xy}^2\right]}{7N^2(3S_{xx}^2 + 3S_{yy}^2 + 2S_{xx}S_{yy} + 4S_{xy}^2)}$$

(3.6)

$$c_2 = \frac{(a - \sqrt{3}b)\left[3(a - \sqrt{3}b)S_{xx}^2 + 3(a + \sqrt{3}b)S_{yy}^2 + 2aS_{xx}S_{yy} + 4aS_{xy}^2\right]}{7N^2(3S_{xx}^2 + 3S_{yy}^2 + 2S_{xx}S_{yy} + 4S_{xy}^2)} \tag{3.7}$$

$$d_0 = \frac{(\sqrt{3}a + b)\left[(\sqrt{3}a + b)S_{xx}^2 + (-\sqrt{3}a + b)S_{yy}^2 - 4bS_{xx}S_{yy} + 6bS_{xy}^2\right]}{14N^2(S_{xx}^2 + S_{yy}^2 - S_{xx}S_{yy} + 3S_{xy}^2)} \tag{3.8}$$

$$d_2 = \frac{(a - \sqrt{3}b)\left[(a - \sqrt{3}b)S_{xx}^2 + (a + \sqrt{3}b)S_{yy}^2 - 4aS_{xx}S_{yy} + 6aS_{xy}^2\right]}{14N^2(S_{xx}^2 + S_{yy}^2 - S_{xx}S_{yy} + 3S_{xy}^2)} \tag{3.9}$$

The relative amplitudes of the decay time constants will provide information about the values of the Cartesian components of the rotational diffusion constant. The parameters a, b, N and Δ are related to the diffusion constant by

$$
\begin{aligned}
a &= \sqrt{3}(D_y - D_x) \\
b &= 2D_z - D_y - D_x + 2\Delta \\
N^2 &= a^2 + b^2 \\
\Delta &= (D_x^2 + D_y^2 + D_z^2 - D_x D_y - D_y D_z - D_x D_z)^{1/2}
\end{aligned}
\tag{3.10}
$$

We use these relationships[16,18,20] and those developed by Johnson and coworkers[21-23] to treat our two photon excited fluorescence anisotropy data on NBDHA in solvents and unilamellar vesicle structures.

Eqs. 3.5 indicate that the two photon anisotropy decay should exhibit two exponential components, and our experimental data yield single exponential decays in all cases (*vide infra*). This result has been observed previously,[21] and obtains under the condition that the experimental time constants are similar, with the single time constant representing a weighted average of the two decay time constants. As is the case for Chuang and Eisenthal's treatment, invoking ellipsoidal rotor shapes for reorientation can

71

serve to simplify the form of the expressions for the decay time constants τ_0 and τ_2. Our

experimental data for one photon excitation suggest that NBD reorients as a prolate rotor,

$D_x \neq D_y = D_z$, (*vide infra*), and we apply this effective rotor shape to the equations for τ_0

and τ_2. The equations derived by the Johnson group[21-23] can be simplified to yield,

$$\tau_{r1}^{PRO} = \frac{S_{xx}^2(7D_x + 17D_z) - 4S_{yy}^2(2D_x - D_z) + (S_{xx}S_{yy} + 2S_{xy}^2)\left(\dfrac{3(D_z^2 + 2D_zD_x)}{2D_x + D_z} + 4D_x - D_z\right)}{8(D_z^2 + 2D_xD_z)(6S_{xx}^2 - 3S_{yy}^2 + S_{xx}S_{yy} + 2S_{xy}^2)} \qquad (3.11)$$

$$\tau_{r2}^{PRO} = \frac{8S_{xx}^2(2D_x + D_z) - 4S_{yy}^2(2D_x - D_z) - (2S_{xx}S_{yy} + 3S_{xy}^2)\left(6D_x - 5D_z + \dfrac{9(D_z^2 + 2D_zD_x)}{2D_x + D_z}\right)}{24(D_z^2 + 2D_xD_z)(2S_{xx}^2 - S_{yy}^2 - 2S_{xx}S_{yy} + 3S_{xy}^2)} \qquad (3.12)$$

The various factors that contribute to the two-photon excited anisotropy decay time

constants are not related in an intuitive manner to the rotational motion of the molecule,

in contrast to the time constant(s) recovered for one photon excitation. Treating NBD as

a prolate rotor, we can determine D_z (Eqs. 3.2) and D_x (Eq. 3.13).

$$D_x = \frac{17S_{xx}^2D_z + 12S_{xy}^2D_z + 2S_{xx}D_z - 48\tau_1S_{xx}^2D_z^2 - 16\tau_1S_{xy}^2D_z^2 - 8\tau_1S_{xx}D_z + 24\tau_1D_z^2}{7S_{xx}^2 + 4S_{xx} - 96\tau_1S_{xx}^2D_z - 32\tau_1S_{xy}^2D_z - 16S_{xx}D_z\tau_1 + 48\tau_1D_z} \qquad (3.13)$$

We use this information to advantage in probing the immediate environment of NBDHA

in a series of solvent and unilamellar vesicle systems of varying composition.

Results and Discussion

As noted in the Introduction, we are interested in understanding the motional dynamics of the chromophore NBDHA in both neat solvents and in the presence of unilamellar vesicles. The issues of primary concern are obtaining a detailed understanding of the dynamics of this chromophore, and whether or not it localizes to specific region(s) within the unilamellar vesicle structures. We consider first the dynamics of NBDHA in selected neat solvents. Previous literature reports have demonstrated that the polarity of the environment surrounding the NBD chromophore plays a significant role in determining its fluorescence lifetime.[5-10] Our data are consistent with these previous results,[6-8,10] showing a decrease in fluorescence lifetime of NBDHA with increasing solvent polarity. The excited state population decay of NBDHA is single exponential in all cases, consistent with the expected first order dynamics of a single emitting species. Fluorescence lifetimes of NBDHA in neat solvents are between 6 and 10 ns. The lifetime values determined by one-photon and two-photon excitation are the same to within the experimental uncertainty, which is expected because radiative emission originates from the same excited electronic state for both modes of excitation. It is difficult to extract detailed chemical information from fluorescence lifetimes because of the system-specific nature of such data and the absence of a comprehensive theoretical framework relating excited state lifetime to either local environment or molecular properties for systems where the emission bands experience significant inhomogeneous broadening.

For these reasons, we turn to the information available from fluorescence anisotropy data. For NBDHA in neat solvents, the one-photon excited fluorescence anisotropy decays are single exponential. Based on Chuang and Eisenthal's treatment, as indicated in Eq. 3.2, the single exponential decay of R(t) indicates that NBDHA is a prolate rotor with $\tau = 1/(6D_z)$[16,20] The one photon reorientation times we recover are related directly to the viscosity of the local medium, as described by the modified Debye-Stokes-Einstein (DSE) equation, [16,18-20]

$$\tau_{OR} = \frac{\eta Vf}{k_B TS} \tag{3.14}$$

Where η is the solvent bulk viscosity, V is the solute hydrodynamic volume $V_{NBDHA} = 245 \ \text{Å}^3$,[25] f is the frictional solvent-solute boundary condition, and S is the solute shape factor. We show in Fig. 3.2 the dependence of τ_{OR} on solvent bulk viscosity, and from those data we determine that $D_z/\eta = 877 \pm 51$ MHz/cP. Despite this useful relationship, there remains the potential ambiguity in determining the Cartesian components of D based on the axis along which the excited transition moment is oriented. We are thus in need of achieving a more thorough understanding of the motional dynamics of NBDHA. In an attempt to lift this ambiguity, we have performed measurements of the transient fluorescence anisotropy of NBDHA for two photon excitation.

For the reorientation data acquired using two-photon excitation, the recovered anisotropy decay times are not related to the viscosity of the local medium in the same manner as the data for one-photon excitation, but are a permutation of D_z, D_x, and the two photon tensor elements. The one-photon anisotropy data for NBDHA suggest that this chromophore reorients as a prolate rotor in the neat solvents we have studied. It is also possible, under

74

certain circumstances, that the one-photon data could be consistent with the behavior of an oblate rotor, depending on the orientation of the transition dipole moments relative to the dominant rotor axis. In an effort to resolve this potential ambiguity and determine whether NBDHA reorients as a prolate rotor or an oblate rotor, we have treated the two-photon data assuming both rotor shapes. Assuming an oblate rotor shape, yields physically unrealistic, negative values for D_x and D_z that are not consistent between the one-photon and two-photon data. Based on these findings, we assert that NBDHA reorients as a prolate rotor in the neat solvents we have studied. We report the values of D_z and D_x in the solvents used here in Table 3.1. These data show that the ratio of diffusion coefficients is $D_z/D_x \sim 2$ for all solvents, a result that is possible only by comparing the two independent data sets, analogous to the information extracted from anisotropy measurements on Rhodamine 640 when excited to two different initial electronic states.[26]

With this information in hand, we now have a relevant framework within which to evaluate the behavior of NBDHA in the presence of unilamellar vesicles. We have synthesized unilamellar vesicles from solutions containing 10^{-4} M NBDHA. A variety of unilamellar vesicle compositions were used to determine whether or not the NBDHA chromophore functions as a sensor of vesicle structure and composition. The addition of cholesterol and sphingomyelin to phospholipid vesicle structures is known to induce phase segregated regions within the bilayer structures.[2-4] Ongoing work in the Blanchard laboratory shows that varying the composition of bilayers does, in fact, influence the dynamics of the constituents.[27] Those results were obtained using chromophores tethered to specific bilayer constituents such as cholesterol or a
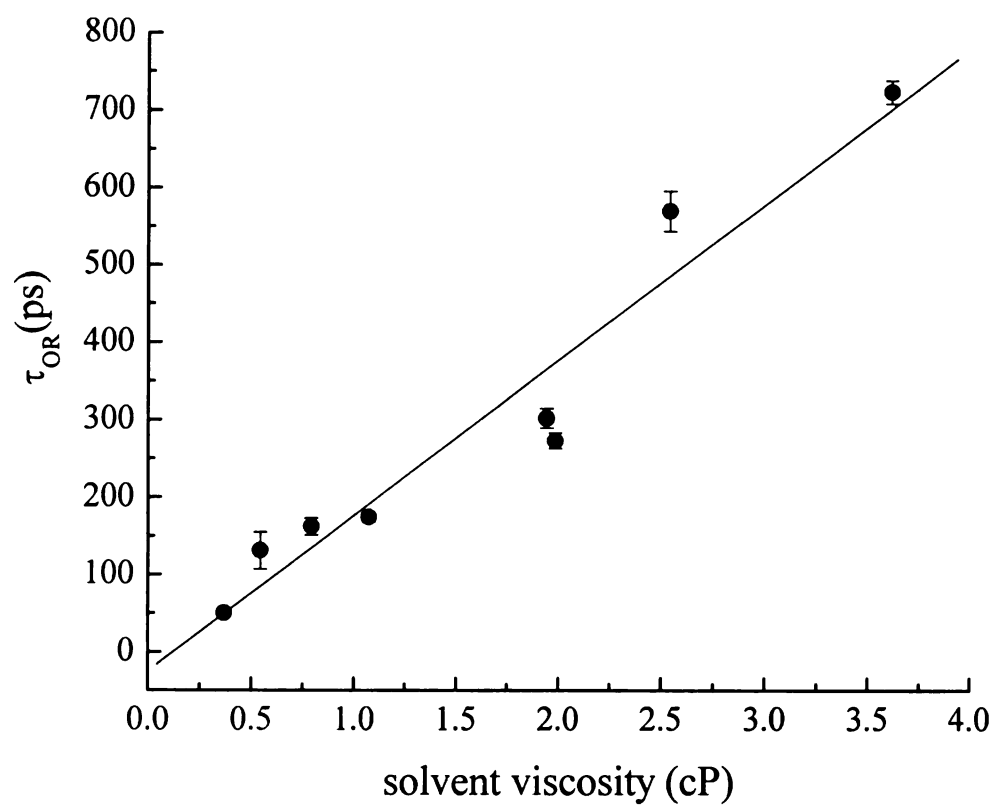
Figure 3.2 Dependence of NBDHA one-photon excited reorientation time constant on solvent viscosity. The slope of the best-fit line is used to extract the viscosity-dependence of the rotational diffusion constant D_z.

phospholipid, and they thus provided information on the region(s) of interest within the bilayer structure. A central goal of this work is to determine whether or not the NBDHA chromophore locates within specific vesicle regions. The underlying question is the structural homology required of a probe molecule in order for it to locate within specific regions of the bilayer.

To help understand the location of NBDHA in vesicle systems, we consider first the fluorescence lifetime of this chromophore. As noted earlier, there is limited information available from fluorescence lifetime measurements by themselves, but when such data are compared to NBDHA lifetimes in other systems, it is possible to garner some useful environmental insight. For each vesicle system, the NBDHA excited state lifetime decays exhibited a single exponential functionality. Previous literature reports have shown that the fluorescence lifetime of NBD in an aqueous or polar environment is typically sub-nanosecond, [6,7,9,10] suggestive of strong interactions between solvent and solute, such as hydrogen bonding and dipolar coupling. We note that there is evidence in the literature for direct chromophore-chromophore interactions between NBD moieties under certain experimental conditions.[11] Given both the functionality and time constant of the lifetime data we recover for our systems, we do not believe that chromophore dimers contribute significantly to our results. We recover the interesting result that, regardless of vesicle composition, the NBDHA lifetimes are all ca. 1 ns, suggesting that the environment sensed by the NBDHA chromophore is of similar polarity in all cases. If this explanation is true, the steady state fluorescence spectra of NBDHA should be similar for all systems, and we consider these data next.

The steady state spectra of NBDHA in vesicles and in water are shown in Fig. 3.3. The NBDHA absorption band maximum and shape is substantially different in water than it is in vesicle-containing solutions. The absorption maximum for NBDHA in vesicle-containing solutions is ~475 nm, and is centered at ~484 nm in water. We conclude from these data that NBDHA is not in the aqueous phase in vesicle-containing solutions. The chromophore NBD is known to have a fluorescence quantum yield that depends sensitively on the polarity of its environment. In water, NBD has a low quantum yield,[7,8] and in our measurements of NBDHA we were unable to detect a significant time-resolved fluorescence signal in water. Based on both the steady state absorption data and the time-resolved emission data, it is clear that in vesicle-containing solutions, NBDHA does not reside in the bulk water region of this system, and that for all vesicle-containing solutions the chromophore senses essentially the same environment.

We consider next the information content of the reorientation data for NBDHA in vesicle-containing solutions. When considering anisotropy decays for NBDHA in the presence of vesicles, we have to decide on the most appropriate model to use in interpreting these data. Depending on where in the solution the chromophore resides, either the DSE (free rotor, Eq. 3.14) model[28-30] or the hindered rotor model[31-33] could be used to interpret the data.

The hindered rotor model has previously been used to describe the motion of a chromophore embedded in a membrane and must be considered here based on the steady state absorption data. In this model, the motion of a chromophore is restricted by its environment, which is modeled as a cone.

Table 3.1 Solvent-dependence of D_z and D_x for NBDHA in neat solvents.

solvent	viscosity (cP)	D_z (MHz)	D_x (MHz)	D_z/D_x
acetonitrile	0.369	3370 ± 6	1887 ± 1	2.1
methanol	0.544	1270 ± 18	610 ± 1	1.7
DMF	0.794	1030 ±7	599 ± 1	1.7
ethanol	1.074	960 ± 3	566 ± 1	1.8
propanol	1.945	550 ± 4	324 ± 1	1.8
DMSO	1.987	610 ± 4	352 ± 1	1.7
butanol	2.544	290 ± 5	165 ± 1	1.7
pentanol	3.619	230 ± 2	128 ± 1	1.8

The cone angle that characterizes the chromophore motional freedom is related to the measured time constant of the anisotropy decay according to Eq. 3.15.

$$\tau = \frac{7\theta_o^2}{24D_w}$$
[3.15]

The time constant associated with motional relaxation of the chromophore is not determined unambiguously because of the dependence of this quantity on both the cone angle in which the chromophore is free to move and on the "wobbling" diffusion constant of the chromophore as it moves about its bond to its anchoring functionality. We note that in this model the measured time constant behaves differently than the quantity τ_{OR} (Eq. 3.14), which is measured for a free chromophore in solution. For the hindered rotor, the anisotropy decay time τ scales with the cone angle swept out. For a restrictive environment (small θ_0), a rapid time constant is measured because the chromophore samples a small volume, and for a relatively free environment (large θ_0), τ is long because of the comparatively greater volume the chromophore has access to. In contrast, for a free rotor, a fast time constant τ_{OR} is reflective of a low viscosity environment and a slow time constant implies a high viscosity, restrictive environment. Also, for hindered rotors, the anisotropy does not decay to zero at t = ∞ as it does in bulk solutions, because a restricted range of motional freedom is available to the chromophore. In principle, the observation of a non-zero R(∞) value would indicate that the hindered rotor is the appropriate model. Because we are using vesicles, however, and restriction in the orientational distribution associated with chromophore confinement within the bilayer is

80
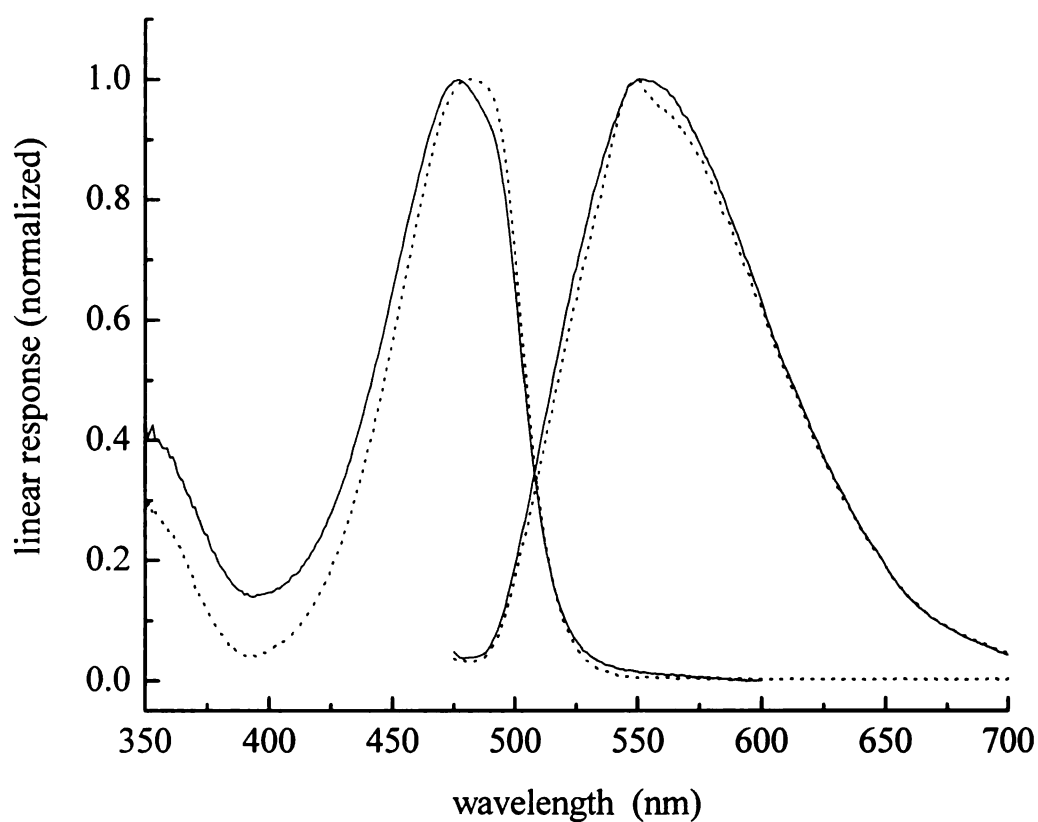
Figure 3.3. Normalized absorption and emission spectra of NBDHA in neat water (dashed line) and in a solution containing DLPC vesicles (solid line). Spectra for all vesicle-containing solutions were identical.

orientationally averaged over 4π steradians macroscopically owing to the spherical shape of the vesicles, R(∞) = 0 for all measurements. The choice of the model most appropriate for the interpretation of our data must therefore be made based on other factors.

We consider that, if NBDHA were bound to the surface of the unilamellar vesicles, it would enjoy substantial motional freedom. We make this structural argument based on the fact that, for the lipids we use, there is a cationic quaternary ammonium species in closest proximity to the water at the lipid-solution interface. Because we make our measurements at pH 8, the NBDHA is fully deprotonated (precluding carboxylic acid tail-to-tail chromophore dimer formation), and if the chromophore were to interact with the vesicle, as suggested by the steady state absorption data, an ionic interaction would be possible. In this picture, the nominally tethered chromophore would experience a cone angle of $2\theta_0 \sim 180°$, which is a limiting case that renders the chromophore equivalent to a free rotor. Also, the strength of the ionic interaction postulated above would be on the order of several kcal/mol at most, and the persistence time for such interactions would be on the order of hundreds of ps. For both of these reasons, we assert that our reorientation data for NBDHA in the presence of vesicles are best understood in the context of the free rotor model rather than the hindered rotor model. Interpreting our reorientation data within the framework of the free rotor model yields the result that NBDHA reorients as a prolate rotor in the presence of vesicles, qualitatively the same as for its behavior in neat solvents. We have synthesized vesicles in a range of compositions, including the use of two different lipids with melting points substantially below (DLPC, mp = -1°C) and substantially above (DSPC, mp = 55°C) room temperature, and with the addition of cholesterol and sphingomyelin. These different vesicle compositions are known to

82

produce phase-segregated bilayer structures, and the local environments created by these different phases vary widely in both their polarity and rigidity.[2-4,34] Despite the wide range of environments within the vesicles that are available to NBDHA, we recover essentially the same one-photon excited reorientation times, regardless of vesicle composition.(Table 3.2, Fig. 3.4) While there may be some slight variation between individual systems, these differences are barely different from the experimental uncertainty. For this reason we do not attempt to provide any more detailed, system-dependent interpretation of these values. We also note that, while the two photon excited anisotropy decays produce different time constants than those seen for the one photon data, as expected, the same behavior is seen for all of the anisotropy decay time data sets.

Treatment of the one-photon excited anisotropy decay times of NBDHA in vesicle-containing solutions in the context of a free rotor allows τ_{OR} to be related to the viscosity of the environment through the DSE equation (Eq. 3.14), and the observation of single exponential anisotropy decays allows assignment of a prolate rotor shape to NBDHA in the presence of vesicles, based on our measurements of NBDHA in neat solvents (*vide supra*). Comparing the reorientation times of NBDHA in vesicle-containing solutions to the same data for NBDHA in neat solvents indicates that the local environment of NBDHA is characterized by a viscosity of ~1 cP, a value fully consistent with an aqueous environment. These data, taken in conjunction with the steady state data (Fig. 3.3), suggest that the probe resides in the polar headgroup region, in the immediate vicinity of the bilayer.

Table 3.2. Dependence of NBDHA one- and two-photon excited anisotropy decay time constants on vesicle composition. Abbreviations: DLPC = 1,2-Dilauroyl-sn-Glycero-3-Phosphocholine; DSPC = 1,2-Distearoyl-sn-Glycero-3-Phosphocholine; chol = cholesterol; spm = sphingomyelin.

Vesicle system	τ_{OR} (one photon, ps)	τ_{linear} (two photon, ps)	$\tau_{circular}$ (two photon, ps)	τ_{fl} (ps)	D_z/D_x
DLPC	163 ± 10	121 ± 5	102 ± 14	1173 ± 88	1.8
DLPC/chol.	166 ± 4	127 ± 5	95 ± 4	1168 ± 66	1.8
DLPC/chol/spm	194 ± 5	132 ± 19	106 ± 16	1177 ± 62	1.7
DSPC	186 ± 6	126 ± 8	97 ± 9	1144 ± 45	1.8
DSPC/chol.	176 ± 6	109 ± 6	107 ± 10	1132 ± 23	1.7
DSPC/chol/spm	165 ± 4	122 ± 4	97 ± 10	1145 ± 44	1.7
DLPC/DSPC	159 ± 6	125 ± 5	102 ± 4	1157 ± 48	1.9
DLPC/DSPC/chol.	161 ± 8	126 ± 8	89 ± 9	1147 ± 40	1.7
DLPC/DSPC/chol/spm	186 ± 5	87 ± 2	75 ± 5	1067 ± 41	2.0
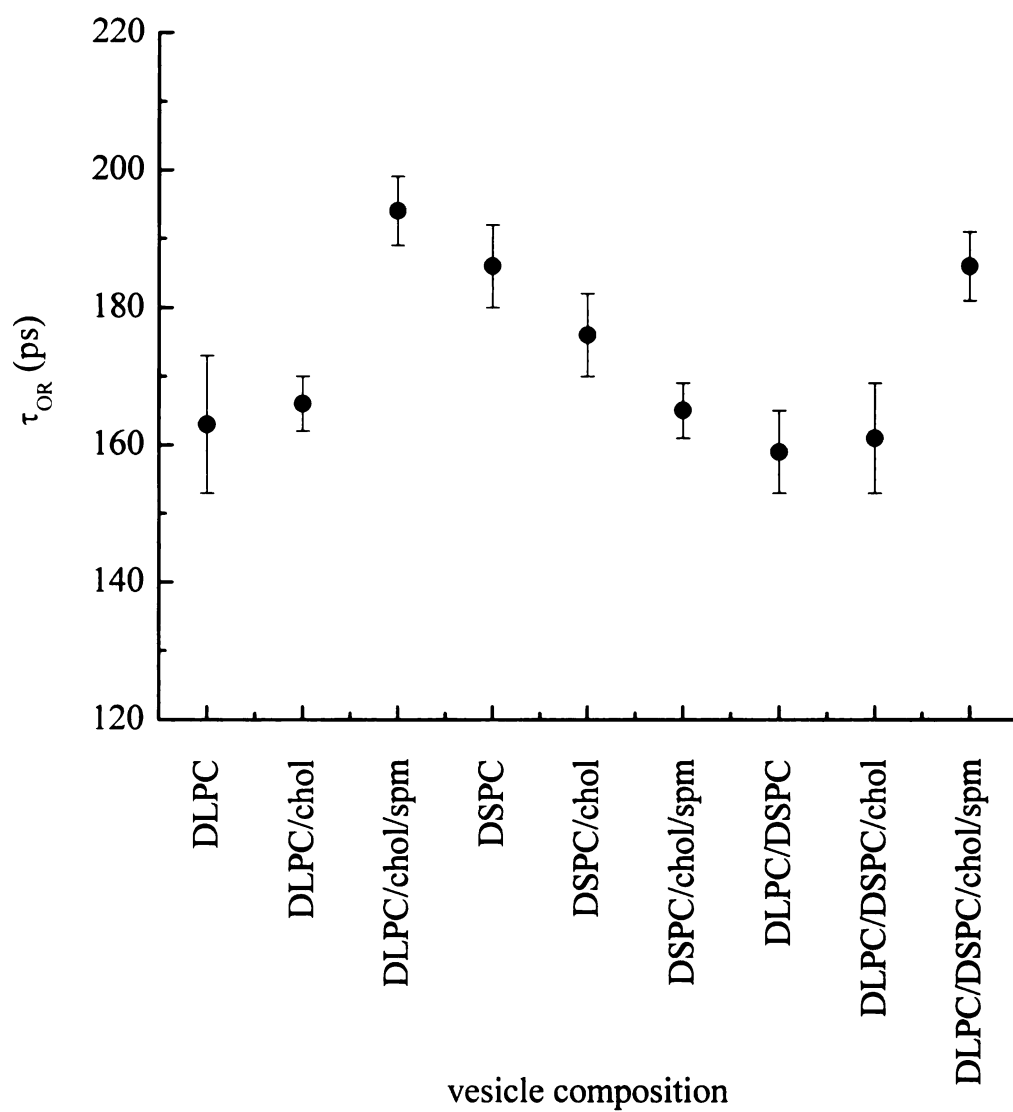
Figure 3.4 Dependence of NBDHA reorientation on vesicle composition.

The two-photon excited anisotropy decays for NBDHA in solvents were modeled as both a prolate and an oblate rotor to determine which model provided results that were consistent with the one photon data. We have treated the two photon data for NBDHA in vesicle-containing solution the same way, and the results of this treatment are that a self-consistent result is obtained only if NBDHA is modeled as a prolate rotor. For the two-photon excited anisotropy data, single exponential decays are seen, and the reorientation times for all systems are the same for both linearly and circularly polarized excitation, regardless of vesicle composition. We apply Eq. 3.13 to our data to extract the quantity D_x. Combining the two-photon and the one-photon data we recover a ratio $D_z/D_x \sim 2$, (Table 3.2) the same ratio that we determined for NBDHA in neat solvents. The consistency of the results between the two different types of environments argues for the applicability of the free rotor model for the interpretation of NBDHA molecular motion in vesicle-containing solutions.

We note that it is, in principle, possible for the NBDHA chromophore to be incorporated to a limited extent (shallow incorporation) into the bilayer structure, and under this condition it would sense a polar environment that is likely not too different than that of bulk water.[35-38] We believe that the reorientation data we have presented allow us to distinguish between the possibility of shallow incorporation and the chromophore being at the bilayer interface. If the chromophore were incorporated to any significant extent within the bilayer structure, the ratio of D_z/D_x would be altered by virtue of its spatial confinement. We find experimentally that the ratio D_z/D_x for NBDHA in vesicle-containing solutions is the same as that in neat liquid solvents, indicating that it resides in an environment that affords substantial orientational freedom

that varies very little if at all with bilayer composition. The only environment that fits these criteria fully is the interface between the bilayer and the bulk liquid.

Conclusions

We have studied the steady state and time resolved optical properties of the chromophore NBDHA in a series of neat solvents and in vesicle-containing solutions. We have used both one photon excitation and two photon excitation for our anisotropy measurements and analyzing these data to find a self-consistent solution allows us to determine that the chromophore reorients as a prolate rotor with $D_z/D_x \sim 2$ in all cases. For NBDHA in vesicle-containing solutions we observe reorientation dynamics that are independent of vesicle composition, even though the steady state absorption and fluorescence lifetime data on these systems indicate that the chromophore does not reside in a purely aqueous environment. The location of the NBDHA chromophore that is most consistent with the entire body of steady state and time-resolved emission data is that the chromophore resides at the bilayer-solution interface, near the zwitterionic phosphocholine headgroups. In this region, interactions between the headgroups and the NBDHA are possible. All solutions are at pH $\sim$8, therefore the NBDHA is essentially all deprotonated, allowing ionic interactions to dominate in this system. The larger implication of this work is that there needs to be a very close match between chromophore side group functionality and a bilayer constituent for there to be incorporation into specific regions of the bilayer structures. We do note that the chromophore interaction with the vesicles is selective for the phospholipid regions, but in a way that is not sensitive to any lipid local organization.

Literature Cited

(1)   Simons, K.; van Meer, G. *Biochemistry* **1988**, *27*, 6197.

(2)   Crane, J. M.; Tamm, L. K. *Biophysical Journal* **2004**, *86*, 2965.

(3)   Hao, M.; Maxfield, F. R. *Journal of Fluorescence* **2001**, *11*, 287.

(4)   Scherfeld, D.; Kahya, N.; Schwille, P. *Biophysical Journal* **2003**, *85*, 3758.

(5)   Chapman, C. F.; Liu, Y.; Sonek, G. J.; Tromberg, B. J. *Photochemistry and Photobiology* **1995**, *62*, 416.

(6)   Chattopadhyay, A.; London, E. *Biochimica et Biophysica Acta, Biomembranes* **1988**, *938*, 24.

(7)   Fery-Forgues, S.; Fayet, J.-P.; Lopez, A. *Journal of Photochemistry and Photobiology, A: Chemistry* **1993**, *70*, 229.

(8)   Lin, S.; Struve, W. S. *Photochemistry and Photobiology* **1991**, *54*, 361.

(9)   Mazeres, S.; Schram, V.; Tocanne, J.-F.; Lopez, A. *Biophysical Journal* **1996**, *71*, 327.

(10)   Mukherjee, S.; Chattopadhyay, A.; Samanta, A.; Soujanya, T. *Journal of Physical Chemistry* **1994**, *98*, 2809.

(11)   Tsukanova, V.; Grainger, D. W.; Salesse, C. *Langmuir* **2002**, *18*, 5539.

(12)   Hunter, D. G.; Frisken, B. J. *Biophysical Journal* **1998**, *74*, 2996.

(13)   Johnson, J. M.; Ha, T.; Chu, S.; Boxer, S. G. *Biophysical Journal* **2002**, *83*, 3371.

(14)   Moscho, A.; Orwar, O.; Chiu, D. T.; Modi, B. P.; Zare, R. N. *Proceedings of the National Academy of Sciences of the United States of America* **1996**, *93*, 11443.

(15)   Patty Philipus, J.; Frisken Barbara, J. *Biophysical journal* **2003**, *85*, 996.

(16)   Chuang, T. J.; Eisenthal, K. B. *Journal of Chemical Physics* **1972**, *57*, 5094.

(17)   Jiang, Y.; Blanchard, G. J. *Journal of Physical Chemistry* **1994**, *98*, 6436.

(18)   Blanchard, G. J. *Journal of Chemical Physics* **1987**, *87*, 6802.

(19)   McPhie, P. *Principles of Fluorescence Spectroscopy, Second Edition* 2000; Vol. 287.

(20)   Tao, T. Time-dependent fluorescence depolarization and Brownian rotational diffusion coefficients of macromolecules. PhD Thesis, 1969.

(21)   Johnson, C. K.; Wan, C. *Topics in Fluorescence Spectroscopy* **1997**, *5*, 43.

(22)   Wan, C.; Johnson, C. K. *Chemical Physics* **1994**, *179*, 513.

(23)   Wan, C.; Johnson, C. K. *Journal of Chemical Physics* **1994**, *101*, 10283.

(24)   Callis, P. R. *Journal of Chemical Physics* **1993**, *99*, 27.

(25)   Edward, J. T. *Journal of Chemical Education* **1970**, *47*, 261.

(26)   Dela Cruz, J. L.; Blanchard, G. J. *Journal of Physical Chemistry A* **2001**, *105*, 9328.

(27)   Koan, M. M., Blanchard, G. J. . *Journal of Physical Chemistry B* **2006**, *110*, 16584.

(28)   Debye, P. *Polar Molecules*; Chemical Catalog Co.: New York, 1929.

(29)   Perrin, F. *Journal de Physique et le Radium* **1936**, *7*, 1.

(30)   Zwanzig, R.; Harrison, A. K. *Journal of Chemical Physics* **1985**, *83*, 5861.

(31) Kinosita, K., Jr.; Ikegami, A.; Kawato, S. *Biophysical Journal* **1982**, *37*, 461.

(32) Kinosita, K., Jr.; Kawato, S.; Ikegami, A. *Biophysical Journal* **1977**, *20*, 289.

(33) Szabo, A. *Journal of Chemical Physics* **1984**, *81*, 150.

(34) Wisniewska, A.; Draus, J.; Subczynski, W. K. *Cellular & Molecular Biology Letters* **2003**, *8*, 147.

(35) Costa, E. J. X.; Shida, C. S.; Biaggi, M. H.; Ito, A. S.; Lamy-Freund, M. T. *FEBS Letters* **1997**, *4116*, 103.

(36) Dhanvantari, S.; Arnaoutova, I.; Snell, C. R.; Steinbach, P. J.; Hammond, K.; Caputo, G. A.; London, E.; Loh, Y. P. *Biochemistry* **2002**, *41*, 52.

(37) Drummen, G. P. C.; van Liebergen, L. C. M.; Op den Kamp, J. A. F.; Post, J. A. *Free Radical Biology & Medicine* **2002**, *33*, 473.

(38) Lee-Gau Chong, P. W. v. d. M., B. Thompson, T.E. . *Biochimica et Biophysica Acta* **1985**, *813*, 253.

CHAPTER 4

ONE- AND TWO-PHOTON EXCITED FLUORESCENCE DYNAMICS OF NBD IN LIPID BILAYERS. DEPENDENCE OF CHROMOPHORE DYNAMICS ON BILAYER COMPOSITION

Introduction

Plasma membranes are central to the existence and function of cellular systems. These membranes are known to contain a large number of constituents, and as our understanding of these complex and dynamic systems has evolved, it has become clear that even simple lipid bilayer membranes are heterogeneous, highly dynamic structures. The discovery of "lipid rafts"[1,2] as a result of exploring the differential solubility of plasma membrane constituents has given rise to a sustained effort aimed at resolving whether or not these structures exist in plasma membranes. Phase separated regions have been readily observed in model bilayer systems composed of three constituents,[2-5] most commonly a phospholipid, a sphingolipid, and cholesterol in varying amounts. However, compelling experimental evidence for the existence of these raft structures in plasma membranes remains to be presented. As a consequence, there is a great deal of effort aimed at understanding the chemical and physical basis for phase separation in the comparatively simpler model systems, so that the structural factors that give rise to phase separation can be evaluated in more complex, natural plasma membranes.

Our interest in heterogeneous bilayer structures is for both pragmatic and fundamental reasons. Ultimately, we want to create a biomimetic interface containing active trans-membrane proteins that can be used for chemical sensing. The first step in

that process is gaining control over the bilayer structure(s) we will use to support the trans-membrane proteins. We are thus interested in understanding the molecular processes that mediate phase separation in model bilayers, and have studied the organization and dynamics of model bilayer systems using a tethered fluorescent probe. We utilize the spectroscopic properties of the tethered chromophore 2-(12-(7-nitrobenz-2-oxa-1,3-diazol-4-yl)amino)dodecanoyl-1-hexadecanoyl-*sn*-glycero-3-phosphocholine (NBD C_{12}-HPC, Figure 4.1) to interrogate local organization in our model bilayers. This chromophore, which is connected to an acyl chain terminus of a phospholipid, incorporates into the bilayer structure of unilamellar vesicles, and we can control the composition of these vesicles readily. We note that the NBD chromophore is well known to exhibit a solvent polarity-dependent fluorescence lifetime,[6-9] but we find that the motional properties of this chromophore shed more light on the organization of the bilayer environment. The transient fluorescence anisotropy decay measurements we use have a well established theoretical framework for their interpretation, both for free and tethered chromophores. In this work we excite the sample using two different spectroscopic processes, one- and two-photon excitation, because the use of two different modes of excitation allows us to extract detailed information on the motional properties of the chromophore. Our data show that the NBD chromophore exists within a significantly restricted environment in phospholipid bilayers, and that both motion about the tethering bond and longer timescale precession within the bilayer structure play a role in the dynamics of this system. When multiple bilayer constituents are added, the dynamics of the NBD chromophore change, with molecular-scale motion in the multi-component medium appearing more rapid and isotropic than in a pure lipid bilayer. Our
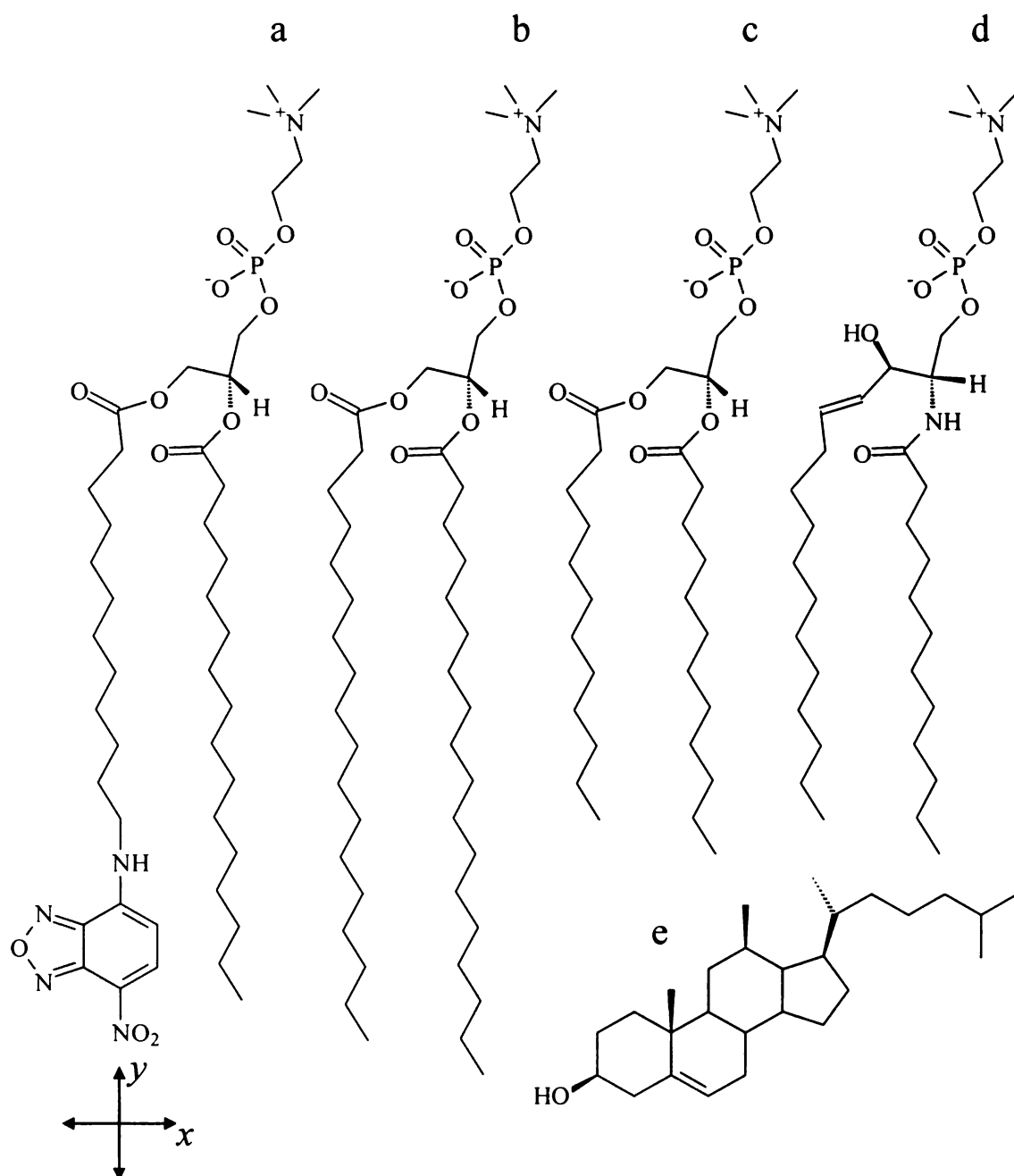
Figure 4.1 Structures of compounds used in this work: (a) NBD-C$_{12}$HCP, (b) DSPC, (c) DLPC, (d) sphingomyelin, and (e) cholesterol.

94

infinite time anisotropy data indicate that the composition of the bilayer mediates the mesoscopic rigidity of the system substantially, with cone angle of chromophore varying from ca. 60° for the pure lipid bilayer to ca. 10° for bilayers comprised of lipid, cholesterol and sphingomyelin. This effect has been seen before[10] and our data point collectively to the creation of molecular scale disorder and a mesoscopic increase in bilayer rigidity. The only structural motif consistent with these findings is that of a heterogeneous, phase separated bilayer structure.

Experimental

Materials. The fluorescent probe 2-(12-(7-nitrobenz-2-oxa-1,3-diazol-4-yl)amino)dodecanoyl-1-hexadecanoyl-*sn*-glycero-3-phosphocholine (NBD C_{12}-HPC) was obtained from Molecular Probes Inc. and used without further purification. The bilayer constituents 1,2-dilauroyl-*sn*-glycero-3-phosphocholine (DLPC, mp = -1°C), 1,2-distearoyl-*sn*-glycero-3-phosphocholine (DSPC, mp = 55°C), egg sphingomyelin (SPM) and powdered cholesterol were obtained from Avanti Polar Lipids, Inc. and used as received.

For the construction of unilamellar vesicles, constituents were prepared in a 1:1:1 mole ratio of phospholipid : cholesterol : sphingomyelin or a 2:1 mole ratio of phospholipid : cholesterol for the multicomponent systems. For the mixed lipid systems, the ratio of phospholipids used was 1:1. A total of six vesicle solutions were produced: NBD C_{12}-HPC/DLPC, NBD C_{12}-HPC/DLPC/cholesterol, NBD C_{12}-HPC/DLPC/cholesterol/SPM, NBD C_{12}-HPC/DSPC, NBD C_{12}-HPC/DSPC/cholesterol, and NBD C_{12}-HPC/DSPC/cholesterol/SPM. NBD C_{12}-HPC. The concentration of NBD C_{12}-HPC in each of these bilayer structures was maintained at $\sim 10^{-4}$ M. Chloroform was evaporated from the lipid solution, then it was dissolved in a 4:1 benzene : methanol solution. The benzene : methanol solvent was then evaporated and the resulting lipid mixture was dissolved in 10 mM Tris® buffer (Aldrich) adjusted for pH~8 in Milli-Q water. For further mixing, the solution was placed in liquid nitrogen for 5 minutes, then in a hot-water bath for 5 minutes, and vortexed for approximately 2 minutes. This process was repeated four more times. The extrusion method was used to produce unilamellar vesicles of ~100 nm diameter. A syringe-based mini-extruder (Avanti Polar

Lipids) was used to extrude the lipid suspension between a polycarbonate filter eleven times to produce unilamellar vesicles of ~100 nm diameter (Figure 4.2).

Steady State Measurements. All absorption spectra were recorded with 1 nm spectral resolution using a Cary model 300 double beam UV-Visible absorption spectrophotometer. All emission spectra were recorded with a Spex Fluorolog 3 spectrometer at a spectral resolution of 3 nm for both excitation and emission monochromators.

Time Correlated Single Photon Counting Measurements. Time-resolved fluorescence lifetime and anisotropy measurements were performed using a time correlated single photon counting (TCSPC) system. This system has been described in detail elsewhere[11] and we provide only a brief recap of its features here. The source laser is a CW mode-locked Nd:YAG laser (Coherent Antares 76-S) that produces 100 ps 1064 nm pulses at a 76 MHz repetition rate. The second or third harmonic of the output of this laser is used to excite a cavity dumped dye laser (Coherent 702-2), operating at 650 nm with Rhodamine 610 dye (Exciton, 532 nm pump) for two photon excitation experiments, or at 460 nm with Stilbene 420 dye (Exciton, 355 nm pump) for one photon excitation experiments. The dye laser outputs were 5 ps pulses at a repetition rate of 4 MHz for both excitation wavelengths. Fluorescence signals were detected using a Hamamatsu R3809U microchannel plate photomultiplier tube detector with a Tennelec 454 quad constant fraction discriminator and Tennelec 864 time-to-amplitude converter and biased amplifier used for signal processing. For this system the instrument response time is ~ 35 ps. Time-resolved fluorescence intensities were collected at 0°, 54.7° and 90° with

respect to the vertically polarized excitation pulse, and the response function was not

deconvoluted from the data.
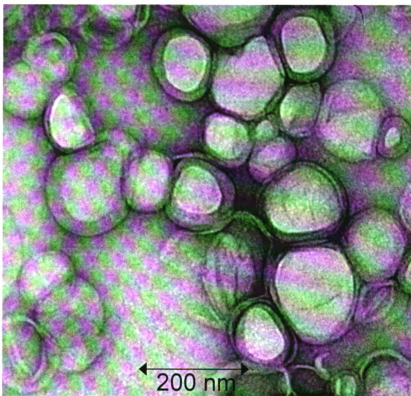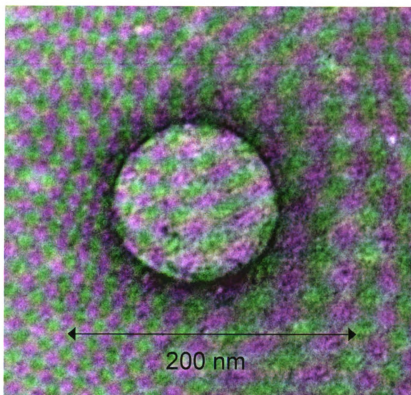
Figure 4.2 TEM micrographs of unilamellar vesicles. Scale bars indicate distances of 200 nm.

Results and Discussion

The central purpose of this work is to understand the molecular scale environment that exists within a lipid bilayer structure and to elucidate the role of bilayer constituents such as cholesterol and sphingomyelin in mediating these dynamics. Information available from this work bears on issues such as the environment available to transmembrane proteins and the local viscosity of these fluid bilayer structures. To evaluate the local environment(s) formed by lipid bilayer structures, we have used the chromophore NBD tethered to a phospholipid (NBD C_{12}-HPC) as a probe in unilamellar vesicle structures. While we are primarily concerned with the dynamics of the chromophore, it is important to have some knowledge of the specific region within the unilamellar vesicle where the tethered chromophore resides. We have addressed both of these issues using time-resolved fluorescence measurements, where lifetime data provide information on the polarity of the chromophore local environment and anisotropy decay data acquired using both one- and two-photon excitation yield detailed information on the motional properties of the chromophore. Because these two types of measurements are sensitive to different aspects of the chromophore environment, we consider the results of each separately.

We first examine the fluorescence lifetime of NBD C_{12}-HPC imbedded in vesicles. For NBD, a substantial body of literature has established that the steady state absorption and emission spectra and the fluorescence lifetime of this compound are sensitive to the polarity of its immediate environment.[6-8,12-14] The absorption and emission maxima for NBD shift to the red with increasing polarity, while the Stokes shift

for this chromophore remains approximately constant over a range of solvents.[6-8,12-14] Our steady state absorbance data show that for all vesicle solutions, the absorption maximum of NBD occurs at ~460 nm and the emission maximum is centered at ~550 nm (Figure 4.3). Time-resolved fluorescence lifetime data show that for both one and two-photon excitation, the S_1 population decay of NBD C_{12}-HPC contains two exponential components in all cases, indicating that the chromophore resides in at least two environments of differing polarity. The long lifetime component for all cases is between ~0.8 and 1.3 ns, while the short lifetime component is between ~100 and 400 ps (Figure 4.4). While these lifetimes are significantly different, the difference in environments for these two sub-populations is likely not very great. From our prior work, we have found that the hexanoic acid derivative of NBD selectively partitions in phosphocholine bilayers into the region near the lipid head group, and for this chromophore the recovered lifetime is ca. 1.1 ns. Other literature[7] reports a short lifetime for NBD derivatives in an aqueous environment, suggesting that our NBD chromophore is in all cases in the vicinity of the lipid head groups. We note that the lifetime of NBD derivatives in solvents of moderate polarity exhibit lifetimes on the order of 8 ns,[15] indicating that for these experiments the tethered NBD chromophore is not in close proximity to the interior of the bilayer. It is reasonable to expect that the acyl chain to which the NBD chromophore is attached has "folded back", leaving the NBD in relatively close proximity to the polar headgroup region of the vesicles, rather than in the nonpolar core region.[12] The immediate environment of a chromophore has long been recognized for having an influence fluorescence lifetime. Molecules that reside in an environment where there is a dielectric gradient on the length scale of the chromophore can experience a substantial

modulation of their fluorescence lifetime, and we believe that to be the situation here.[16-19]

Within the bilayer structure, there is a gradient in dielectric response from the acyl region

($\varepsilon \sim 4$) to the aqueous region ($\varepsilon \sim 82$) over a distance of several Ångströms. Where in

this gradient the NBD chromophore resides, and the orientation of its transition moment

relative to the gradient, will influence its fluorescence lifetime. Thus, the presence of two

distinct fluorescence lifetime components in our data should not be taken as a necessary

indication of two substantially different environments, but rather, these data signify

subtle positional differences for sub-populations of the tethered chromophore. These data

do not provide sufficient information by themselves, however, to draw any firm structural

or organizational conclusions. In order to understand the local environment of the NBD

chromophore in more detail, we turn to fluorescence anisotropy measurements.

For our experimental conditions, the fluorescence anisotropy data for NBD C_{12}-

HPC in vesicles result from molecular reorientation. There is a well established

theoretical framework for the interpretation of fluorescence anisotropy data, under

conditions of both one and two photon excitation. For both means of excitation, the

essential physics of the relaxation process remains the same – an initially anisotropic

population returns to an equilibrium orientational distribution. The difference between

one and two photon excitation measurements lies in the initial orientational distribution

of the anisotropic photo-selected population and the relationship between the incident

electric field polarization(s) and the excited state orientational distribution. For this

reason, the relationship between the time constant(s) of the induced orientational

anisotropy decay and the Cartesian components of the rotational diffusion constant will
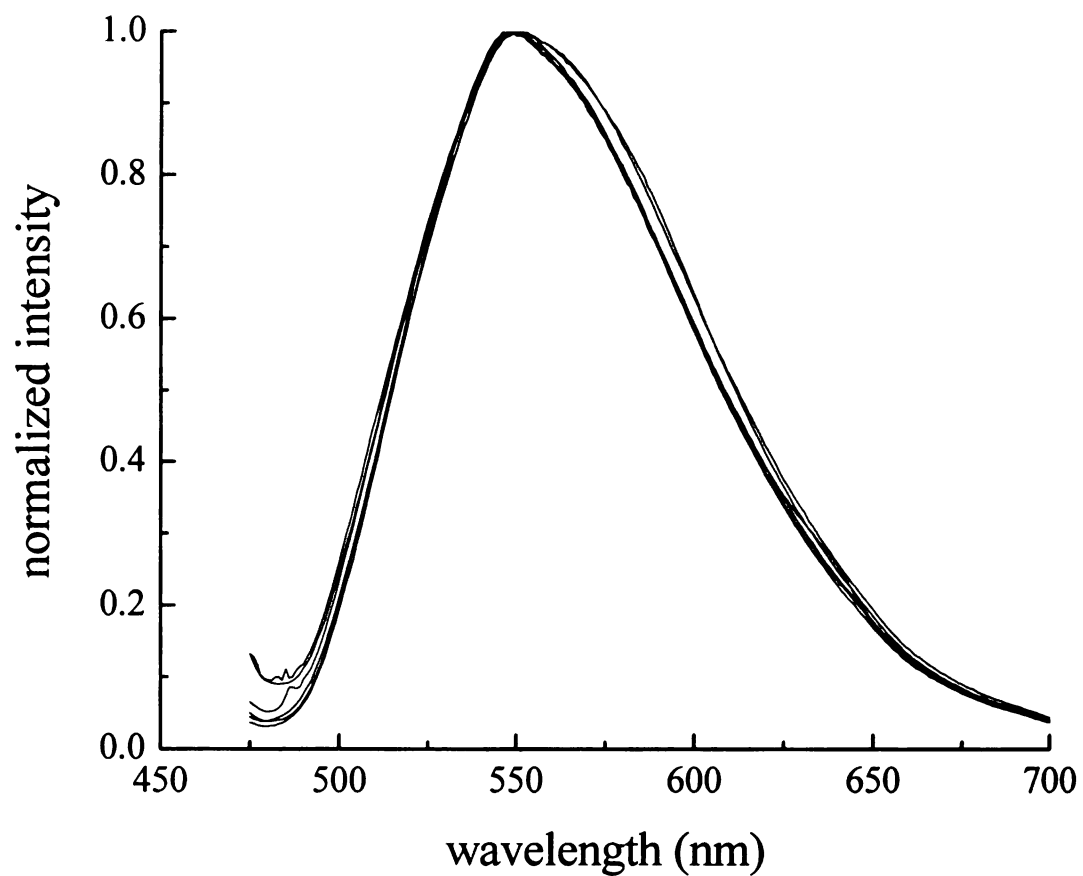
Figure 4.3. Normalized emission spectra for NBD-C$_{12}$HPC in unilamellar vesicles. Emission maxima are centered at ca. 550 nm in all cases.
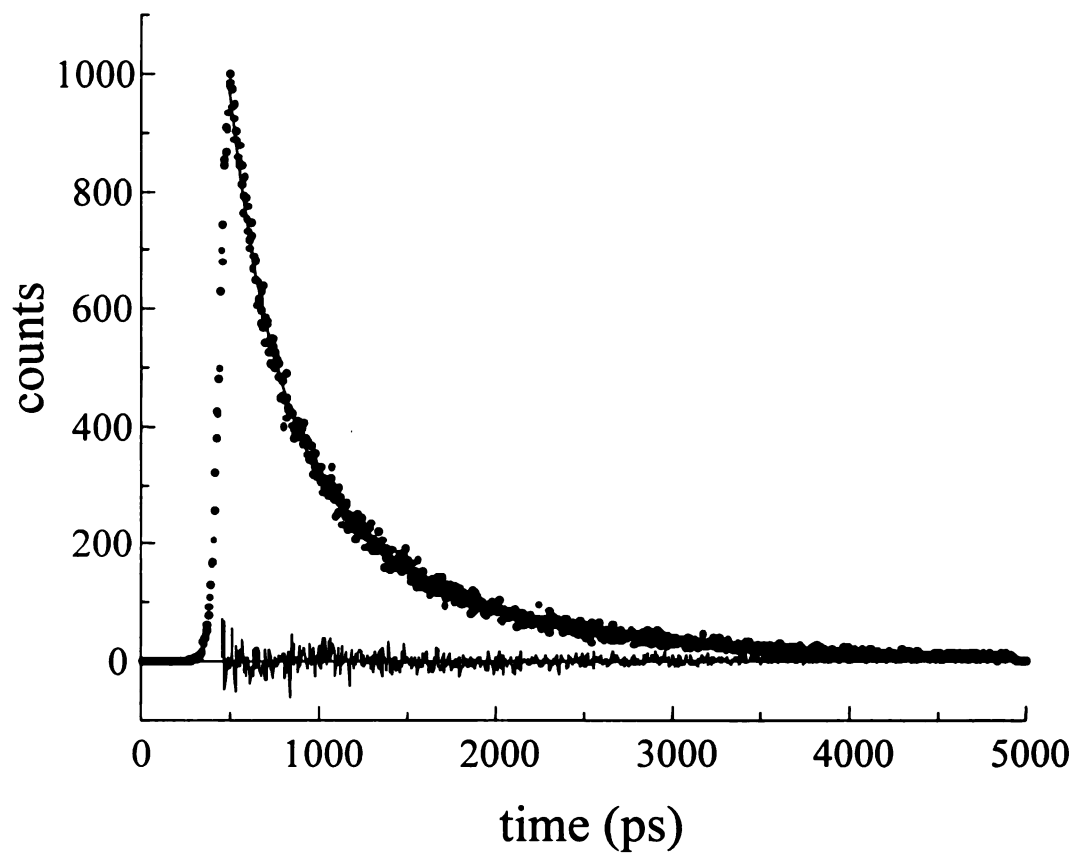
Figure 4.4. Lifetime decay of NBD-C$_{12}$HPC in unilamellar vesicles composed of DLPC. The lifetime is a double exponential decay with τ_1=321 ± 22 ps and τ_2=1331 ± 147 ps.

differ for the two modes of excitation, and we take advantage of this difference to extract information which is not available from either measurement individually.For one-photon excitation, the induced orientational anisotropy function, R(t), is generated from the polarized emission transients according to Eq.4.1,

$$R(t) = \frac{I_{\parallel}(t) - I_{\perp}(t)}{I_{\parallel}(t) + 2I_{\perp}(t)} \qquad (4.1)$$

where $I_{\parallel}(t)$ and $I_{\perp}(t)$ are the emission intensities polarized parallel and perpendicular to the vertically polarized excitation pulse. The chemical information extracted from these measurements is contained in the number of exponential decays and their time constant(s) that constitute R(t). A note is in order about the experimental data we present here. Our instrument response time is typically 35 ps fwhm and several of the anisotropy decay time constants we report here are ca. 100 ps. Our past experience has consistently shown that the deconvolution of the instrument response function from our raw data changes the observed anisotropy decay time constant by less than the experimental uncertainty, even for decays with time constants as fast at 100 ps. Because of the limited S/N ratio that characterize our data and our desire to not manipulate the experimental data more than necessary, we have not attempted deconvolution.

While R(t) may be characterized by up to five decays, typically only one or two decays are resolved experimentally. The relationship between the functionality of R(t) and the chromophore molecular properties has been described in detail previously.[20-22] Chuang and Eisenthal's treatment of R(t) allows for this function to be simplified to two general cases, where the shape of the rotor describes the time-averaged volume swept out

by the rotating species.[22] A Type I rotor is characterized by a distortion along the axis coincident with the transition moment axis and a Type II rotor is characterized by a distortion from a spherical shape along an axis perpendicular to the transition moment axis. These rotor designations correspond to the more traditional descriptions of prolate and oblate rotor as follows: For a Type I rotor with the transition moments along the ith axis, $D_i > D_j = D_k$ (i,j,k = x,y,z) are prolate, and $D_i < D_j = D_k$ are oblate. For a Type II rotor, $D_k > D_i = D_j$ is prolate and $D_k < D_i = D_j$ is oblate. We prefer to use the Type I and Type II designations here because the notion of prolate and oblate rotors is not necessarily physically clear in the context of a restricted or tethered environment. There are two general solutions to these cases.[21,22] For the transition moment polarized along the ith axis, with $D_i \neq D_j = D_k$,

$$R(t) = 0.4 \exp(-6 D_k t) \tag{4.2}$$

And for $D_k \neq D_i = D_j$,

$$R(t) = 0.1 \exp(-6 D_i t) + 0.3 \exp(-(2 D_i + 4 D_k) t) \tag{4.3}$$

Despite these simplifications to the time-averaged shape of the reorienting species, there remains ambiguity in the interpretation of anisotropy decay data, arising form the orientations of the absorbing and emitting transition dipole moments. In order to resolve which of these conditions obtains for our results, we must have knowledge of the absorption and emission transition dipole moment orientations for NBD C_{12}-HPC. For the NBD chromophore, the one photon absorption and emission transition dipole moments are in the π-system plane with x designating the long molecular axis and y designating the short axis. Based on this assignment, and the location of the connection

of the phospholipid acyl chain to the chromophore (Figure 1), the motional constraints relevant to NBD C_{12}-HPC are $D_y \neq D_x = D_z$. With this axis assignment Eqs. 4.2 and 4.3 can be modified to describe the possible decay functionalities for R(t) in terms of the Cartesian axes,

$$\text{x-polarized transition} \quad R(t) = 0.3\exp\left(-\left(4D_y + 2D_x\right)t\right) + 0.1\exp(-6D_x t) \quad (4.4)$$

$$\text{y-polarized transition} \quad R(t) = 0.4\exp(-6D_x t) \quad (4.5)$$

The fact that we recover single exponential decay anisotropies for all one-photon excited measurements (*vide infra*) suggests that the $S_1 \leftrightarrow S_0$ transitions are y-axis polarized for NBD. While it is possible that our S/N ratio does not allow us to resolve a second component, analysis of the two photon excited data for either x- or y-polarized emission yields physically meaningful results (*i.e.* $D_i > 0$) only for y-polarized emission (*vide infra*). The recovered time constant for one photon excitation is therefore related to the motion about the x-axis. A simplistic interpretation of this treatment implies that the chromophore is free to rotate in solution, which is not the case with NBD C_{12}-HPC. The information obtained on D_x must therefore be reflective of motions within the bilayer structure that are either precessional or random walk in nature, and we discuss this point in more detail below, after considering the information content of two-photon excited anisotropy data.

We borrow from Johnson's excellent treatment of two-photon excited anisotropy decay data to interpret our results.[9,23-26] Induced orientational anisotropy decay functions are generated for both linearly ($r_1(t)$) and circularly ($r_2(t)$) polarized light and are given by:

$$r_1(t) = \frac{I_{\parallel}^{linear}(t) - I_{\perp}^{linear}(t)}{I_{\parallel}^{linear}(t) + 2I_{\perp}^{linear}(t)}$$

$$r_2(t) = \frac{I_{\parallel}^{circular}(t) - I_{\perp}^{circular}(t)}{2I_{\parallel}^{circular}(t) + I_{\perp}^{circular}(t)}$$

(4.6)

For both excitation polarizations, the anisotropy decays are characterized by two time constants, τ_0 and τ_2, weighted according to the properties of the chromophore.[9,24,26]

$$r_1(t) = r_1(0)\left[c_0 \exp(-t/\tau_0) + c_2 \exp(-t/\tau_2)\right]$$

$$r_2(t) = r_2(0)\left[d_0 \exp(-t/\tau_0) + d_2 \exp(-t/\tau_2)\right]$$

(4.7)

The relative contributions of the time constants are given by the prefactors c_i and d_i. These prefactors are[25]

$$c_0 = \frac{(\sqrt{3}a + b)\left[3(\sqrt{3}a + b)S_{xx}^2 + 3(-\sqrt{3}a + b)S_{yy}^2 + 2bS_{xx}S_{yy} + 4bS_{xy}^2\right]}{7N^2(3S_{xx}^2 + 3S_{yy}^2 + 2S_{xx}S_{yy} + 4S_{xy}^2)}$$

(4.8)

$$c_2 = \frac{(a - \sqrt{3}b)\left[3(a - \sqrt{3}b)S_{xx}^2 + 3(a + \sqrt{3}b)S_{yy}^2 + 2aS_{xx}S_{yy} + 4aS_{xy}^2\right]}{7N^2(3S_{xx}^2 + 3S_{yy}^2 + 2S_{xx}S_{yy} + 4S_{xy}^2)}$$

(4.9)

$$d_0 = \frac{(\sqrt{3}a + b)\left[(\sqrt{3}a + b)S_{xx}^2 + (-\sqrt{3}a + b)S_{yy}^2 - 4bS_{xx}S_{yy} + 6bS_{xy}^2\right]}{14N^2(S_{xx}^2 + S_{yy}^2 - S_{xx}S_{yy} + 3S_{xy}^2)}$$

(4.10)

$$d_2 = \frac{(a - \sqrt{3}b)\left[(a - \sqrt{3}b)S_{xx}^2 + (a + \sqrt{3}b)S_{yy}^2 - 4aS_{xx}S_{yy} + 6aS_{xy}^2\right]}{14N^2(S_{xx}^2 + S_{yy}^2 - S_{xx}S_{yy} + 3S_{xy}^2)}$$

(4.11)

The relative amplitudes of the decay time constants will provide information about the values of the Cartesian components of the rotational diffusion constant. The parameters a, b, N and Δ are related to the diffusion constant by

$$a = \sqrt{3}(D_y - D_x)$$
$$b = 2D_z - D_y - D_x + 2\Delta$$
$$N^2 = a^2 + b^2$$
$$\Delta = (D_x^2 + D_y^2 + D_z^2 - D_x D_y - D_y D_z - D_x D_z)^{1/2}$$

(4.12)

While Eqs. 4.7 indicate that two anisotropy decay time constants should be recovered for two photon excitation measurements, this is not always the case. For cases where τ_0 and τ_2 are similar, the time constants observed experimentally are τ_{r1} (linear polarization) and τ_{r2} (circular polarization), which are weighted averages of τ_0 and τ_2.[25] It is also possible, depending on the spectroscopic and motional properties of the chromophore, that one or more of the terms c_i and d_i could assume values of zero, and in this case, the time constant observed is simply the time constant not associated with the zero-coefficient term. This situation obtains for our experimental conditions, with $D_x = D_z$, leading to the term $(\sqrt{3}a + b) = 0$. The imposition of this condition causes the prefactors c_0 and d_0 to become zero, and for our experimental conditions, $\tau_{r1} = \tau_2$, and $\tau_{r2} = \tau_2$ where $\tau_2 = (6D + 2\Delta)^{-1}$.[25] The reorientation times recovered from linearly polarized excitation and circularly polarized excitation are predicted to be identical, and τ is related to both D_y and D_x.[25]

$$\tau_2 = \frac{1}{(2D_x + 4D_y)}$$

(4.13)

The time constant recovered from two-photon excited decays contains contributions from both D_y and D_x, while the one-photon excited anisotropy decay time constant is related to D_x. From these two measurements we can, in principle, determine D_x and D_y uniquely. We caution, however, that the chromophore motions are restricted to some extent by the

fact that they are tethered to the phospholipid, and we consider the consequences of this structural condition next.

At this point it is useful to note that the R(0) values that we extract from our experimental data do not approach the theoretical limits of either the one or two photon treatments of the data. The quantity R(0), for both one and two photon excitation, is related to the angle between the excited and emitting transition dipole moments. This quantity is not related to the rotational diffusion coefficient, and there is a measurable perturbation of the recovered time constants only where R(0) ~ 0.[27] This condition occurs for an angle of 54.7° between the transition moments for one photon excitation and at 35.3° for two photon excitation.[28] The fact that our R(0) values all lie in the ~0.1-0.3 range indicates that the determination of the rotational diffusion coefficients are essentially unaffected by the angle between the transition moments for either type of excitation.[21,27]

The theoretical constructs used to interpret fluorescence anisotropy data depend on the constraints imposed on the chromophore by its local environment. When the motional freedom of a molecule is restricted in some manner, such as incorporation into a bilayer structure and/or tethering to an interface, the data are typically treated within the framework of the hindered rotor model.[29-32] This model takes into account the fact that the initially non-random chromophore distribution selected by the excitation pulse is not free to rerandomize completely. The inability of the chromophore to relax into a fully random orientational distribution is manifested as a non-zero infinite-time anisotropy, R(∞). The decay time constant for the anisotropy function is the time required for the

system to relax from the non-random orientational distribution selected by the excitation pulse to its steady state orientational distribution, and this time constant is given by

$$\tau_{HR} = \frac{7\theta_o^2}{24D_w}$$

(4.14)

Where θ_0 is the semi-angle of the cone which the (tethered) molecule sweeps out as it moves within its confines, and D_w is the "wobbling diffusion constant" which describes the motion of the chromophore about its tethering bond. This description of molecular motion is not determined sufficiently for our purposes. While the quantity θ_0 is useful as a measure of average disorder in the system, the quantity D_w provides very little in the way of detailed molecular scale insight into chromophore motion.

It is important to consider at this point the role of symmetry and timescale in extracting $R(\infty)$ information from our data. This issue arises because of the number of phenomena that are operating simultaneously on the chromophore. Specifically, the translational mobility of the chromophore within the vesicle walls and the rotational motion of the vesicle as a whole need to be considered. Based on the average size of our vesicles (ca. 100 nm diameter), we estimate its rotational diffusion time to be ca. 125 μs. The time scale of vesicle reorientation is thus long relative to chromophore local rotational motion. Translational motion of the vesicle constituents ($D_T \sim 50$ μm^2/s) allows the chromophore to sample the surface area of the vesicle in ca. 500 μs. Thus, on the time scale of chromophore reorientation, neither vesicle rotation nor chromophore translation will contribute to any discernible extent. Our ps time scale measurements sample exclusively the molecular rotational motion of the chromophore. We can thus

extract meaningful R(∞) values from our experimental data, and relate that information to local organization within the vesicle wall.

For a hindered rotor, the time-course of R(t) behaves according to Eq. 4.15:

$$R(t) = R(\infty) + (R(0) - R(\infty))\exp(-t/\tau_{HR})$$ (4.15)

Where τ_{HR} is given by Eq. 4.14. The quantity R(∞) is related to the size of the cone in which the chromophore resides,

$$\left(\frac{R(\infty)}{R(0)}\right)^{1/2} = 0.5\left(\cos\theta_0\left(1+\cos\theta_0\right)\right)$$ (4.16)

Our experimental data for R(0) and R(∞) are tabulated in Table 4.5, and from these data we calculate cone angles θ_0 in the range of ~60° to ~10° for these bilayer structures. We will return to consideration of the significance of these data after dealing with the motional component of our signals.

If we were to interpret our experimental anisotropy data simply in the context of the hindered rotor model, we would be left in all cases with the anisotropy decay time constant being associated with the same physical quantities θ_0 and D_w, and this situation would not account for the excitation and system dependencies we see in our data. Our experimental data (Table 4.1) demonstrate that this is not the case, so that a more detailed interpretation than is afforded by Eq. 4.15 is required. We are not aware of any treatments in the literature that attempt to make correspondence between the hindered rotor model[20,32,33] and the more general treatment[22] for fluorescence anisotropy decays which consider explicitly the Cartesian components of the rotational diffusion coefficient.

Regardless of the extent of confinement, the relaxation of the excited chromophore population will scale as $P_2[\mu(0){\cdot}\mu'(t)]$ for one photon excitation, and as $P_2[S(0){\cdot}\mu'(t)]$ for two photon excitation. Both of these expressions can be cast in terms of D_x, D_y and D_z.[9]

As discussed above, we can treat the fluorescence anisotropy data for one and two photon excitation according to Chuang and Eisenthal[22] and Johnson et al.,[9,23-26] and can extract values for D_x and D_y for NBD C_{12}-HPC from the data. Based on the functional form of the anisotropy decays for both one and two photon excitation, the NBD chromophore reorients as a Type I rotor with $D_y \neq D_x = D_z$, with the absorption and emission transition dipole moments oriented along the chromophore y-axis. Attempts to locate the transition dipole moment(s) along the chromophore x (long) axis yield expressions that are inconsistent with the functional form and time constants of our experimental data. For an x-polarized transition, our experimental data yield at least one negative diffusion coefficient, and the results for one- and two-photon excitation are not self-consistent. The anisotropy decay treated by the various models must represent the same physical phenomenon; the re-randomization of an initially non-random orientational distribution, and there must thus be a connection between the two models.

For NBD-C_{12}-HPC, the y-axis corresponds to that axis along which the chromophore is tethered, x is the long in-plane axis and z is perpendicular to the x-y plane. In this model, the unique motion for the tethered chromophore will be about the tethering, y-axis. Apparent rotational motions about the x- and z- axes will actually be either precessional or random walk motions within the (nominally) conic volume the

113

tethered chromophore sweeps out. We consider next the experimental data, and how the anisotropy decay times differ due to the different modes of excitation.

We present in Tables 4.1 – 4.3 the fluorescence lifetime and anisotropy decay time data for excitation of NDB C_{12}-HPC by one photon excitation at 460 nm (Table 4.1), and by two photon excitation with linearly (Table 4.2) and circularly (Table 4.3) polarized light at 650 nm. For each system we recover a two component fluorescence lifetime, and for a given vesicle system, the lifetimes we recover are the same to within the experimental uncertainty for all modes of excitation because the emitting state is the same in all cases. The anisotropy decay data shown in Tables 4.1 – 4.3 reveal a dependence on both the bilayer composition and on the mode of excitation.

We have interrogated the dynamics of NBD C_{12}-HPC unilamellar vesicles comprised solely of the phospholipid as well as vesicles containing cholesterol and/or sphingomyelin in addition. The intent of these experiments was to understand the constraints imposed on the chromophore by the phospholipids and to evaluate the role of the added constituents on bilayer organization over a range of length scales. The one-photon excited anisotropy decay time constant is related to the rotational diffusion coefficient by $\tau = (6D_x)^{-1}$. For a Type I ellipsoid tethered along its y-axis, $D_x = D_z$ and the recovered one-photon reorientation time constants represent motion that lies between precessional and random walk, as constrained by its tether. This motion, while not fully rotational, reflects an angular displacement with time, and will appear as a nominally rotational motion to our experiment because of the inherent distribution of environments that the chromophore occupies. In comparison, for two-photon excited measurements,

114

Table 4.1 One photon excitation, fluorescence lifetimes and anisotropy decay time constants in vesicles of different compositions. Chol = cholesterol, SPM = sphingomyelin.

Vesicle composition	Fluorescence Lifetime τ_1 (ps)	Fluorescence Lifetime τ_2 (ps)	τ_{OR} (ps)
NBD-C_{12}HPC, DLPC	321 ± 22 (60±1%)	1331 ± 147 (40±1%)	572 ± 55
NBD-C_{12}HPC, DLPC, chol	179 ± 18 (83±1%)	808 ± 64 (17±1%)	215 ± 35
NBD-C_{12}HPC, DLPC, chol, SPM	132 ± 20 (67±2%)	581 ± 71 (33±2%)	191 ± 18
NBD-C_{12}HPC, DSPC	144 ± 25 (42±3%)	1044 ± 158 (58±3%)	789 ± 17
NBD-C_{12}HPC, DSPC, chol	119 ± 4 (72±3%)	793 ± 9 (28±3%)	110 ± 19
NBD-C_{12}HPC, DSPC, chol, SPM	135 ± 8 (97±3%)	750 ± 60 (3±3%)	94 ± 11

where the anisotropy decay time constant has contributions from D_x and D_y (Eq. 4.13), we anticipate that the time constants will, in general be different, and this is seen experimentally. We note that, as predicted on theoretical grounds, the anisotropy decay times acquired for linearly and circularly polarized two photon excitation yield the same time constants for a given system.

We present in Table 4.4 the calculated diffusion coefficients D_x and D_y for NBD-C_{12}-HPC in vesicles of varying composition, along with the calculated viscosity and the D_y/D_x aspect ratio. There are several interesting pieces of information in these data which provide significant insight into the organization of our bilayers. We have extracted the values for D_x and D_y from the experimental anisotropy decay data (Tables 4.1-4.3) and Eqs. 4.5 and 4.13. In order to estimate the local viscosity sensed by our chromophore, we have used the modified Debye-Stokes-Einstein equation.[20-22,34,35]

$$\tau_{OR} = \frac{\eta V f}{k_b T S} = \frac{1}{6D} = \frac{1}{4D_x + 2D_y}$$ (4.17)

where η is the viscosity of the medium surrounding the reorienting moiety, V is the solute hydrodynamic volume, which we take to be the volume of the NBD chromophore for this work, $V_{NBD} = 106 \ \text{Å}^3$,[36] f is the frictional solvent-solute boundary condition, and S is the solute shape factor. We calculate the value of D from our experimental quantities D_x and D_y and with the assumption that $D_x = D_z$. D is defined as the average of the Cartesian components, $D = (D_x+D_y+D_z)/3 = (2D_x+D_y)/3$. The modified DSE equation was derived to describe the rotational motion of an ellipsoid in a continuum fluid, where there is no

116

Table 4.2. Two photon excitation (linear polarization), fluorescence lifetimes and anisotropy decay time constants in vesicles of different compositions.

Lipid composition	Fluorescence Lifetime τ_1 (ps)	Fluorescence Lifetime τ_2 (ps)	τ_{OR} (ps)
NBD-C$_{12}$HPC, DLPC	247 ± 8 (58±2%)	1029 ± 17 (42±2%)	123 ± 9
NBD-C$_{12}$HPC, DLPC, chol	166 ± 11 (76±8%)	1061 ± 82 (24±8%)	183 ± 9
NBD-C$_{12}$HPC, DLPC, chol, SPM	127 ± 5 (57±14%)	944 ± 13 (43±14%)	106 ± 6
NBD-C$_{12}$HPC, DSPC	115 ± 6 (68±2%)	890 ± 13 (32±2%)	189 ± 7
NBD-C$_{12}$HPC, DSPC, chol	118 ± 15 (63±3%)	931 ± 37 (37±3%)	156 ± 7
NBD-PC, DSPC, chol, SPM	106 ± 8 (70±5%)	883 ± 33 (30±5%)	105 ± 3

Table 4.3. Two photon excitation (circular polarization), fluorescence lifetimes and anisotropy decay time constants in vesicles of different compositions.

Lipid composition	Fluorescence Lifetime τ_1 (ps)	Fluorescence Lifetime τ_2 (ps)	τ_{OR} (ps)
NBD-C_{12}HPC, DLPC	266 ± 9 ($60 \pm 1\%$)	1110 ± 15 ($40 \pm 1\%$)	117 ± 13
NBD-C_{12}HPC, DLPC, chol	171 ± 9 ($51 \pm 1\%$)	1087 ± 24 ($49 \pm 1\%$)	166 ± 18
NBD-C_{12}HPC, DLPC, chol, SPM	128 ± 13 ($53 \pm 7\%$)	910 ± 38 ($47 \pm 7\%$)	80 ± 11
NBD-C_{12}HPC, DSPC	142 ± 6 ($66 \pm 1\%$)	1039 ± 18 ($34 \pm 1\%$)	176 ± 3
NBD-C_{12}HPC, DSPC, chol	202 ± 21 ($48 \pm 4\%$)	1014 ± 44 ($52 \pm 4\%$)	160 ± 8
NBD-C_{12}HPC, DSPC, chol, SPM	114 ± 9 ($67 \pm 3\%$)	879 ± 29 ($33 \pm 3\%$)	101 ± 9

118

tethering attachment. While our application of Eq. 4.17 to a bilayer structure is clearly at odds with the original intent of the model, we believe that we are justified in making this approximation because of the fluid nature of the bilayer system. As noted above, it is fair to consider that there will be motions associated with both the chromophore and with the vesicle itself. We assert that these motions are well isolated from one another in the time domain. Specifically, if we apply Eq. 4.17 to the vesicle as a whole, (r ~ 500 Å), we calculate a reorientation time of 126 μs; six orders of magnitude longer than the chromophore reorientation time. Even if this calculation were in error by as much as a factor of two, such a difference in time scales would render the overall motion of the vesicle undetectably slow on the timescale of our measurements.

We recognize that the viscosity values we extract from the DSE model are likely characterized by a systematic offset from the actual viscosities, but our primary purpose in using this model is that it allows a basic comparison to be made across the range of experimental conditions we have employed here. We obtain values of ca. 7.8 cP for NBD C_{12}-HPC in DLPC (mp = -1°C) and ca. 11.6 cP for NBD C_{12}-HPC in DSPC (mp = 55°C). These values are entirely consistent with recent data we have acquired for DMPC above and below its gel-to-fluid transition temperature using a different, non-tethered probe.[37] We note that the aspect ratio, D_y/D_x, is significantly greater than unity for the NBD chromophore in the pure lipid bilayer, consistent with molecular-scale motional freedom constrained by the presence of significant lipid acyl chain organization. With the addition of cholesterol to the bilayer, we see two noteworthy changes. The first is a decrease in the measured viscosity (much more pronounced for DSPC), indicating a

Table 4.4. Cartesian components of the rotational diffusion coefficient for NBD C_{12}-HPC, and resulting viscosities calculated from these D values.

Lipid composition	D_x (MHz)	D_y (MHz)	η from D	D_y/D_x
NBD-C_{12}HPC, DLPC	291	1938	7.8	6.7
NBD-C_{12}HPC, DLPC, chol	775	1041	7.5	1.3
NBD-C_{12}HPC, DLPC, chol, SPM	873	2252	4.9	2.6
NBD-C_{12}HPC, DSPC	211	1261	11.6	6.0

Table 4.5 Calculated cone angles for hindered rotor model based on zero and infinite time anisotropy data for NBD-C_{12}-HPC in vesicles of varying composition.

Vesicle composition	τ HR (ps)	R(0)	R(∞)	θ_0
NBDPC, DLPC	572 ± 55	0.15 ± 0.01	0.02 ± 0.01	61 ± 7
NBDPC, DLPC, chol	215 ± 35	0.19 ± 0.02	0.10 ± 0.04	37 ± 12
NBDPC, DLPC, chol, SPM	191 ± 18	0.37 ± 0.07	0.35 ± 0.04	11 ± 16
NBDPC, DSPC	789 ± 17	0.15 ± 0.03	0.04 ± 0.01	51 ± 8
NBDPC, DSPC, chol	110 ± 19	0.20 ± 0.07	0.09 ± 0.05	41 ± 18
NBDPC, DSPC, chol, SPM	94 ± 11	0.19 ±0.02	0.14 ± 0.03	26 ± 11

decrease in the organization of the bilayer on a molecular length scale. Along with this change we see that D_y/D_x changes from 6.7 to ca. 1.3 for DLPC, and from 6.0 to 0.5 for DSPC. This remarkable change is a direct indication of the local disorder introduced by cholesterol in the region sensed by NBD. Examination of D_y and D_x values reveals that D_y decreases upon addition of cholesterol, while D_x increases slightly. The decrease in D_y implies that the cholesterol added to the system is either interacting with the NBD chromophore providing some type of impediment to motion,[10] but the implications of the changes in D_x are less clear. The addition of sphingomyelin continues these trends, consistent with the further disruption of *local* organization in the portion of the bilayer structure sensed by the NBD chromophore. Taken collectively, these data point to significant interactions between the chromophore and all the bilayer constituents, indicating that the addition of multiple constituents to the bilayer gives rise to a loss of short-range organization.

To this point we have considered the transient anisotropy decay and the information contained within it relative to short-range bilayer organization. The infinite time anisotropy information contained in the one-photon excited anisotropy data shed light on the longer-range structural heterogeneity of the bilayers. We consider these results in the context of the hindered rotor model, where the measured infinite time anisotropy (Figure 4.5, Eq. 4.16) is related to the volume swept out by the probe. We observe (Table 4.5) that with the addition of cholesterol and sphingomyelin to the bilayers, there is a monotonic trend to smaller cone semi-angles, θ_o, which is seen for both lipids. On its face, such a trend would appear to be in conflict with the reorientation data. We believe that there is no conflict. It is well known that the addition of

cholesterol to bilayers makes the bilayers more rigid.[10] The increase in rigidity is consistent with a heterogeneous system, where the packing of mesoscopic domains give rise to greater rigidity, and less translational mobility in the overall system. The fact that we sense local loss of organization with the reorientation transients and mesoscopic increase of organization with the infinite time anisotropy data suggests that the NBD chromophore resides relatively near the domain boundaries in these systems.

With this information on the reorientation dynamics of NBD C_{12}-HPC, we return to the issue of the two component fluorescence lifetime decay. The time constants recovered from the lifetime data (ca. 200 ps, 1.1 ns) are both indicative of polar environments, and it is likely that they represent two different configurations where the chromophore is "folded back" to approach more closely the polar interface between the bilayer head groups and the aqueous environment. Both of these populations apparently sense relatively similar local environments and are thus sensitive to the same loss of short range organization associated with the addition of cholesterol and sphingomyelin to the bilayer. The remarkable changes we note in the anisotropy dynamics are likely averaged over some range of "depths" within the bilayer structure, and owing to the polarity sensitivity of this chromophore, the lifetime data reflect this particular aspect of the local environment with greater sensitivity than the reorientation data.
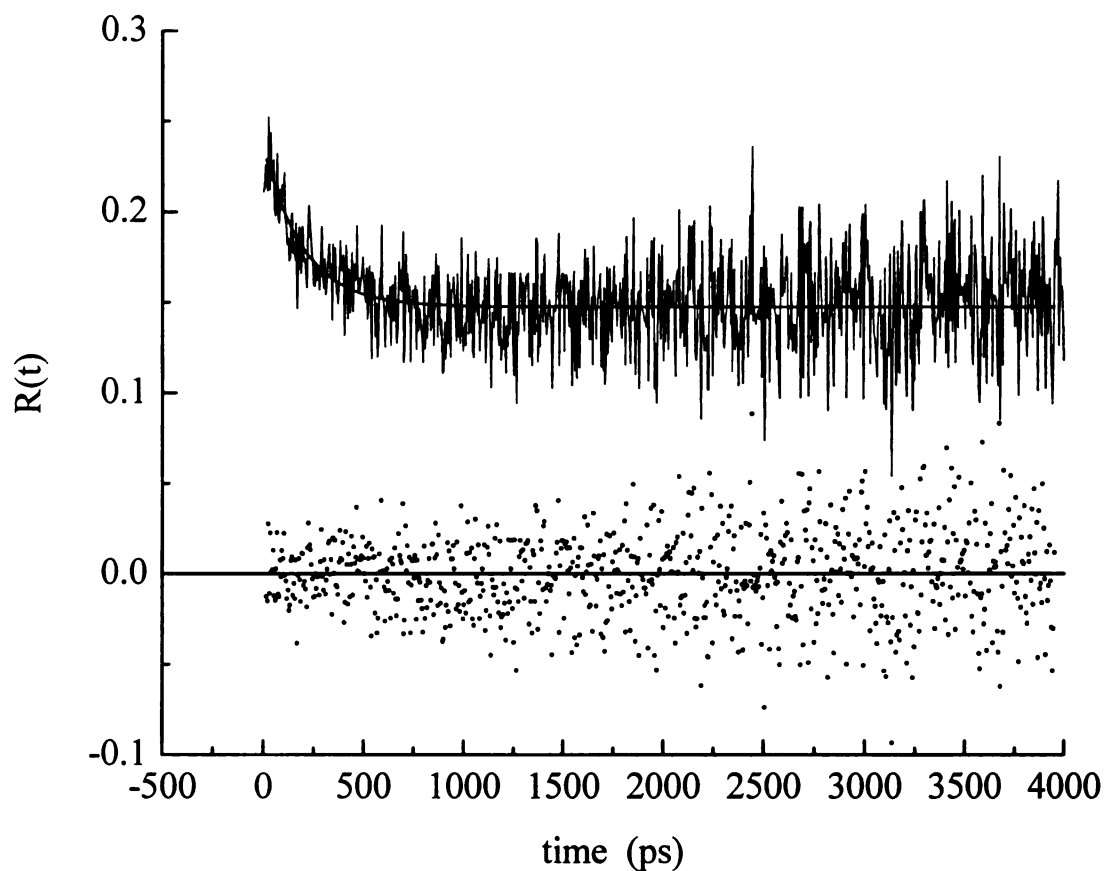
Figure 4.5. Anisotropy decay for one-photon excitation of NBD-C_{12}HPC in unilamellar vesicles composed of DLPC and cholesterol. Residuals of the fit to the data are shown as solid circles. For this particular run, $\tau = 195 \pm 27$ ps and $R(\infty) = 0.15 \pm 0.01$.

124

Conclusions

We have studied the steady state and time resolved optical properties of the chromophore NBD-C_{12}HPC in vesicles containing aqueous solutions. We used both one- and two-photon excitation to gather the information required to determine both D_y and D_x. From these measurements, we estimate the viscosity of the local medium of the chromophore, as well as D_y/D_x. For vesicles comprised of pure phospholipid, we determine a viscosity of 11.6 cP for gel phase DSPC and 7.8 cP for fluid phase DLPC, consistent with other recent reports on bilayer viscosity.[37] Upon the addition of cholesterol, the bilayer viscosity decreases due to changes in the local organization within the bilayer structure(s), and the addition of sphingomyelin causes a further decrease in bilayer viscosity. For pure phospholipid vesicles, $D_y/D_x \sim 1$, and for vesicles comprised of two or more components, $D_y/D_x \sim 1$. Such changes underscore the extent of the local disorder being imposed on the bilayer. Infinite time anisotropy data reveal that longer range organization in the bilayers is enhanced with the addition cholesterol and sphingomyelin, consistent with the formation of a heterogeneous bilayer structure. Taken collectively, our reorientation and cone angle data on NBD-C_{12}-HPC in a range of bilayer systems point to the chromophore residing in relatively close spatial proximity to the boundaries between heterogeneous regions within these bilayers. For these complex bilayer systems, local and mesoscopic organization change in different ways with the addition of cholesterol and sphingomyelin.

Literature Cited

(1)   Simons, K.; Ehehalt, R. *Journal of Clinical Investigation* **2002**, *110*, 597.

(2)   Simons, K.; van Meer, G. *Biochemistry* **1988**, *27*, 6197.

(3)   Crane, J. M.; Tamm, L. K. *Biophysical Journal* **2004**, *86*, 2965.

(4)   Hao, M.; Maxfield, F. R. *Journal of Fluorescence* **2001**, *11*, 287.

(5)   Scherfeld, D.; Kahya, N.; Schwille, P. *Biophysical Journal* **2003**, *85*, 3758.

(6)   Chattopadhyay, A.; London, E. *Biochimica et Biophysica Acta, Biomembranes* **1988**, *938*, 24.

(7)   Fery-Forgues, S.; Fayet, J.-P.; Lopez, A. *Journal of Photochemistry and Photobiology, A: Chemistry* **1993**, *70*, 229.

(8)   Mazeres, S.; Schram, V.; Tocanne, J.-F.; Lopez, A. *Biophysical Journal* **1996**, *71*, 327.

(9)   Wan, C.; Johnson, C. K. *Chemical Physics* **1994**, *179*, 513.

(10)   Cao, H.; Tokutake, N.; Regen, S. L. *Journal of the American Chemical Society* **2003**, *125*, 16182.

(11)   DeWitt, L.; Blanchard, G. J.; LeGoff, E.; Benz, M. E.; Liao, J. H.; Kanatzidis, M. G. *Journal of the American Chemical Society* **1993**, *115*, 12158.

(12)   Huster, D.; Muller, P.; Arnold, K.; Herrmann, A. *Biophysical Journal* **2001**, *80*, 822.

(13)   Lin, S.; Struve, W. S. *Photochemistry and Photobiology* **1991**, *54*, 361.

(14)   Mukherjee, S.; Chattopadhyay, A.; Samanta, A.; Soujanya, T. *Journal of Physical Chemistry* **1994**, *98*, 2809.

(15)   Greenough, K. P.; Blanchard, G. J. *Journal of Physical Chemistry A* **2007**, *111*, 558.

(16)   Drexhage, K. H. *Journal of Luminescence* **1970**, *1,2*, 693.

(17)   Girard, C.; Martin, O. J. F.; Dereux, A. *Physical Review Letters* **1995**, *75*, 3098.

(18)   Lukosz, W.; Kunz, R. E. *Optics Communications* **1977**, *20*, 195.

(19)   Lukosz, W.; Kunz, R. E. *Journal of the Optical Society of America* **1978**, *67*, 1607.

(20)   Tao, T. Time-dependent fluorescence depolarization and Brownian rotational diffusion coefficients of macromolecules. PhD Thesis, 1969.

(21)   Blanchard, G. J. *Journal of Chemical Physics* **1987**, *87*, 6802.

(22)   Chuang, T. J.; Eisenthal, K. B. *Journal of Chemical Physics* **1972**, *57*, 5094.

(23)   Johnson, C. K.; Wan, C. *Topics in Fluorescence Spectroscopy* **1997**, *5*, 43.

(24)   Lakowicz, J. R.; Gryczynski, I.; Gryczynski, Z.; Danielsen, E.; Wirth, M. J. *Journal of Physical Chemistry* **1992**, *96*, 3000.

(25)   Pauls, S. W.; Hedstrom, J. F.; Johnson, C. K. *Chemical Physics* **1998**, *237*, 205.

(26)   Wan, C.; Johnson, C. K. *Journal of Chemical Physics* **1994**, *101*, 10283.

(27)   Blanchard, G. J.; Wirth, M. J. *Journal of Chemical Physics* **1985**, *82*, 39.

(28)   Cho, M. *Journal of Chemical Physics* **2003**, *119*, 7003.

(29)   Karpovich, D. S.; Blanchard, G. J. *Langmuir* **1996**, *12*, 5522.

(30)   Kinosita, K., Jr.; Ikegami, A.; Kawato, S. *Biophysical Journal* **1982**, *37*, 461.

(31)   Kinosita, K., Jr.; Kawato, S.; Ikegami, A. *Biophysical Journal* **1977**, *20*, 289.

(32)   Szabo, A. *Journal of Chemical Physics* **1984**, *81*, 150.

(33)   Lipari, G.; Szabo, A. *Biophysical Journal* **1980**, *30*, 489.

(34)   Zwanzig, R.; Harrison, A. K. *Journal of Chemical Physics* **1985**, *83*, 5861.

(35)   McPhie, P. *Principles of Fluorescence Spectroscopy, Second Edition* 2000; Vol. 287.

(36)   Edward, J. T. *Journal of Chemical Education* **1970**, *47*, 261.

(37)   Koan, M. M., Blanchard, G. J. . *Journal of Physical Chemistry B* **2006**, *110*, 16584.

CHAPTER 5

DYNAMICS OF A TETHERED CHROMOPHORE IN PHOSPHOGLYCEROL VESICLES

Introduction

Plasma membranes are central to the function of mammalian cells. Despite the fact that a single mammalian plasma membrane may contain as many as 500 different lipid and sterol compounds, it has emerged that their distribution within the membrane is not homogeneous.[1-7] Lipid bilayer membranes are heterogeneous, complex structures, exhibiting phase separation even in comparatively simple model systems. The existence of such phase separation has given rise to the notion of "lipid rafts",[2-5,8-20] and their presence and characterization in both model bilayers and plasma membranes is an area of active research. Although there is ample evidence of phase separation in two- and three-component systems, the existence of lipid raft structures in plasma membranes remains to be proven. We are interested in these heterogeneous bilayer systems to determine whether or not such "rafts" in simple model systems can be used to support transmembrane proteins in their active forms. To address this issue, we have investigated organization and dynamics within one, two and three component model bilayer structures and have examined how organization and dynamics varies with the chemical functionalities present, in both the polar and nonpolar regions of the bilayers.[21,22] In this manuscript, we consider the role of the lipid head group identity in mediating the dynamics of chromophores placed in close spatial proximity to the bilayer head groups.

In the vicinity of the lipid bilayer head group region, the environment is dominated by the presence of water, and optical spectroscopic probes indicate that this environment is slightly more viscous than bulk water.[23] Despite the distinct structural differences between the polar and nonpolar regions of lipid bilayers, it is clear that each has a structural influence on the other, both in terms of the local motional freedom available to individual molecules, and in terms of longer range translational freedom. A key issue in understanding the organization of lipid bilayer structures is knowledge of how the polar phospholipid head groups interact with the aqueous environment in which they are in contact. The most widely used phospholipid family for such studies is the phosphocholines (PCs). The headgroups of these lipids are terminated by a trimethylamino moiety that carries a formal charge which is strongly solvated by water, but does not possess lone pairs which hydrogen bond extensively with surrounding water. The phosphoester functionality, however, does possess the lone pairs with which to hydrogen-bond with water. Phosphoglycerols (PGs), in addition to having the phosphoester functionality, also contain two hydroxyl moieties, enabling more extensive hydrogen bonding with water. The issue we are concerned with in this paper is whether or not the structural differences between the PC and PG lipid head groups gives rise to significant differences in the dynamics of bilayers made from these lipids, and we interrogate the bilayer dynamics by means of a tethered chromophore.

We use the chromophore 7-nitrobenz-2-oxa-1,3-diazole, NBD, a molecule that has been used extensively for interrogating biological and biomimetic systems.[24-32] This chromophore is characterized by a fluorescence spectral profile and lifetime that both depend sensitively on the polarity of its immediate environment.[24-32] In addition, the

chromophore NBD is available with a variety of sidegroups, or attached to lipid head groups or acyl chains, making it a particularly attractive choice for the study of lipid bilayers.

We have reported previously on the dynamics of NBD tethered to a PC lipid.[21] In that work we examined the fluorescence lifetime and induced orientational anisotropy decay of the NBD chromophore as a function of bilayer composition. We used NBD tethered to a phospholipid acyl chain, and found that the environment experienced by the chromophore depends sensitively on the composition of the bilayer. The addition of cholesterol and sphingomyelin to the phospholipid bilayer reduced the organization of the chromophore environment significantly but did not influence the (conic) volume of the restricted region in which the chromophore can orientationally relax. The functional form of the anisotropy and lifetime data pointed to the chromophore residing in the proximity of the bilayer polar head group region with the local viscosity of the bilayer region sensed by the probe being ca. 2 cP. The most plausible explanation for this finding is that the chromophore tethered to the lipid acyl chain is able to "loop back" and reside in proximity to the phospholipid head group.[28] In this work, we examine the lifetime and anisotropy decay dynamics of the molecule (1-Palmitoyl-2-[12-[(7-nitro-2-1,3-benzoxadiazol-4-yl)amino]dodecanoyl]-sn-Glycero-3-[Phospho-rac-(1-glycerol)] (NBD-PG). Use of this chromophore allows us to gauge the effect of the lipid headgroup on interactions with their local environment for a system that is expected to hydrogen-bond extensively both among lipid headgroups and with surrounding water. We use one- and two-photon excitation to determine fluorescence lifetime and anisotropy decay

dynamics. The data we present here show that the identity of the lipid headgroup plays a significant role in chromophore behavior.

Experimental

Materials. The fluorescent probe 1-Palmitoyl-2-[12-[(7-nitro-2-1,3-benzoxadiazol-4-yl)amino]dodecanoyl]-*sn*-Glycero-3-[Phospho-*rac*-(1-glycerol)] (NBD-PG) was obtained from Avanti Polar Lipids, Inc. and was used without further purification. For the construction of unilamellar vesicles, the lipids 1,2-Dilauroyl-*sn*-Glycero-3-[Phospho-*rac*-(1-glycerol)] (DLPG, mp = -3°C), 1,2-Distearoyl-*sn*-Glycero-3-[Phospho-*rac*-(1-glycerol)] (DSPG, mp = 55°C), egg sphingomyelin (SPM) and powdered cholesterol were obtained from Avanti Polar Lipids, Inc. The vesicle constituents were prepared in a 1:1:1 mole ratio of phospholipid : cholesterol : sphingomyelin or a 2:1 mole ratio of phospholipid : cholesterol for the multicomponent systems. The tagged phospholipids in these systems were present at 10^{-4} M. A total of six vesicle solutions were produced: (1) NBD-PG/DLPG, (2) NBD-PG/DLPG/cholesterol, (3) NBD-PG/DLPG/cholesterol/SPM, (4) NBD-PG/DSPG, (5) NBD-PG/DSPG/cholesterol, and (6) NBD-PG/DSPG/cholesterol/SPM. Chloroform was evaporated from the lipid solution, and the remaining solid was dissolved in a 4:1 benzene : methanol solvent system. The benzene : methanol solvent was then evaporated, and the resulting lipid mixture was dissolved in 10 mM Tris® buffer (Aldrich) adjusted to pH~8 in MilliQ water. The resulting concentration of NBD-PG in each vesicle solution was ~10^{-4} M. For further mixing, the solution was put through five freeze-thaw-vortex cycles, where for each cycle the sample is placed in liquid nitrogen for 5 minutes, then in a hot water bath for 5 minutes, then vortexed for 2 minutes. A syringe-based mini-extruder from Avanti Lipids was used to extrude the lipid suspension

through a polycarbonate filter eleven times to produce unilamellar vesicles of ~100 nm diameter.[11,23]

Steady State Measurements. Absorption spectra were recorded on a Cary model 300 double beam UV-Visible absorption spectrophotometer, with 1 nm spectral resolution. Emission spectra were recorded on a Spex Fluorolog 3 spectrometer at a spectral resolution of 3 nm for both excitation and collection monochromators.

Time Correlated Single Photon Counting Measurements. All lifetime and anisotropy data were acquired using a time correlated single photon counting (TCSPC) system. This system has been described in detail elsewhere,[21,23,33,34] and we recap only its salient features here. The source laser is a CW mode-locked Nd:YAG laser (Coherent Antares 76-S) that produces 30 W average power at 1064 nm with 100 ps pulses at 76 MHz repetition rate. The second harmonic (532 nm, 3W average power) or third harmonic (355 nm, 1 W average power) of the output of this laser excites a cavity dumped dye laser (Coherent 702-2), operating with Rhodamine 610 dye (Exciton, 532 nm pump) for two photon excitation experiments, or with Stilbene 420 dye (Exciton, 355 nm pump) for one photon excitation experiments. The dye laser output is typically 5 ps pulses at a repetition rate of 3.8 MHz for both excitation wavelengths. Fluorescence signals are spectrally filtered using a subtractive double monochromator (American Holographic) and are detected using a Hamamatsu R3809U-51 microchannel plate photomultiplier tube (MCP-PMT) detector. The signals are processed using a Tennelec 454 quad constant fraction discriminator and Tennelec 864 time-to-amplitude converter and biased amplifier. For this system the instrument response time is ca. 35 ps fwhm. Fluorescence was collected at 0°, 54.7° and 90° with respect to the vertically polarized

excitation pulse. Collection wavelength, polarization and data acquisition were controlled using National Instruments LabVIEW® 7.1 software.

Pressure-Area Isotherms. Pressure-area isotherms were generated using a Langmuir-Blodgett Trough (Nima Technology Ltd. Model 612D). The lipid solutions were prepared at a concentration of 1 mg/mL in chloroform, with a 2:1 molar ratio of phospholipid:cholesterol and 1:1:1 phospholipid, cholesterol, SPM. For these experiments, the fluorescent lipid and the phospholipid were present in equimolar amounts.

Results and Discussion

We are interested in understanding the motional dynamics of 1-Palmitoyl-2-[12-[(7-nitro-2-1,3-benzoxadiazol-4-yl)amino]dodecanoyl]-*sn*-Glycero-3-[Phospho-*rac*-(1-glycerol)] (NBD-PG) (Figure 5.1) in unilamellar vesicles comprised of phosphoglycerol lipids, sphingomyelin and cholesterol. We are concerned not only with the dynamics of the chromophore, but also the specific region within the unilamellar vesicle where the tethered chromophore localizes. We have obtained pressure-area isotherm data to gauge the organization of our bilayers and the extent to which the presence of the chromophore perturbs the bilayer. We have measured both the fluorescence lifetime and anisotropy decay using one- and two-photon excitation of the chromophore incorporated into the vesicles. Using two different excitation methods provides access to mutually complementary information regarding the motion of the chromophore. With these data, we can evaluate the Cartesian components of the rotational diffusion coefficient, a task which is not possible using either of these excitation methods individually.

Previous literature reports have demonstrated that the polarity of the NBD chromophore environment plays a significant role in determining its fluorescence lifetime.[23,25-32] NBD is a polar chromophore, and it is reasonable to expect this molecule to reside preferentially in a polar environment.[21,25,27,28] The absorption maximum for NBD shifts to the red in polar solvents,[25-27,30] and our steady state absorbance data show that for all vesicle-containing solutions, the NBD absorption maximum is ~460 nm and its emission maximum is ~550 nm (Figure 5.1), consistent with a polar environment. This finding is consistent with what is known about tethered NBD is bilayer systems.
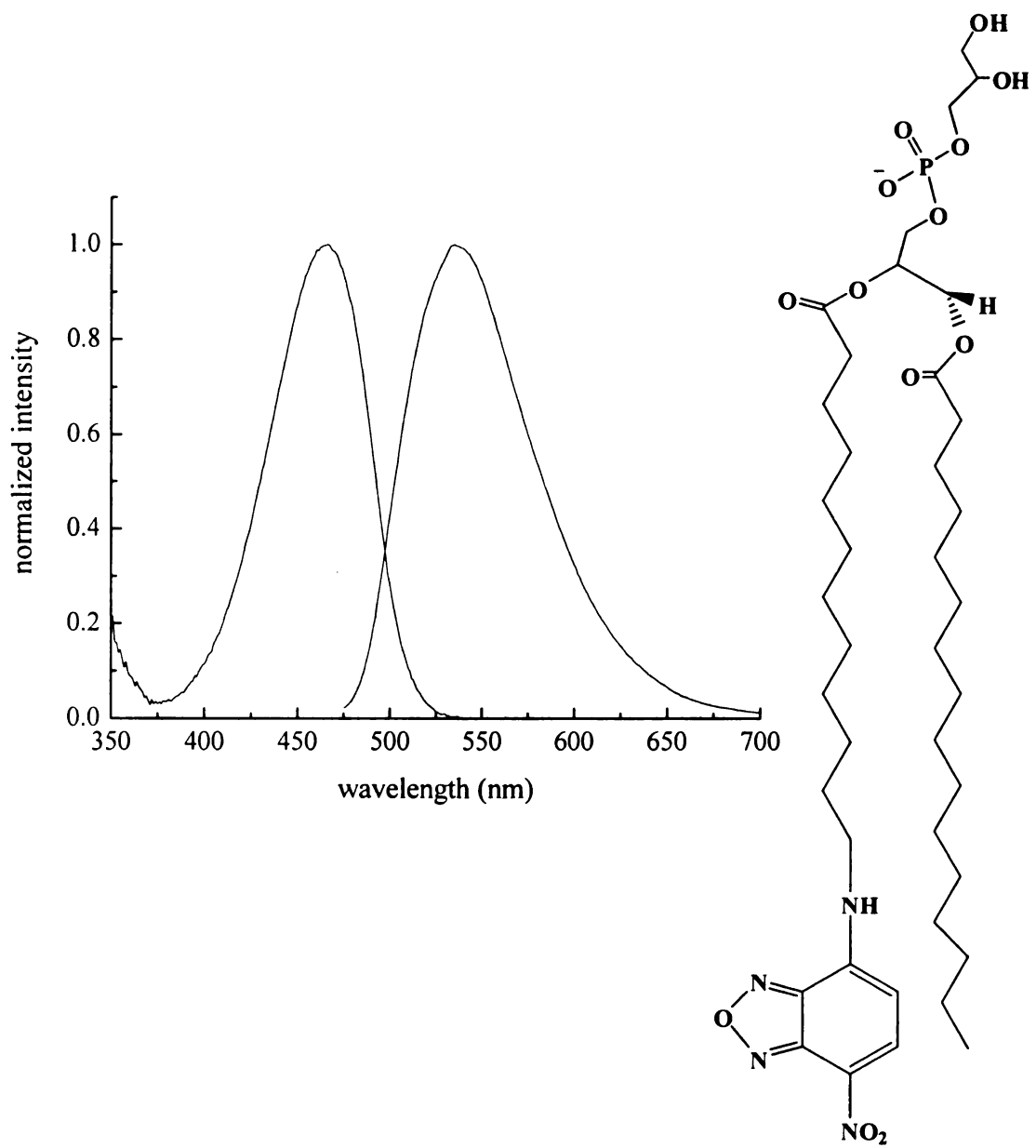
136

Figure 5.1 Normalized absorption and emission spectra of NBD-PG in ethanol (left) and structure of 16:0-12:0 NBD-PG (right).

When NBD is attached to the acyl chain of a lipid and incorporated into a lipid bilayer, it is known that the NBD moiety will "loop back" into the polar region of the bilayer, in close proximity to the lipid head group.[21,25,28]

The NBD fluorescence lifetime data for both one- and two-photon excitation yield the same result, which is an expected result because the emitting state for both means of excitation is the S_1 (π^*) state. Time-resolved fluorescence lifetime data show that the excited state population decay of NBD-PG in vesicles contains at least two exponential components in all cases (Figure 5.2), indicating the presence of the probe in multiple environments characterized by a range of polarities. The long lifetime component for all cases ranges from ~1300 ps to 2200 ps, while the short lifetime component is between 300 ps and 400 ps. These two lifetimes differ significantly in each vesicle system, and their fractional contribution to the overall decay also varies with the composition of the vesicle (Table 5.1). These environmentally-dependent differences in lifetime can be attributed to the gradient in the dielectric response of the bilayer across the headgroup region, ranging from ε~2 in the nonpolar portion of the bilayer to ε~80 in the aqueous region above the head group region, a distance of ca. 10 Å. It is this significant dielectric gradient across the bilayer head group region that modulates the NBD lifetime data,[35-38] rather than significant differences in chromophore position within the bilayer. Thus, the two-component lifetime should not be taken to indicate two radically different environments; rather, the chromophore senses a large change in dielectric response as a result of subtle positional differences within the bilayer head group region.

To evaluate the organization of the phospholipids and the extent to which the presence of the NBD chromophore affects organization, pressure-area isotherms of Langmuir-Blodgett monolayers were obtained for each of the six vesicle-forming solutions (after mixing but not extruded), both with and without the tethered chromophore (Figures 5.3a and 5.3b). For ordered systems characterized by a high T_m, such as DSPG, the pressure-area isotherm shows a slight increase in lateral packing density as well as an apparent slight increase in organization with the addition of cholesterol (Figure 5.3b), and we note this same qualitative trend for DLPG, although the isotherms appear to be more liquid-like under all conditions for this lipid (Figure 5.3b).[5,6,9,39] Upon addition of SPM to DSPG films, there is notable expansion of the bilayer; the opposite is seen for the disorganized monolayer of DLPG when SPM is added (Figure 5.3b). Such results have been observed previously,[4,39-48] and this behavior most often attributed to the cooperative effect of SPM and cholesterol when both are present in the bilayer.[39,40,43-45] The surface monolayers that did not contain the NBD-tagged lipid showed that DSPG films exist as solids, presumably with ordered acyl chains, and the DLPG films behave as liquids. The addition of the chromophore-containing lipid to the monolayer caused the monolayers to become more liquid-like in all cases, owing to the disorder induced by the presence of this species. Similar results were seen for the isotherms obtained for phosphocholine lipid monolayers (Figure 5.4). These data underscore the significant role that the lipid acyl chains as well as non-lipid constituents play in determining overall organization within the layers.
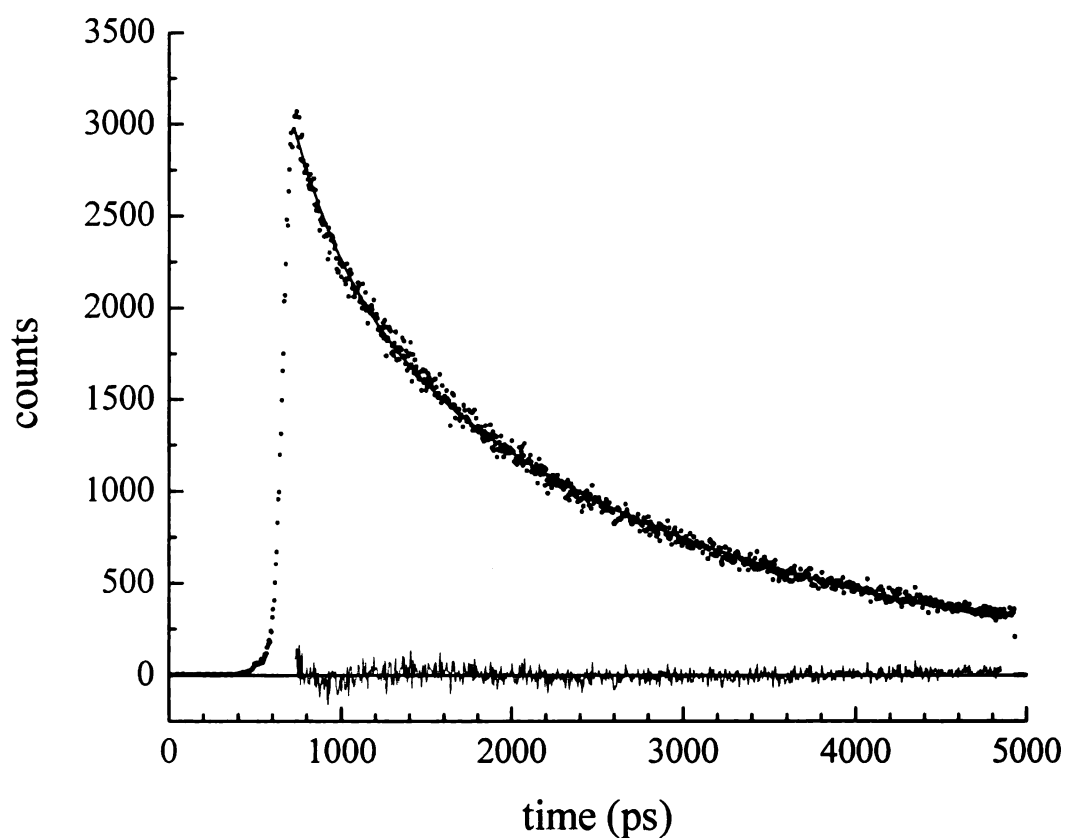
Figure 5.2 Example fluorescence lifetime data (points) for DLPG vesicles containing NBD-PG, showing a fit to a double exponential decay functionality. (τ_1=327 ps, τ_2=2123 ps) The solid line through the data is the fit, with the residuals plotted as fluctuations about zero intensity.

Table 5.1. One-photon excited fluorescence lifetimes of NBD-PG in vesicles. Experimental data were fit to the function $f(t) = A_1exp(-t/\tau_1) + A_2exp(-t/\tau_2)$. Uncertainties are $\pm 1\sigma$ for at least six individual determinations.

Vesicle system	τ_1 (ps)	τ_2 (ps)	$A_1/(A_1+A_2)$
NBD-PG, DLPG	347 ± 20	2211 ± 31	0.27 ± 0.01
NBD-PG, DLPG, chol	425 ± 17	1394 ± 38	0.40 ± 0.02
NBD-PG, DLPG, chol, SPM	332 ± 5	2232 ± 50	0.81 ± 0.003
NBD-PG, DSPG	415 ± 20	1305 ± 16	0.34 ± 0.01
NBD-PG, DSPG, chol	374 ± 13	1800 ± 70	0.64 ± 0.01
NBD-PG, DSPG, chol, SPM	390 ± 8	1340 ± 19	0.62 ± 0.02

Figure 5.3 Pressure-area isotherms for Langmuir-Blodgett monolayers of (a):
DLPG (1), DLPG + Cholesterol (2), DLPG + Cholesterol + sphingomyelin
(3), DLPG + NBD-PG (4), DLPG + NBD-PG + Cholesterol (5), DLPG +
NBD-PG + Cholesterol +sphingomyelin (6).   (b): DSPG (1), DSPG +
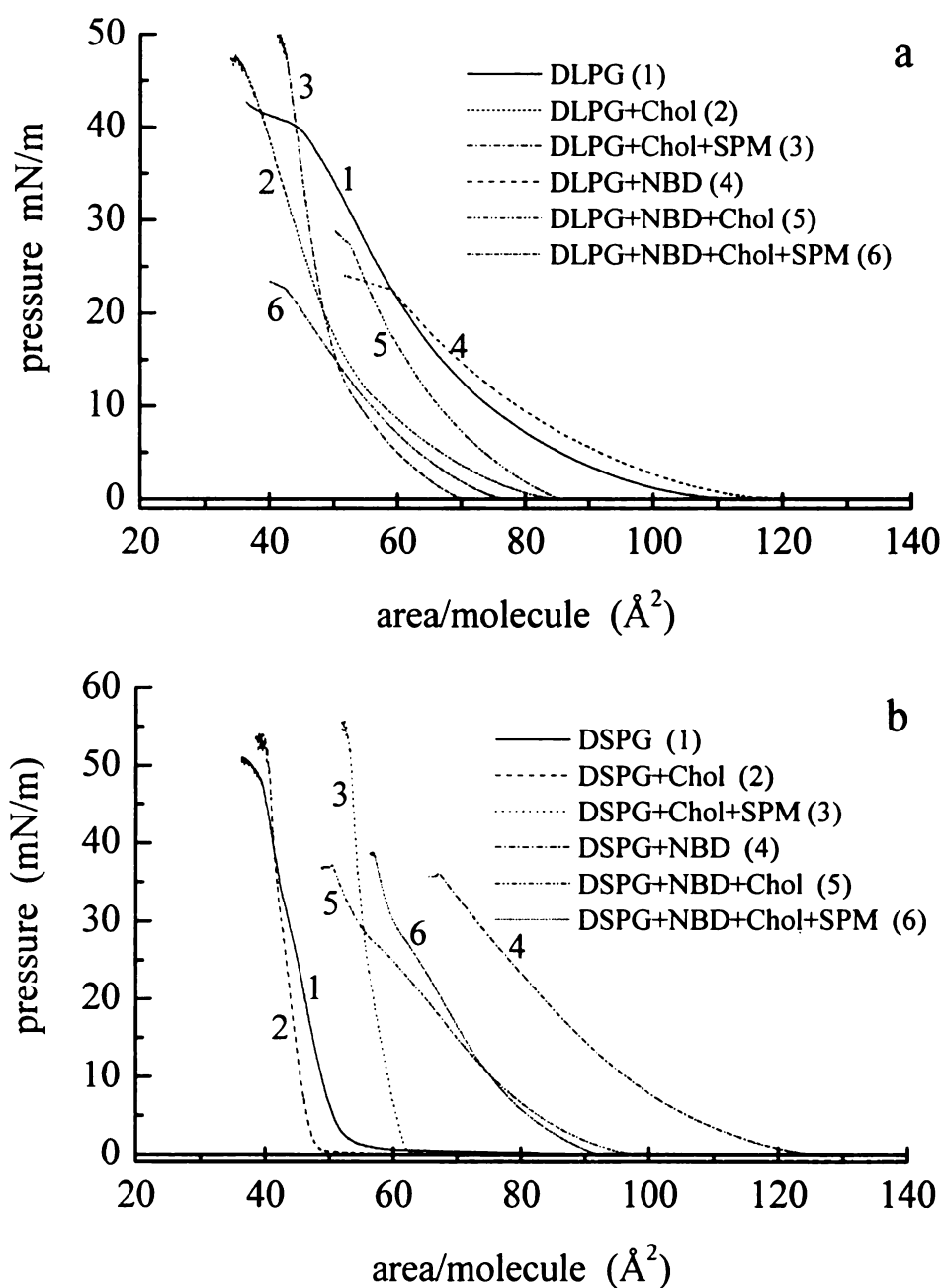Cholesterol (2), DSPG + Cholesterol + sphingomyelin (3), DSPG + NBD-PG
(4), DSPG + NBD-PG + Cholesterol (5), DSPG + NBD-PG + Cholesterol
+sphingomyelin (6).

When NBD-PG is incorporated into the LB monolayers, a significant amount of disorder results. With the addition of tethered NBD, DSPG/PC lipid monolayers exhibit pressure-area isotherms characteristic of liquids at room temperature (Figures 5.3b and 5.4). This is not a surprising result, because the NBD-containing lipid is comparatively large and bulky, a condition which will interfere with tight lipid packing. Following cholesterol incorporation into the chromophore-containing monolayers, we do not observe an increase in fluidity. For LB films that do not contain the chromophore, the addition of cholesterol gives rise to a reduction in organization, producing an isotherm with a more fluid-like transition than is seen for the lipid-only monolayer (Figures 5.3a and 5.3b). The chromophore concentrations used in these isotherm measurements are higher than those used for the spectroscopic measurements to make clear the role of the chromophore in layer organization. It is reasonable to expect that the presence of the chromophores perturbs *local* organization for any chromophore concentration, and it is this environment that is sensed by the probe spectroscopic response. Despite the limitations to this type of measurement, we find that the local organization of our bilayer vesicles is affected measurably by the addition of cholesterol and sphingolipid, and we consider these issues next.

Anisotropy decay data for NBD-PG in vesicle systems are capable of revealing significant detail about the chromophore local environment. Interpretation of anisotropy decay data obtained using one- and two-photon excitation differs because of the different initial orientational distribution selected by these two methods and the different contributions of spectroscopic and diffusional terms to the anisotropy decays. The information obtained from the one-photon excitation is complementary to that extracted
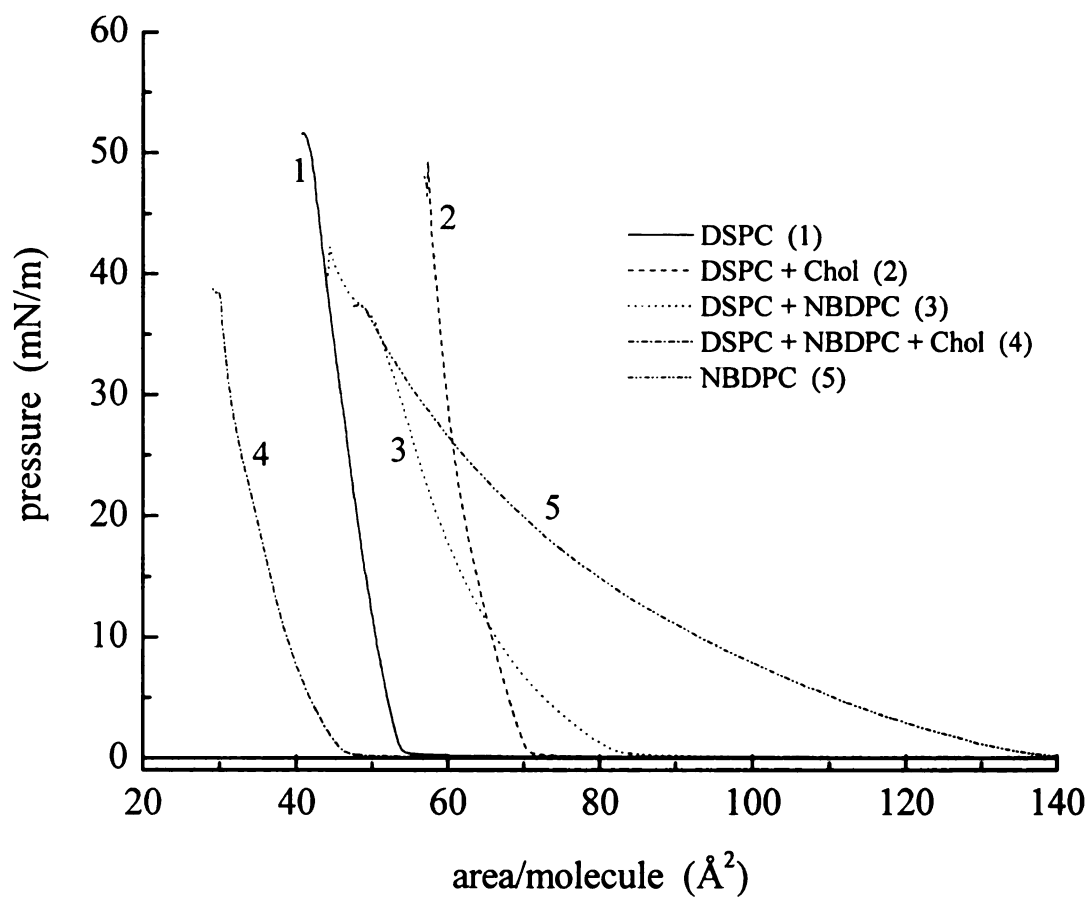
Figure 5.4. Pressure-area isotherms for Langmuir-Blodgett monolayers of DSPC (1), DSPC + Cholesterol (2), DSPC + NBDPC (3), DSPC + NBDPC + Cholesterol (4), NBDPC (5).

from the two-photon excitation measurements. These data, taken collectively, provide a detailed description of tethered NBD motion in lipid bilayers. We treat the information contained in each body of data separately before considering that available through a comparison of the two data sets.

For one photon excitation, there is a well-established framework for the interpretation of anisotropy decay data.[34,49-55] The induced orientational anisotropy function, R(t), is generated from the polarized fluorescence signal intensities (Eq. 5.1),

$$R(t) = \frac{I_{\parallel}(t) - I_{\perp}(t)}{I_{\parallel}(t) + 2I_{\perp}(t)} \tag{5.1}$$

where the excitation is vertically polarized and the quantities $I_{\parallel}(t)$ and $I_{\perp}(t)$ are the polarized emission transients. The chemical information extracted from these data is contained in the functional form of R(t). While up to five exponential decays may be present in R(t),[50] the most common case is to observe one or two exponential decays. The relationship between the decay functionality of R(t) and the chromophore transition moment(s) and rotational diffusion constant has been described in detail.[34,49-55] Chuang and Eisenthal's treatment[50] described R(t) as a function of rotor shape and transition moment orientation, with the limiting cases being either a Type I or Type II rotor, which simplifies the general expression for R(t). A Type I rotor is characterized by a distortion along the axis containing the transition moment, and a Type II rotor is characterized by a distortion along an axis perpendicular to the transition moment.[21] For a transition moment along the ith axis (one of the Cartesian axes), there are two general solutions to the anisotropy decay:

Type I $\quad R(t) = 0.4 \exp(-6 D_k t)$ (5.2)

Type II $\quad R(t) = 0.1 \exp(-6 D_i t) + 0.3 \exp(-(2 D_i + 4 D_k)t)$ (5.3)

The information that can be extracted from R(t) thus depends on the orientation of the absorption and emission transition dipole moments of the chromophore. The NBD transition moment lies in the π plane, where we take the x-axis to be the long molecular axis, and the y-axis is coincident with the short in-plane axis. The bond tethering the NBD moiety to the lipid molecule therefore is oriented along the y-axis, and under this condition, NBD is characterized by $D_y \neq D_x = D_z$. For this system, the anisotropy can decay as either a single or double exponential, depending on the orientation of the transition (x or y axis):

x-polarized transition $\quad R(t) = 0.3 \exp(-(4 D_y + 2 D_x)t) + 0.1 \exp(-6 D_x t)$ (5.4)

y-polarized transition $\quad R(t) = 0.4 \exp(-6 D_x t)$ (5.5)

Our experimental data are, to within our ability to determine, single exponential anisotropy decays, suggesting that the transition is y-axis polarized, and the recovered reorientation time is reflective of motions about the chromophore x- and z-axes. Specifically, the recovered anisotropy decay time constant for one photon excitation is given by $(6 D_x)^{-1}$. We recognize that, owing to the presence of the tether, NBD is not allowed to rotate freely about the x-axis, and the recovered time constant is representative of wobbling and angular tilting about the tethering bond. It is clear, however, that the motional relaxation behavior of NBD in our vesicle structures is not well characterized when one photon excited fluorescence anisotropy is the only method used. This

146

information becomes more useful when compared to the results from two photon excitation, and we consider these data next.

A brief word is in order regarding the assignment of rotor shape for these data. The interpretation of our results in the context of the one-photon excited anisotropy decay being a single exponential ultimately relies on the S/N ratio of our data, which is limited (Figure 5.5). We note that in the limit of an isotropic rotor ($D_x \sim D_y \sim D_z$), Eqs. 5.4 and 5.5 reduce to the same functional form. Comparing the one- and two-photon excitation data, which we discuss next, we find that, except for one system, we in fact recover isotropic rotor behavior for the tethered NBD chromophore (*vide infra*), rendering the issue of distinguishing between Eq. 5.4 and Eq. 5.5 largely moot for this system.

To understand the anisotropy decay data acquired using two-photon excitation, we borrow from the treatment presented by the Johnson group.[56-62] Induced orientational anisotropy decay functions are generated for both linearly ($r_1(t)$) and circularly ($r_2(t)$) polarized excitation (Eqs. 5.6),

$$
\begin{aligned}
r_1(t) &= \frac{I_{\parallel}^{linear}(t) - I_{\perp}^{linear}(t)}{I_{\parallel}^{linear}(t) + 2I_{\perp}^{linear}(t)} \\
r_2(t) &= \frac{I_{\parallel}^{circular}(t) - I_{\perp}^{circular}(t)}{2I_{\parallel}^{circular}(t) + I_{\perp}^{circular}(t)}
\end{aligned}
\tag{5.6}
$$

For both excitation polarizations, the anisotropy decays are characterized by two time constants, τ_0 and τ_2, weighted according to the spectroscopic and motional properties of
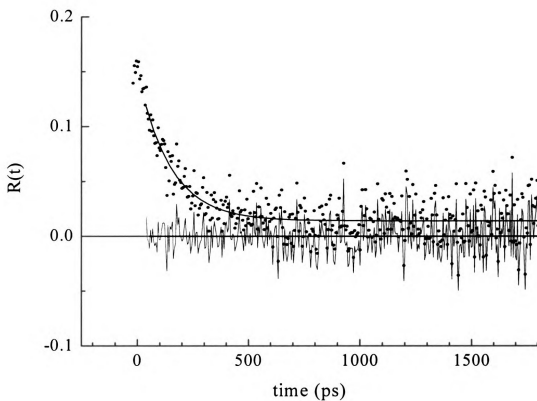
147

Figure 5.5 Two photon excited anisotropy decay for vesicles containing DSPG,
NBD-PG and cholesterol. Points are experimental data, solid line is the fit of
the data to an exponential decay and the residuals of the fit are shown
centered about the zero intensity line.

the chromophore. The anisotropy decays are given by,[58,59,61,62]

$$r_1(t) = r_1(0)\left[c_0 e^{-t/\tau_0} + c_2 e^{-t/\tau_2}\right]$$

$$r_2(t) = r_2(0)\left[d_0 e^{-t/\tau_0} + d_2 e^{-t/\tau_2}\right] \tag{5.7}$$

Where the exponential prefactors are[60]

$$c_0 = \frac{(\sqrt{3}a+b)\left[3(\sqrt{3}a+b)S_{xx}^2 + 3(-\sqrt{3}a+b)S_{yy}^2 + 2bS_{xx}S_{yy} + 4bS_{xy}^2\right]}{7N^2(3S_{xx}^2 + 3S_{yy}^2 + 2S_{xx}S_{yy} + 4S_{xy}^2)} \tag{5.8}$$

$$c_2 = \frac{(a-\sqrt{3}b)\left[3(a-\sqrt{3}b)S_{xx}^2 + 3(a+\sqrt{3}b)S_{yy}^2 + 2aS_{xx}S_{yy} + 4aS_{xy}^2\right]}{7N^2(3S_{xx}^2 + 3S_{yy}^2 + 2S_{xx}S_{yy} + 4S_{xy}^2)} \tag{5.9}$$

$$d_0 = \frac{(\sqrt{3}a+b)\left[(\sqrt{3}a+b)S_{xx}^2 + (-\sqrt{3}a+b)S_{yy}^2 - 4bS_{xx}S_{yy} + 6bS_{xy}^2\right]}{14N^2(S_{xx}^2 + S_{yy}^2 - S_{xx}S_{yy} + 3S_{xy}^2)} \tag{5.10}$$

$$d_2 = \frac{(a-\sqrt{3}b)\left[(a-\sqrt{3}b)S_{xx}^2 + (a+\sqrt{3}b)S_{yy}^2 - 4aS_{xx}S_{yy} + 6aS_{xy}^2\right]}{14N^2(S_{xx}^2 + S_{yy}^2 - S_{xx}S_{yy} + 3S_{xy}^2)} \tag{5.11}$$

and the quantities a, b, N and Δ are related to the rotational diffusion constant D by

$$a = \sqrt{3}(D_y - D_x)$$

$$b = 2D_z - D_y - D_x + 2\Delta$$

$$N^2 = a^2 + b^2 \tag{5.12}$$

$$\Delta = (D_x^2 + D_y^2 + D_z^2 - D_xD_y - D_yD_z - D_xD_z)^{1/2}$$

While Eqs. 5.7 predict two exponential decay components for each excitation

polarization, we recover only one decay time constant in each case, and this is a

commonly observed situation. Further, for each system studied here, the anisotropy

149

decay time constant for linear and circular excitation polarization is the same, τ_{r1} (linear) = τ_{r2} (circular). The most general interpretation of single exponential decays for two photon excitation is that the recovered time constants are simply weighted averages of τ_0 and τ_2,[60]

$$\tau_{r_1} = \frac{(c_0\tau_0 + c_2\tau_2)}{c_0 + c_2}$$

$$\tau_{r2} = \frac{(d_0\tau_0 + d_2\tau_2)}{d_0 + d_2}$$

(5.13)

This condition does not, in general lead to the same decay time constant for both linear and circular excitation polarization. Because $D_x \sim D_z$ for our systems (from one photon excitation data), the term $(\sqrt{3}a+b)$ in Eqs 5.8 and 5.10 is zero, making the prefactors c_0 and d_0 equal to zero for $D_x \geq D_y$, and this condition is met to within the experimental uncertainty, save for one case (*vide infra*). The time constants we recover are thus $\tau_{r1}=\tau_2$, and $\tau_{r2}=\tau_2$ where $\tau_2=(6D+2\Delta)^{-1}$.[60,61] This situation is consistent with the fact that we recover the same time constants, to within the experimental uncertainty for both linear and circular excitation polarization, and for these conditions, τ has contributions from both D_y and D_x:

$$\tau_2 = \frac{1}{(4D_y + 2D_x)}$$

(5.14)

We determine D_x from one-photon excitation, and use that information, in combination with two-photon data to determine D_y. We recognize that the values of D_x and D_y we recover are not free rotational motions about each axis because of the tethering attachment to the phospholipid. These quantities represent random walk (D_x and D_z) and

150

predominantly rotational (D_y) motions of the chromophore. With this information in hand, we are now in a position to consider the changes in chromophore local environment associated with variations in bilayer composition.

The anisotropy decay time constants, calculated values of D_y and D_x, and D_y/D_x are summarized in Table 5.2. Vesicles comprised of DLPG vesicles are characterized by $D_y/D_x = 5.7$, suggesting a substantially anisotropic environment for the chromophore, where there is relatively little lateral (D_z, D_x) freedom and the dominant motion is about the y-axis. With the addition of cholesterol and/or sphingomyelin to the bilayers, the ratio D_y/D_x decreases to 1.3 ± 0.1 (cholesterol) and 1.1 ± 0.2 (cholesterol and sphingomyelin). The approach to an isotropic environment suggests that there is a decrease in organization of the bilayer structure with the addition of cholesterol and/or sphingomyelin, in agreement with our earlier findings for phosphocholine bilayers formed with DLPC and DSPC.[21] The reduction of the ratio D_y/D_x in these bilayers suggests that these structures are becoming less organized and perhaps more fluid, consistent with the functional form of the pressure area isotherms for the corresponding Langmuir Blodgett monolayers (Figures 5.3a and 5.3b).

The anisotropy data on D_y/D_x shows a consistent trend for DLPC, DSPC, and DLPG, with comparative confinement in the phospholipid vesicles, and an increase in the motional freedom when cholesterol and/or sphingomyelin are added. However, DSPG vesicles show a different bilayer composition dependence through D_y/D_x, even though the isotherms change in a manner similar to the other monolayers when the NBD-containing

151

Table 5.2. Experimental reorientation time constants and calculated values of rotational diffusion coefficients for NBD-PG in the vesicles of compositions indicated in the first column.

Vesicle system	$\tau_{OR} \pm 1\sigma$ (one photon, ps)	$\tau_{OR} \pm 1\sigma$ (two photon, ps)	D_x (MHz)	D_y (MHz)	D_y/D_x
DLPG	678 ± 34	167 ± 21	246 ± 13	1400 ± 7	5.7 ± 0.3
DLPG, chol	93 ± 5	77 ± 13	1797 ± 97	2272 ± 49	1.3 ± 0.1
DLPG, chol, SPM	81 ± 10	79 ± 13	2081 ± 249	2199 ± 125	1.1 ± 0.2
DSPG	138 ± 11	153 ± 27	1212 ± 96	1059 ± 48	0.87 ± 0.1
DSPG, chol	117 ± 21	121 ± 29	1490 ± 291	1427 ± 146	0.96 ± 0.2
DSPG, chol, SPM	82 ± 14	88 ± 22	2084 ± 380	1841 ± 190	0.88 ± 0.2

lipid is added. The DSPG vesicles that contain the tethered NBD are characterized D_y/D_x = 0.87 ± 0.10, and that value remains constant to within the experimental uncertainty with the addition of cholesterol (D_y/D_x = 0.96 ± 0.20) and sphingomyelin (D_y/D_x = 0.88 ± 0.20). This finding indicates the environment probed by the NBD-PG for DSPG-based systems does not change its effective shape with the addition of cholesterol and/or sphingomyelin. The ratio of D_y/D_x does not provide the complete picture, however. When examining trends in $D = \frac{1}{3}(D_x+D_y+D_z)$, we see that D increases for both DSPC and DSPG lipids with the addition of cholesterol, and increases slightly more with the addition of sphingomyelin in addition (Table 5.2). Thus the qualitative organization of the local environment does not appear to change for DSPG vesicles with the addition of cholesterol and/or sphingomyelin, but the addition of these species does introduce more fluidity into the portion of the bilayer sensed by the tethered chromophore. There are a few characteristics of the DSPG bilayers that could account for these observations. Comparisons between DSPC and DSPG show differences in organization of pure phospholipid bilayers. Although the transition temperatures are comparable, the difference between the two lipids lies in the identity of the headgroup. The glycerol headgroup will participate in a network of hydrogen bonding with the neighboring headgroups while choline does not. The extensive hydrogen bonding results in stronger interactions between lipids and chromophore, and thus more ordered bilayers. Although this factor could account for differences between DSPG and DSPC, a comparison must be made between DLPG and DSPG systems. Both DLPG and DSPG contain the glycerol headgroup that will participate extensively in hydrogen bonding between headgroups, the aqueous layer outside the bilayer, and the NBD group as it folds back to be in close

153

proximity to the hydrophilic head group region of the bilayer. The difference in behavior for NBD in the DLPG and DSPG vesicles suggests that for DSPG the local environment of NBD is more isotropic than it is for DLPG. Given the commonality in head group structure for DLPG and DSPG, and our data indicating the lifetimes of tethered NBD are the same in DLPG and DSPG vesicles, the only factor that can be responsible of the observed behavior is the length of the acyl chains, and differences in bilayer organization that result from this difference. Because the chromophore has a C16 acyl chain, if this chain were all-*trans*, it would span the DLPG monolayer and penetrate to some extent into the opposing leaflet, whereas for DSPG this is not the case. The consequences of this difference may be that the chromophore-containing lipid is more translationally constrained in DLPG. The functional form of this finding is somewhat surprising because DSPG has a higher melting point than DLPG, and intuition would suggest behavior analogous to that seen for DSPC and DLPC. Further investigation is required to understand this behavior fully.

For chromophores imbedded in an intrinsically anisotropic medium, such as the lipid bilayers we examine here, the data are often treated using the hindered rotor model. The chromophore we use in this work, NBD-PG, consists of an NBD moiety attached to the aliphatic chain of a phosphoglycerol lipid. Due to attachment of the chromophore to a lipid, the hindered rotor model is an appropriate model for describing the behavior of NBD-PG. This model has been used previously to describe the one-photon excited anisotropy decay behavior of other chromophores embedded in a bilayer.[57,63,64] In this model, the motion of the chromophore is restricted by its environment as well as its attachment to a membrane constituent; we anticipate the motion of the NBD

chromophore to sweep out a conical volume. The cone angle ($2\theta_0$) that characterizes chromophore motion is related to the infinite time anisotropy, $R(\infty)$, and the zero time anisotropy, $R(0)$.

$$\left(\frac{R(\infty)}{R(0)}\right)^{1/2} = 0.5\left(\cos\theta_0\left(1+\cos\theta_0\right)\right)$$

(5.15)

Where $R(\infty)$ is related to the degree of confinement imposed by the chromophore environment and $R(0)$ is related to the spectroscopic properties of the probe. From our experimental data we extract $R(0)$ and $R(\infty)$, and calculate the cone semi-angle θ_0 according to Eq. 5.15. We present these results for NBD-PG in our vesicles in Table 5.2. Notably, the cone angle values are the same to within the experimental uncertainty for all systems studied, and are relatively large, indicating the local environment of the NBD chromophore is reasonably constant and disordered for the PG lipids. This finding is in contrast to previous results we reported for phosphocholine lipids,[21] where the addition of cholesterol and sphingomyelin produced a marked decrease in cone angle, reflective of the system becoming more organized (Table 5.2). The comparative constancy of the cone angle for the PG lipids, with or without cholesterol and/or sphingomyelin, is consistent with the hydrogen-bonding amongst the PG head groups mediating layer organization as sensed by the NBD chromophore, in contrast to PC lipids, where acyl chain organization is thought to dominate.

Conclusions

We have investigated the dynamics of the tethered NBD-PG chromophore contained within unilamellar vesicles comprised of phosphoglycerols DLPG and DSPG, with or without cholesterol and sphingomyelin added. Our data point to some similarities between vesicles comprised of phosphoglycerol and phosphocholine lipids, but the ability of the phosphoglycerol head groups to form hydrogen bonded networks provides an additional means of mediating bilayer organization in the proximity of the polar head groups. These findings point to comparatively subtle differences between the phosphocholine and phosphoglycerol bilayers, and underscore the ability of spectroscopic probes to interrogate these differences. Using both one- and two-photon excitation for the acquisition of time-domain fluorescence data, we are able to extract information on the Cartesian components of the rotational diffusion constant, revealing variations in the confinement of the chromophore by the bilayer that depend on the bilayer constituents. The apparently constant cone of confinement experienced by the chromophore suggests a significant role of head group hydrogen bonding in mediating organization within the polar regions of phosphoglycerol lipid bilayers.

Literature Cited

(1)   Araiso, T., Koyama, T. *Japanese Journal of Physiology* **1995**, *45*, 187.

(2)   Brown, D. A., London, E. *Biochemical and Biophysical Research Communications* **1997**, *240*, 1.

(3)   Brown, D. A., London, E. *Journal of Membrane Biology* **1998**, *164*, 103.

(4)   McConnell, H. M., Radhakrishnan, A., Xin-Min, L., Brown, R.E. *Biochimica et Biophysica Acta* **2001**, *1511*, 1.

(5)   Scherfeld, D.; Kahya, N.; Schwille, P. *Biophysical Journal* **2003**, *85*, 3758.

(6)   Simons, K.; van Meer, G. *Biochemistry* **1988**, *27*, 6197.

(7)   Wisniewska, A.; Draus, J.; Subczynski, W. K. *Cellular & Molecular Biology Letters* **2003**, *8*, 147.

(8)   Brown, R. E. *Journal of Cell Science* **1998**, *111*, 1.

(9)   Crane, J. M.; Tamm, L. K. *Biophysical Journal* **2004**, *86*, 2965.

(10)   Hao, M.; Maxfield, F. R. *Journal of Fluorescence* **2001**, *11*, 287.

(11)   Hunter, D. G.; Frisken, B. J. *Biophysical Journal* **1998**, *74*, 2996.

(12)   Lee-Gau Chong, P. W. v. d. M., B. Thompson, T.E. . *Biochimica et Biophysica Acta* **1985**, *813*, 253.

(13)   McConnell, H. M., Radhakrishnan, A. *Biochimica et Biophysica Acta* **2003**, *1610*, 159.

(14)   McMullen, T. P. W., Lewis, R.N.A.H, McElhaney, R.N. . *Current Opinion in Colloid and Interface Science* **2004**, *8*, 459.

(15) Mitchell, D. C., Litman, B.J. *Biophysical Journal* **1998**, *75*, 896.

(16) Samsonow, A. V., Mihalyov, I., Cohen, F.S. *Biophysical Journal* **2001**, *81*.

(17) Sankaram, M. B., Thompson, T.E. *Biochemistry* **1990**, *29*, 10670.

(18) Silvius, J. R. *Biochimica et Biophysica Acta* **2003**, *1610*, 174.

(19) Slotte, J. P. *Chemistry and Physics of Lipids* **1999**, *102*, 13.

(20) Webb, S. J., Greenaway, K., Bayati, M., Trembleau, L. *Organic and Biomolecular Chemistry* **2006**, *4*, 2399.

(21) Greenough, K. P. a. B., G. J. *Chemical Physics* **2007**.

(22) Koan, M. M., Blanchard, G. J. . **2006**.

(23) Greenough, K. P. a. B., G. J. *The Journal of Physical Chemistry B* **2006**, *110*, 6351.

(24) Chapman, C. F.; Liu, Y.; Sonek, G. J.; Tromberg, B. J. *Photochemistry and Photobiology* **1995**, *62*, 416.

(25) Chattopadhyay, A.; London, E. *Biochimica et Biophysica Acta, Biomembranes* **1988**, *938*, 24.

(26) Fery-Forgues, S.; Fayet, J.-P.; Lopez, A. *Journal of Photochemistry and Photobiology, A: Chemistry* **1993**, *70*, 229.

(27) Greenough, K. P. a. B., G. J. *The Journal of Physical Chemistry A* **2007**, *111*, 558.

(28) Huster, D.; Muller, P.; Arnold, K.; Herrmann, A. *Biophysical Journal* **2001**, *80*, 822.

(29) Lin, S.; Struve, W. S. *Photochemistry and Photobiology* **1991**, *54*, 361.

(30)   Mazeres, S.; Schram, V.; Tocanne, J.-F.; Lopez, A. *Biophysical Journal* **1996**, *71*, 327.

(31)   Mukherjee, S.; Chattopadhyay, A.; Samanta, A.; Soujanya, T. *Journal of Physical Chemistry* **1994**, *98*, 2809.

(32)   Tsukanova, V.; Grainger, D. W.; Salesse, C. *Langmuir* **2002**, *18*, 5539.

(33)   Goldie, S. N., Blanchard, G.J. *Journal of Physical Chemistry A* **1999**, *103*, 999.

(34)   Jiang, Y.; Blanchard, G. J. *Journal of Physical Chemistry* **1994**, *98*, 6436.

(35)   Drexhage, K. H. *Journal of Luminescence* **1970**, *1,2*, 693.

(36)   Girard, C.; Martin, O. J. F.; Dereux, A. *Physical Review Letters* **1995**, *75*, 3098.

(37)   Lukosz, W.; Kunz, R. E. *Optics Communications* **1977**, *20*, 195.

(38)   Lukosz, W.; Kunz, R. E. *Journal of the Optical Society of America* **1978**, *67*, 1607.

(39)   Bittman, R., Kasireddy, C. R. , Mattjus, P., Slotte, J.P. *Biochemistry* **1994**, *33*, 11776.

(40)   Koopman, E. Sphingomyelin-cholesterol superlattices as detected with Langmuir isotherms: their potential role in myelin and demyelination; Husted, C. A., Ed.; University of California, Santa Barbara, 2003; Vol. 1.

(41)   Korchowiec, B., Paluch, M., Corvis, Y., Rogalska, E. *Chemistry and Physics of Lipids* **2006**, *144*, 127.

(42)   Prenner, E., Honsek, G., Honig, D., Mobius, D., Lohner, K. *Chemistry and Physics of Lipids* **2007**, *145*, 106.

(43)   Rog, T., Pasenkiewicz-Gierula, M. *Biophysical Journal* **2006**, *91*, 3756.

(44)   Smaby, J. M., Brockman, H.L., Brown, R.E. *Biochemistry* **1994**, *33*, 9135.

(45)   Smaby, J. M., Momsen, M., Kulkarni, V. S., Brown, R.E. *Biochemistry* **1996**, *35*, 5696.

(46)   Stottrup, B. L., Stevens, D.S., Kellar, S.L. *Biophysical Journal* **2005**, *88*, 269.

(47)   Terova, B., Heczko, R., Slotte, J.P. *Biophysical Journal* **2005**, *88*, 2661.

(48)   Yuan, C., Johnston, L.J. *Journal of Microscopy* **2002**, *205*, 136.

(49)   Blanchard, G. J. *Journal of Chemical Physics* **1987**, *87*, 6802.

(50)   Chuang, T. J.; Eisenthal, K. B. *Journal of Chemical Physics* **1972**, *57*, 5094.

(51)   Debye, P. Polar Molecules. In *Chemical Catalog Co.* New York, 1929.

(52)   Dela Cruz, J. L.; Blanchard, G. J. *Journal of Physical Chemistry A* **2001**, *105*, 9328.

(53)   Lakowicz, J. R.; Gryczynski, I.; Gryczynski, Z.; Danielsen, E.; Wirth, M. J. *Journal of Physical Chemistry* **1992**, *96*, 3000.

(54)   McPhie, P. *Principles of Fluorescence Spectroscopy, Second ed. Joseph R. Lakowicz*, 2000; Vol. 287.

(55)   Zwanzig, R.; Harrison, A. K. *Journal of Chemical Physics* **1985**, *83*, 5861.

(56)   Callis, P. R. *Journal of Chemical Physics* **1993**, *99*, 27.

(57)   Chen, S. Y.; Van Der Meer, B. W. *Biophysical Journal* **1993**, *64*, 1567.

(58)   Johnson, C. K.; Wan, C. *Topics in Fluorescence Spectroscopy* **1997**, *5*, 43.

(59)   Johnson, J. M.; Ha, T.; Chu, S.; Boxer, S. G. *Biophysical Journal* **2002**, *83*, 3371.

(60)   Pauls, S. W.; Hedstrom, J. F.; Johnson, C. K. *Chemical Physics* **1998**, *237*, 205.

(61)   Wan, C.; Johnson, C. K. *Chemical Physics* **1994**, *179*, 513.

(62)   Wan, C.; Johnson, C. K. *Journal of Chemical Physics* **1994**, *101*, 10283.

(63)   Lipari, G.; Szabo, A. *Biophysical Journal* **1980**, *30*, 489.

(64)   Szabo, A. *Journal of Chemical Physics* **1984**, *81*, 150.

CHAPTER 6

CONCLUSIONS

In this work, we have studied the fluorescence lifetime and anisotropy decay of chromophores from the NBD family, both as free probe molecules and those tethered to phospholipid molecules. These fluorescent behavior of these chromophores were examined using one- and two-photon excitation as a means to determine the Cartesian components of the rotational diffusion coefficient in both solvents and in model lipid bilayers. The information gained from this work will provide an initial understanding of the phase segregation within lipid bilayers.

Prior to incorporation into a bilayer, the fluorescence behavior of three substituted NBD chromophores was studied in solvents. Chapter 2 showed that, despite different side group attachments on the NBD chromophores, the dynamics of these molecules are similar. The fluorescence lifetimes were dependent on the solvent polarity, while the rotational diffusion coefficients found by both one- and two-photon excitation yielded a ratio of $D_z/D_x \sim 2$ regardless of the identity of the solvent. Comparing the experimental data with the Debye-Stokes-Einstein model it was found that the reorientation time was much longer that the predicted time constant. We attributed this to a contribution from dielectric friction, which, when accounted for the discrepancies between the predicted and experimental time constants. Overall, the identity of the sidegroup on the chromophore played little role in determining the rotational dynamics of the chromophore in solution.

An NBD chromophore, NBD-hexanoic acid, was incorporated into bilayers composed of phospholipids, cholesterol, and sphingomyelin. Chapter 3 reports on the fluorescence behavior of the chromophore in vesicle systems. The fluorescence lifetime values suggested that, regardless of vesicle composition, NBD-hexanoic acid was located at the bilayer-aqueous interface. Similar results obtained for the anisotropy data, with the free chromophore reorienting in the same manner in each vesicle system. These data taken together suggest that in order to gain information about phase segregation and overall organization of the bilayer, a chromophore tethered to a lipid molecule must be used in these studies.

In Chapter 4, an NBD moiety tethered to a phospholipid molecule was used to probe lipid bilayer heterogeneity. Again, both one- and two-photon excitation were utilized to determine the fluorescence lifetime and anisotropy in lipid vesicles. Using the tethered chromophore, double exponential lifetime decays were obtained, indicating the chromophore was sensing two environments. The experimental anisotropy decay was measured, and from that, the viscosity of the probe's surroundings and the Cartesian components of the rotational diffusion coefficient were calculated. Significant changes in viscosity were measured upon the addition of both cholesterol and sphingomyelin to the phospholipid. These changes in viscosity were attributed to changes in local organization within the bilayer structure. The ratio D_y/D_x was used as a measure of bilayer organization, and substantial decreases of D_y/D_x were the result of cholesterol and sphingomyelin being added to the system. Furthermore, changes in the cone angle showed increased organization within the bilayer upon addition of components. Taken

collectively, the data point to the NBD group residing near boundaries between heterogeneous regions within the model lipid bilayers.

Vesicles comprised of lipids with a glycerol headgroup, as opposed to a choline headgroup were used for studies outlined in chapter 5. NBD tethered to a phosphoglycerol lipid was the chromophore incorporated into bilayers. The experimental data show some similarities in chromophore behavior as compared to the phosphocholine vesicles, yet the ability of the phosphoglycerol headgroups to participate in hydrogen bonding provide an additional means of mediating bilayer organization in the proximity of the lipid headgroup region of the bilayer.

Overall, this work shows the benefits of utilizing both one- and two-photon excitation to examine the fluorescent behavior and rotational dynamics of a chromophore. When incorporated into model bilayer systems, these experiments probe the organization of lipid bilayers and show that even in simple systems, formation of phase segregation occurs within the bilayer providing further evidence of heterogeneity of lipid bilayer systems.